FLOWING AFTERGLOW STUDIES OF TEMPERATURE DEPENDENCIES FOR ELECTRON-ION DISSOCIATIVE RECOMBINATION OF HYDROCARBON IONS: RELEVANCE TO THE ATMOSPHERE OF TITAN AND THE INTERSTELLAR MEDIUM

by

JASON LEE MCLAIN

(Under the Direction of NIGEL G. ADAMS)

ABSTRACT

A temperature-variable flowing afterglow with an electrostatic Langmuir probe (VT-FALP) has been used to determine the rate coefficients, α_e, for the dissociative recombination (DR) of a series of molecular ions with electrons. The α_e for O_2^+, CH_5^+, $C_2H_5^+$, c-$C_3H_3^+$, l-$C_3H_3^+$, c-$C_6H_7^+$, $HCNH^+$, CH_3CNH^+, $CH_3CH_2CNH^+$, $(HCN)_2H^+$, $(CH_3CN)_2H^+$, and $(CH_3CH_2CN)_2H^+$ have been determined at temperatures ranging from 80 to 600 K. The DR of these ions is important to molecular synthesis and the ionization balance in interstellar clouds and the ionosphere of Titan, which has been probed by the Cassini-Huygens spacecraft since 2004. The DR of O_2^+ was the standard calibration test for recombination measurements. The α_e's for O_2^+ over the temperature range of 100-500 K followed a single power law dependence of $T^{-0.7}$, which is consistent with previous data in this temperature range. A series of different types of molecular ions were chosen to study for which the α_e and their temperature dependence have not been obtained previously, and which were relevant to the applications. These temperature dependencies are represented as power laws in the range of $T^{-0.5 \text{ to } -1.5}$. Until recently, most recombination measurements have been obtained only at room temperature. However, typically the environments where DR is important are not at this temperature. The α_e's obtained in the

present studies exhibit significant dependencies on temperature usually consistent with simple theoretical models based on a combination of the direct and indirect mechanisms. The production of proton bound cluster ions has also been investigated. These cluster ions are produced by association when large reactant concentrations are used. Here, this association can compete with DR of the protonated ions, creating a plasma containing two simultaneously recombining ions. All of the α_e's vary significantly depending on the ion type. The number of atoms, type of bonding, and whether the ions are cyclic or linear can all affect the α_e. The relevance of the present data to the applications is also discussed.

INDEX WORDS: Dissociative Recombination, Electron-Ion Recombination, VT-FALP, Direct Mechanism, Indirect Mechanism

FLOWING AFTERGLOW STUDIES OF TEMPERATURE DEPENDENCIES FOR ELECTRON-ION DISSOCIATIVE RECOMBINATION OF HYDROCARBON IONS: RELEVANCE TO THE ATMOSPHERE OF TITAN AND THE INTERSTELLAR MEDIUM

by

JASON LEE MCLAIN

Bachelors of Chemical Engineering, Auburn University, 2001

A Dissertation Submitted to the Graduate Faculty of The University of Georgia in Partial Fulfillment of the Requirements for the Degree

DOCTOR OF PHILOSOPHY

ATHENS, GEORGIA

2008

FLOWING AFTERGLOW STUDIES OF TEMPERATURE DEPENDENCIES FOR ELECTRON-ION DISSOCIATIVE RECOMBINATION OF HYDROCARBON IONS: RELEVANCE TO THE ATMOSPHERE OF TITAN AND THE INTERSTELLAR MEDIUM

by

JASON LEE MCLAIN

Major Professor: Nigel G. Adams

Committee: Geoffrey D. Smith
I. Jonathan Amster

Electronic Version Approved:

Maureen Grasso
Dean of the Graduate School
The University of Georgia
August 2008

DEDICATION

There are so many things that came together at the right time to make this all possible. First, would be the creation of the universe, without it, nothing would exist. Second, would be manifestation of light, without it, seeing would have been impossible. Thirdly, would be the synthesis of matter, without it, we would all be just chaotic energy. Fourthly, all of the people who believed in me, (which I endeavored to not let down), as well as the people who did not, (which I strived to prove wrong). But sincerely, I am dedicating this to my mother and father. Thank you for your support and patience through these many trying years.

ACKNOWLEDGEMENTS

Firstly, I would like to thank my major advisor and friend, Nigel G. Adams. I feel like one of the luckiest persons on the face of the Earth just because I got to know someone of his caliber.

I would also like give an extra special thanks to Greg Grieves. First, for the time he devoted to helping me write the Langmuir probe data acquisition program, and secondly, for his insightful conversations about chemistry and the universe. I cannot express enough how much my deepest gratitude goes out to him for his support and kindness.

I am very grateful to a number of professors and graduate students who I have interacted with throughout graduate school. Particularly graduate students: Dalila Fondren, Chris and Karen Molek, Timothy Ayers, Nathan De Yonkers, Andy Simmonett, Allen Ricks, Leah Stavish, Eric Gale, Jeremy Grove, Matt Tessier, Francesco Evangelista, Caroline Watson, Wendy Nkari, Joe Valasquez, Brian Ticknor, Prosser Carnegie, David Osborne and many others. And particularly Professors: Goeff Smith, Jon Amster, Sarah Haydock, Michael Duncan, Gary Douberly, Dennis Phillips, George Majetich, John Stickney, Bobby Stanton, and Allen King.

TABLE OF CONTENTS

Page

LIST OF TABLES

Page

LIST OF FIGURES

Page

CHAPTER 1

INTRODUCTION

Dissociative electron-ion recombination (DR) is an energetic and complex process that involves the production of excited resonant intermediate states that can either autoionize back to the reactants or fragment into an almost unpredictable distribution of excited neutral products. The rate coefficients (α_e) for these reactions are large 10^{-8} cm^3 s^{-1} to 10^{-5} cm^3 s^{-1}, and depend significantly on whether a surface crossing exist between the ion potential surface and the repulsive, dissociative potential surface of the neutralized products, the direct mechanism. Although the presence of such surface crossings permits rapid recombination, it is not a prerequisite. Other mechanisms have been proposed, i.e.; intermediate and resonant Rydberg states,[1, 2] core excited states,[3] dissociative state mixing,[4] broad cross-section interference,[5] tunneling,[6] and the electronic indirect mechanism[7] that can circumvent this lack of a curve crossing and generate moderately rapid recombination rates. DR rate coefficients are usually much larger than those for other recombination mechanisms. Other types of recombination are collisional/radiative recombination which has of recombination rate coefficients between 10^{-9} to 10^{-17} cm^3 s^{-1}, and dielectronic recombination with recombination rate coefficients between 10^{-11} to 10^{-12} cm^3 s^{-1}.[8, 9] Ternary processes with a third body can also neutralize ionization and have binary rate coefficients in the range of 10^{-10} to 10^{-13} cm^3 s^{-1} at a pressure of 1 Torr.[8, 9] Therefore, DR is an extremely important ionization loss process in plasma containing molecular ions such as interstellar clouds,[10-12] cometary comae,[13] planetary ionosphere,[13, 14] and even man-made plasma applications.[15-17] A conference

series on DR began in 1989 and the proceedings of the first six meetings have been published.[3, 4, 18-21] There are also presently many reviews[22-24] on DR and databases[25-28] which contain recombination rate coefficients and, when available, neutral products of DR.

When DR was first accepted as a rapid process, two mechanisms were proposed to explain the incontrovertible experimental data on dissociative recombination, the direct and indirect mechanisms. In the direct mechanism, proposed by Bates,[29-31] the electron is captured directly onto an accessible repulsive, dissociative curve of the neutralized ion. The recombining electron excites an electron in the ion and in a double-electron radiationless transition is resonantly captured to form the doubly excited repulsive state, $(ABC)_R^{**}$. Initially, this state $(ABC)_R^{**}$ can autoionize back to the reactants. However, as the neutral products start to separate, the potential energy of the ion is converted into kinetic energy of separation. Once the potential energy goes below the lowest rotational/vibrational level of the recombining ion, recombination becomes inevitable.

$$ABC^+ + e^- \rightleftharpoons (ABC)_R^{**} \rightharpoonup AB^* + C^* \qquad (1.1a)$$

$$\rightharpoonup BC^* + A^* \qquad (1.1b)$$

This process requires a favorable crossing between the potential curve of the ion and the repulsive curve. The rate coefficient for direct recombination can be expressed in the form[1]:

$$\alpha_{DR} = \frac{4\pi^3\hbar^2 r}{\left(2\pi m^3 k T_e\right)^{1/2}} \Gamma_c \frac{\left|\xi_0(R_c)\right|^2}{\left|E_d'(R_c)\right|} \qquad (1.2)$$

where Γ_c is the capture width which is related to the strength of the interaction between states and thus the transition probability, ξ_0 is the wavefunction of the nuclear motion

governing the dissociation with the subscript *0* indicating that it is for the ground vibrational level. E_d' = dE(R)/dR is the potential function varying with internuclear separation, R. R_c is the separation at which the repulsive curve is at the energy of the crossing point with the ion potential curve. This is essentially the starting point of the dissociation. The r is the ratio between the multiplicity of the resonant molecular state and that of the initial state of the molecular ion. Thus, the recombination coefficient is predicted to vary as $T_e^{-1/2}$, the subscript e denotes the electron temperature or, if the particle energies are thermalized, the plasma temperature, T.

In the indirect mechanism proposed by Bardsley,[1, 31, 32] the captured electron vibrationally excites the ion in a radiationless transition and is then resonantly captured into a vibrational level of a Rydberg state, $(ABC)^*_{Ryd}$

$$ABC^+ + e^- \rightleftharpoons (ABC)_R^* \rightleftharpoons (ABC)_R^{**} \rightharpoonup AB^* + C^* \qquad (1.3a)$$

$$\rightharpoonup BC^* + A^* \qquad (1.3b)$$

where the electron is orbiting far away from the ion core. This state undergoes a second radiationless transition to the same doubly excited repulsive state as in the direct process, $(HCNH)_R^{**}$. The indirect recombination rate coefficient is given by[1]:

$$\alpha = \sum_s \frac{4\pi^3\hbar^2 r}{(2\pi mkT)^{3/2}} \frac{\Gamma_{sa}\Gamma_{sd}}{\Gamma_s} \exp\left(-\frac{E_s - E_0}{kT}\right) \qquad (1.4)$$

where Γ's are capture widths with the subscript s identifying the resonant state (Γ being the total width) and subscripts a and d referring to the Γ's for autoionization and predissociation to neutral products respectively. E_s and E_0 are the potential energies of the resonance and the initial molecular ion and R_s is the value of R_c at zero energy. Note that the temperature dependencies are very different in the two mechanisms being $T_e^{-1/2}$ for direct recombination and $T^{-3/2}$ for the indirect process. Also, these two mechanisms

can in general occur in parallel, depending on the relative efficiencies of the two first stages. This situation is automatically treated in multichannel quantum defect theory (MQDT).[33]

DR was initially studied using stationary (time dependent) afterglows (SA). In a stationary afterglow, a mixture of gases within a spherical or cylindrical chamber is ionized by a pulse of microwaves or a RF discharge. The ionization density decay is then measured with a Langmuir probe as function of time. An advantage of the stationary afterglow is the lengthy time scale for the measurements, ideal for measuring slow α_e's. This can be as long as 100 msec, which for flowing afterglows, the residence time is only 10–30 msec. The main disadvantage for SA is that the ion identity and abundances can change during the measurement due to ion-molecule reactions because the entire gas mixture is exposed to the discharge.[31, 34]

In the beginning, the flowing afterglow (FA) technique was used to study ion-molecule reactions.[35] However, the Selected Ion Flow Tube (SIFT) technique developed by Adams and Smith proved to be far more superior for these types of reactions.[36, 37] Therefore, the FA was applied to recombination studies in conjunction with electrostatic Langmuir probing techniques,[38] and will be discussed in detail in Chapter 2. In the FA, reactant gases can be added at various distances along the flow tube i.e., at various afterglow times, making it possible to have a single ion type dominating the molecular ion plasma. FA's have also been integrated with spectroscopic techniques,[39-42] and spectrometric techniques have been used to identify reionized neutral products.[43] The main disadvantage of the FA is that some molecular ions cannot be exclusively

synthesized because certain ion-molecule reactions give a distribution of ionized products.

Along with afterglow techniques, the ion storage ring technique has been used to study DR rate coefficients and products. In the storage ring technique, an electron beam merges with an ion beam and the cross-sections, σ_e, are determined. This technique is ideal for measuring reactivity as a function of electron energy over a broad energy range, and since ions can be injected into the ring, recombination cross-sections and thus rate coefficients, equation 1.5, can be obtained for molecular ions that the afterglow experiments cannot measure, e.g. H_2^+, due to H_2^+ rapidly converting into H_3^+ in H_2 plasma.

$$\alpha_e(T) = \int_0^\infty v f(v) \sigma_e(v) dv \tag{1.5}$$

where $\alpha_e(T)$ is related to the velocity-dependent cross-sections, $\sigma_e(v)$, for the process via an integration over the velocity weighted by the Maxwell-Boltzmann velocity distribution, $f(v)$. In principle, the storage ring experiments are perfect for studying DR, but unfortunately many sources of uncertain error have to be resolved. Significant errors can occur in both the measurements of the beam currents, and the length of the interaction region. The ion excitation states have also not often been well determined, and the neutral particle detectors have a resolution larger than an amu.[44]

As indicated above, DR rate coefficients are predicted by theory to have inverse temperature dependencies. The extent of this dependence varies depending on the competition between the direct and indirect mechanism, and especially if the other mechanisms are involved. These temperature dependencies for DR are of critical importance because where these reactions are observed, rarely are they at ambient room

temperature, where most experimental recombination measurements have been made. In the present studies, the temperature dependencies of α_e for several important molecular ion have been obtained, i.e.; O_2^+, CH_5^+, $C_2H_5^+$, c-$C_3H_3^+$, l-$C_3H_3^+$, c-$C_6H_7^+$, $HCNH^+$, CH_3CNH^+, $CH_3CH_2CNH^+$, $(HCN)_2H^+$, $(CH_3CN)_2H^+$, and $(CH_3CH_2CN)_2H^+$. These species exhibit a variety of behaviors. All of these ions have been produced in a H_3^+/e^- dominated flowing afterglow plasma, except for O_2^+. H_3^+ will rapidly donate a proton to most molecules, especially hydrocarbons. The H_3^+ ions also have a relatively small α_e of 1×10^{-7} cm^3 s^{-1}, so that considerably large ionization densities, $\sim1\times10^{10}$ cm^{-3}, can be obtained. These data are presented and their relevance to theory and observation will be discussed.

1.1 REFERENCES

[1] Bardsley, J. N., The Theory of Dissociative Recombination. *J. Phys. B.* **1968,** 1, 365-380.

[2] Guberman, S. L., Dissociative Recombination without a Curve Crossing. *Phys. Rev. A* **1994,** 49, R4277.

[3] Mitchell, J. B. A.; Guberman, S. L., *Dissociative Recombination: Theory, Experiment and Applications I.* World Scientific: Singapore, 1989.

[4] Zajfman, D.; Mitchell, J. B. A.; Schwalm, D.; Rowe, B. R., *Dissociative Recombination: Theory, Experiment and Applications III*. World Scientific: Singapore, 1996.

[5] Larson, A.; Orel, A. E., Ion-pair formation and product branching ratios in dissociative recombination of HD^+. *Phys Rev. A* **2001,** 64, (6), 062701-1.

[6] Bates, D. R., Dissociative Recombination: Crossing and Tunneling Modes. *Adv. Atom. Molec. Opt. Phys.* **1994,** 34, 427-486.

[7] Hickman, A. P., Dissociative recombination of electrons with H_2^+. *J Phys. B* **1987,** 20, (9), 2091.

[8] Flannery, M. R., Recombination Processes. In *Molecular Processes in Space*, Watanabe, T.; Shimamura, I.; Shimizu, M.; Itikawa, Y., Eds. Plenum: New York, 1990; p 145.

[9] Adams, N. G.; Babcock, L. M.; McLain, J. L., Electron-Ion Recombination. In *Encyclopedia of Mass Spectrometry: Theory and Ion Chemistry, Vol.1*, Armentrout, P., Ed. Elsevier: Amsterdam, 2003; Vol. 1, pp 542-555.

[10] Herbst, E., Ion-Molecule Chemistry in Interstellar Clouds: Successes and Problems. *Adv. Gas Phase Ion Chem.* **1998,** 3, 1-47.

[11] Millar, T. J., *Chemistry in Expanding Circumstellar Envelopes.* Kluwer: Dordrecht, 1988; p 287-308.

[12] Dalgarno, A., Dissociative Recombination in Astrophysical Environments. In *Dissociative Recombination: Theory, Experiment and Applications IV*, Larsson, M.; Mitchell, J. B. A.; Schneider, I. E., Eds. World Scientific: Singapore, 2000; pp 1-12.

[13] Cravens, T. E., Dissociative Recombination in Cometary Ionospheres. In *Dissociative Recombination of Molecular Ions with Electrons*, Guberman, S. L., Ed. Kluwer: New York, 2003; pp 385-400.

[14] Fox, J. L., Dissociative Recombination in Planetary Ionospheres. In *Dissociative Recombination Theory, Experiment and Applications II*, Rowe, B. R.; Mitchell, J. B. A.; Canosa, A., Eds. Plenum: New York, 1993; p 219.

[15] Goodings, J. M.; Karellas, N. S.; Hasanali, C. S., Comparison of Electron Scavengers in a Hydrocarbon Flame: Anion Formation with Sulfur Hexafluoride, $(CF_3SO_2)_2O$, Sulfur Dioxide and Chloromethane Additives. *Int. J. Mass Spectrom. Ion Proc.* **1989,** 89, 205-226.

[16] Post, D. E., The Role of Atomic Collisions in Fusion. In *Physics of Ion-Ion and Ion-Electron Collisions*, Brouillard, F.; McGowan, J. W., Eds. Plenum Press: New York, 1983; pp 37-99.

[17] Biondi, M. A., Principles of Laser Plasmas. In *Recombination.*, Bekefi, G., Ed. Wiley: New York, 1976; p 125.

[18] Rowe, B. R.; Mitchell, J. B. A.; Canosa, A., *Dissociative Recombination: Theory, Experiment and Applications II*. Plenum: New York, 1993.

[19] Wolf, A.; Lammich, L.; Schmelcher, P., *Sixth International Conference on Dissociative Recombination: Theory, Experiments and Applications*. Inst. Phys. J. Phys.: Conf. Ser. 6: London, 2005; Vol. 6.

[20] Larsson, M.; Mitchell, J. B. A.; Schneider, I. E., *Dissociative Recombination: Theory, Experiment and Applications IV*. World Scientific: Singapore, 2000.

[21] Guberman, S., *Dissociative Recombination of Molecular Ions with Electrons*. Kluwer New York, 2003; Vol. 5.

[22] Adams, N. G.; Poterya, V.; Babcock , L. M., Electron Molecular Ion Recombination: Product Excitation and Fragmentation. *Mass Spectrom. Revs.* **2006,** 25, 798-828.

[23] Florescu-Mitchell, A. I.; Mitchell, J. B. A., Dissociative Recombination. *Physics Reports-Review Section of Physics Letters* **2006,** 430, 277-374.

[24] Mitchell, J. B. A.; Rebrion-Rowe, C., The Recombination of Electrons with Complex Molecular Ions. *Int. Rev. Phys. Chem.* **1997,** 16, 201-213.

[25] Woodall, J.; Agundez, M.; Markwick-Kemper, A. J.; Millar, D. P., The UMIST Database of Astrochemistry. *http://www.udfa.net/* **2008**.

[26] Johnson III, R. D. NIST Computational Chemistry Comparison and Benchmark Database: NIST Standard Reference Database Number 101. http://srdata.nist.gov/cccbdb

[27] Dere, K. P.; Landi, E., CHIANTI Database. *Ap. J. Suppl.* **2006,** 162, 261.

[28] Garrod, R.; Herbst, E., Ohio State University Database. *https://kb.osu.edu/dspace/index.jsp* **2007**.

[29] Bates, D. R., Electron Recombination in Helium. *Phys. Rev.* **1950,** 77, 718-719.

[30] Bates, D. R., Dissociative Recombination. *Phys. Rev.* **1950,** 78, 492-493.

[31] Bardsley, J. N.; Biondi, M. A., Dissociative Recombination. *Adv. At. Mol. Phys.* **1970,** 6, 1-57.

[32] Bardsley, J. N., Configuration Interaction in the Continuum States of Molecules. *J. Phys. B.* **1968,** 1, 349-364.

[33] Guisti, A., A Multichannel Quantum Defect Approach to Dissociative Recombination. *J. Phys. B.* **1980,** 13, 3867-3894.

[34] Johnsen, R., Microwave Afterglow Measurements of the Dissociative Recombination of Molecular Ions with Electrons. *Int. J. Mass Spectrom. Ion Proc.* **1987,** 81, 67-84.

[35] Ferguson, E. E.; Fehsenfeld, F. C.; Schmeltekopf, A. L., Flowing Afterglow Measurements of Ion-Neutral Reactions. *Adv. At. Mol. Phys.* **1969,** 5, 1-56.

[36] Adams, N. G.; Smith, D., Product-Ion Distributions for Some Ion-Molecule Reactions. *J. Phys. B.* **1976,** 9, 1439-51.

[37] Adams, N. G.; Smith, D., The Selected Ion Flow Tube (SIFT); A Technique for Studying Ion-Neutral Reactions. *Int. J. Mass Spectrom. Ion Phys.* **1976,** 21, 349-59.

[38] Smith, D.; Adams, N. G.; Dean, A. G.; Church, M. J., The Application of Langmuir Probes to the Study of Flowing Afterglow Plasmas. *J. Phys. D.* **1975,** 8, 141-152.

[39] Adams, N. G., Spectroscopic Determinations of the Products of Electron-Ion Recombination. *Adv. Gas Phase Ion Chem.* **1992,** 1, 271-310.

[40] Adams, N. G., Flowing Afterglow Studies of Electron-Ion Recombination using Langmuir Probes and Optical Spectroscopy. In *Dissociative Recombination: Theory, Experiment and Applications,* Rowe, B. R.; Mitchell, J. B. A., Eds. Plenum Press: New York, 1993; pp 99-111.

[41] Adams, N. G.; Babcock, L. M., Optical Emissions from the Dissociative Electron Recombination of N_2H^+ and HCO^+. *J. Phys. Chem.* **1994,** 98, 4564-4569.

[42] Adams, N. G.; Babcock, L. M., Vibrational Excitation in the Products of Electron-Ion Recombination: A Test of Theory for Ions of Interstellar Significance. *Astrophys. J.* **1994,** 434 184-187

[43] Adams, N. G.; Molek, C. D.; McLain, J., New Flowing Afterglow Technique for Determining Products of Dissociative Recombination: CH_5^+ and N_2H^+. *J. Phys. Conf. Ser.* **2008**, in press.

[44] Larsson, M., Dissociative Recombination in Ion Storage Rings. *Int. J. Mass Spectrom Ion Proc.* **1995,** 149-50, 403-14.

CHAPTER 2

EXPERIMENTAL ARRANGEMENT AND PROCEDURE

2.1 BASIC DESIGN

The measurements described in this dissertation were made in the University of Georgia's Variable Temperature Flowing Afterglow with an axial Langmuir Probe (VT-FALP) apparatus. This chapter includes; (i) and overview of the flowing afterglow technique, (ii) a detailed discussion of the Langmuir probe technique, (iii) the basics of the Langmuir probe program written to obtain and analyze the data, (iv) the techniques developed to control and measure the temperature, and (v) the procedure and analysis for determining the ion velocities. A synopsis of the electron density data for determining the recombination rate coefficients, α_e, is also presented.

The UGA (VT-FALP) apparatus, see figure 2.1-2, is an extremely versatile instrument which was designed to be used as either a flowing afterglow (FA) or a Selected Ion Flow Tube (SIFT). The two separate ion sources are located outside a vacuum vessel encasing the flow tube. This vessel isolates the flow tube from the surroundings and this will be discussed in detail in section 2.2. The two ion sources enter through the vacuum vessel via two bellows designed to flex as the main flow tube expands and contracts upon heating and cooling. The main flow tube is 7.3 cm diameter which has 6 positions that contain 2 vertical and 2 horizontal ports, giving a total of 12 vertical ports and 12 horizontal ports. Four additional windows are located in the ion

detection system for spectroscopic measurements. The ion detection system is equipped with a quadrupole mass spectrometer with an electron impact ionizer for ionizing neutral molecules. The ions are detected with a discrete dynode electron multiplier (ETP model AF553H). The main 24 ports have conflat flanges which can support windows for spectroscopic measurements, or can support injectors for reactant gases. The gases are introduced into the flow tube through a complex arrangement of vacuum valves and stainless steal tubing, which will not be described. A carrier gas, typically helium, can flow into the tube through 4 different routes. The valves on the FA and reaction port 1 (RP1) allow helium to flow through the glass tube located upstream of the microwave cavity discharge. The valve on the SIFT allows the He to flow through a Venturi type nozzle downstream of the SIFT injection orifice disk, which is essential for injecting ions in a flow tube. The SIFT has not been used in these studies and will not be described further. It has been discussed in detail in the literature. The final He injection line is accessed through the valve on injector RP2-A. This is the most used injector because the gas line is connected to the Cu jacket surrounding the flow tube, see section 2.2, and first runs up and down the entire length of the flow tube jacket to achieve thermal equilibrium. It also allows the electron density to vary over the range 10^8 to 10^{11} cm^{-3} by moving the cavity discharge. This gas line enters at the flowing afterglow source. A specialized glass tube injector is positioned inside the main glass tube and runs upstream of the microwave cavity region until a 180° bend points the injector in the downstream direction, see figure 2.2. This guarantees that with extreme temperature changes, the gas entering the flow is completely thermalized. The apparatus has 4 reactant systems which can be utilized to inject gases into the flow. Each reactant system is connected to a series

of injectors, where the valves are designated RP2-B through RP6. RP2B, typically used for the addition of Ar, also first runs the entire length of the flow tube's Cu jacket, and enters the flow tube 22 centimeters downstream of the microwave discharge. RP3, 5 and 6 valves are ring type injectors having 6 holes pointing upstream to rapidly mix the gas into the He flow, RP4 is a straight nozzle injector pointed upstream at a 45° angle off axis.

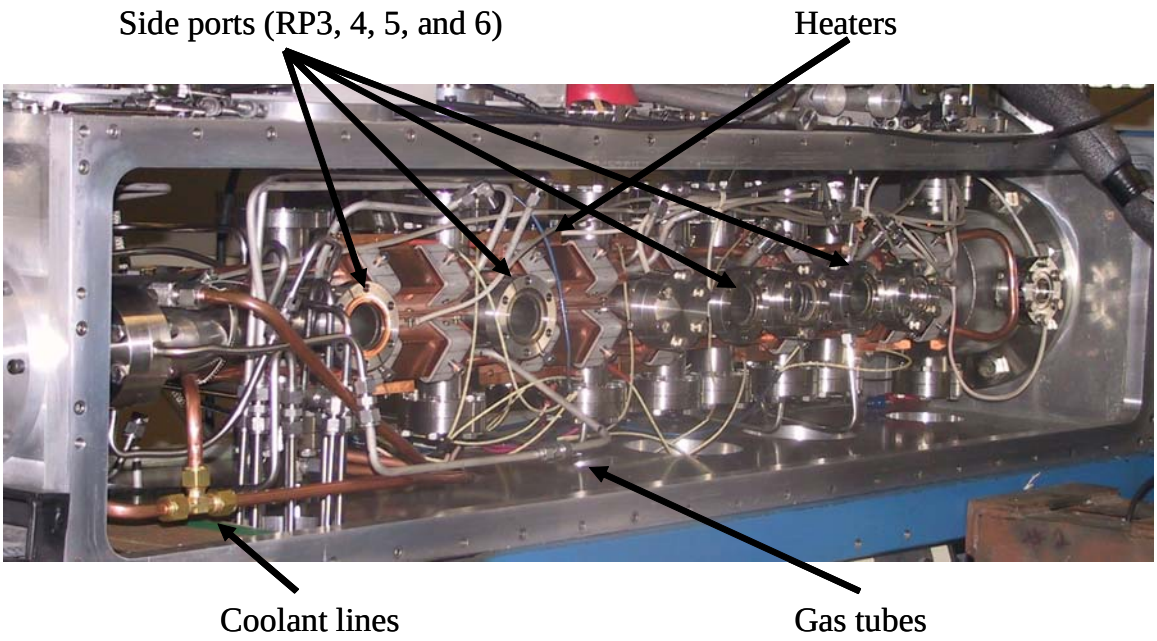

Figure 2.1. A picture of the variable temperature flowing afterglow at UGA with the side plate taken off of the vacuum vessel.

2.2 Temperature Control

For temperature variation, the entire flow tube is encased in a vacuum chamber, and this is evacuated to a pressure of ~10^{-6} Torr with a diffusion pump. This reduces conductive and convective heat transfer from the flow tube to the surroundings when at a temperature different from room temperature. Aluminum foil surrounds the flow tube

inside the evacuated chamber to reduce radiative heat transfer. The flow tube is fitted with an array of copper jackets that serve several purposes, see figure 2.1. The main purpose of the Cu jackets is to maximize conductive heat transfer from the heating and cooling elements to the flow tube. Mounted inside the Cu jackets are 10 Watlow firesticks, six 300 watt heaters and four 200 watt heaters. These firesticks are resistive heaters that are paired together vertically and are controlled with five variable transformers. The highest flow tube temperature that can be achieved with these heaters is approximately 700 K, but caution must be used to operate at this maximum temperature due to several optical windows on the flow tube with o-rings that could fail if this temperature is maintain for long times. Although o-ring failure has never occurred, heaters have failed operating at the maximum voltage of the variable transformers of 140 V.

The Cu jackets are also brazened to 3/8" Cu tubing for cooling the flow tube using a cryogenic fluid, typically liquid nitrogen. The supply line runs into a tee which divides the flow into two separate tubes. These run up and down the entire length of flow tube jacket. Then these tubes run into another tee, which allows the flow to exit through a single return line, see figure 2.1. These supply and return lines are connected to a pump specifically designed to pump liquid nitrogen. The liquid nitrogen pump had to be designed by the author after an exhaustive effort was made to find a commercial source for a simple, inexpensive liquid nitrogen pump. The University of Georgia Instrument Shop constructed the pump, which was designed to fit inside of a MVE 30 L dewar. The pump's general design was a modified FTS systems® ICS-40-0 cryogenic pump, which was inadequate to pump liquid nitrogen. The pumping mechanism is simply a spinning

Teflon disk nestled into a larger housing which is connected to a ¼" diameter tube. Liquid can flow into this disk from the bottom, via a ½" opening, and then into a series of radial vanes. Centrifugal force pressurizes the fluid and forces it up through the tube. With this unique pump, liquid nitrogen can be used to reach a temperature as low as ~80 K, only slightly above the normal temperature of liquid nitrogen (78 K).

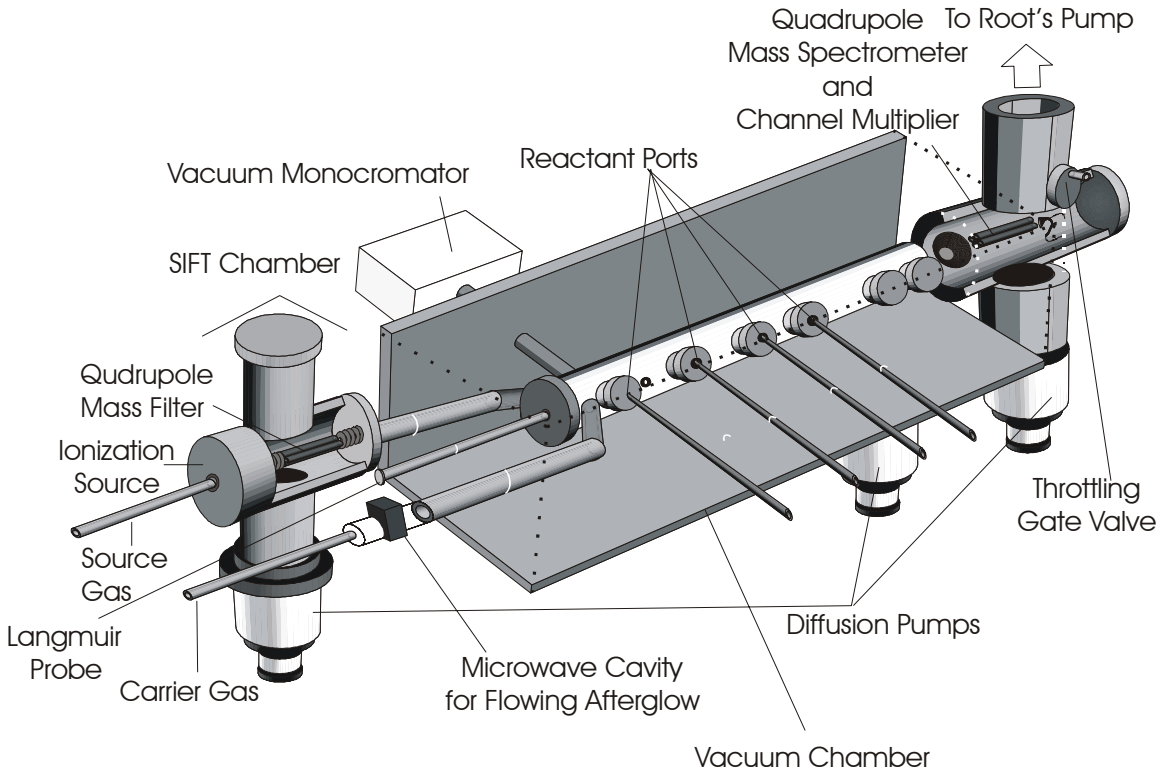

Figure 2.2. Schematic of the University of Georgia's Variable Temperature Flowing Afterglow has a movable axial Langmuir Probe (VT-FALP) for measuring electron-ion recombination rate coefficients and products.

Intermediate temperatures between 80 K and 300 K can also be achieved by periodically turning the liquid nitrogen pump on and off. The measurements can be completed in relatively short times, 20 minutes or less, and therefore the temperature fluctuations are small < 5° K.

The temperatures around the system are measured using six Type K thermocouples. These 6 thermocouples are spaced equally down the flow tube. An average temperature is calculated from these readings. To minimized temperature gradients, sections of the jacket are kept at temperatures less than 5° K apart to ensure that the entire reaction region is at a uniform temperature.

2.3 LANGMUIR PROBE MEASUREMENTS

The Langmuir probe wire is a specially designed tungsten wire 25 μm in diameter coated with 100 μm diameter nickel, which was custom made. The nickel coating serves as a protective sleeve to support the tungsten wire, and prevents the wire from touching the glass tube that holds it in place, figure 2.3.

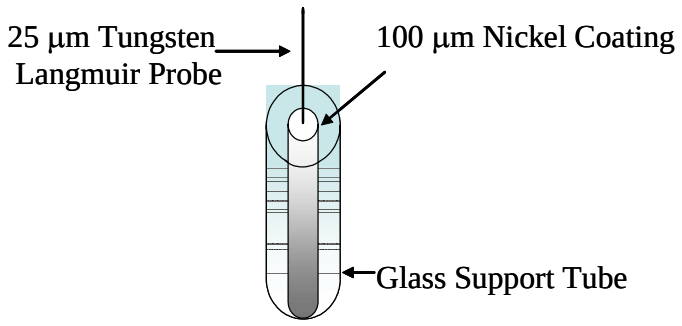

Figure 2.3. A simplistic illustration of the glass support tube for the Langmuir probe.

The glass support tube, although initially insulating, can become coated with a conducting layer of chemicals that can distort the probe characteristics and lead to

erroneous electron densities. The nickel coating was removed in an acidic solution to expose a tungsten wire measuring 4.3 mm long. The diameter of the probe was measured using optical diffraction with a He/Ne laser, and the length from a magnified image projected onto a screen.

For the probe diameter and electron densities available, the Langmuir probe is operated in the orbital limited region. Here, the probe's diameter is much smaller than its length and therefore, the electrostatic sheath takes the form of a cylinder. In this configuration, the electrons orbit the probe and the measured electron flux can be expressed as:

$$[e^-] = \sqrt{\frac{slope \cdot \pi^2 \cdot m_e}{2 \cdot a^2 \cdot e^3}} \tag{2.1}$$

where the *slope* is obtained from the plot of I^2 vs Vp. *a* represents the surface area of a cylinder equal to $2\pi rh$, where r and h are the radius and length of the probe. m_e and *e* are the mass and charge of an electron, respectively. Note that, if the probe's length is too short, the electrostatic sheath takes the form of a sphere and the characteristics I^2 vs Vp become nonlinear.

A positive ramp voltage sweep (V_a), typically 0-5 V, is applied to the probe circuitry. This attracts electrons from the plasma, creating a current and an amplified voltage, (V_{out}), is measured. The voltage the probe receives, (V_p), is determined by the expression $V_p = V_a - V_{in}$, where $V_{in} = (V_{out} - V_{offset})/G$. The V_{offset} and the gain of the amplifier (G) were measure to be 34 mV and 108.6, respectively. The current (I) is then calculated from Ohm's Law from V_{in}/R, where R is the resistor value selected for a particular ionization density, see section 2.6.

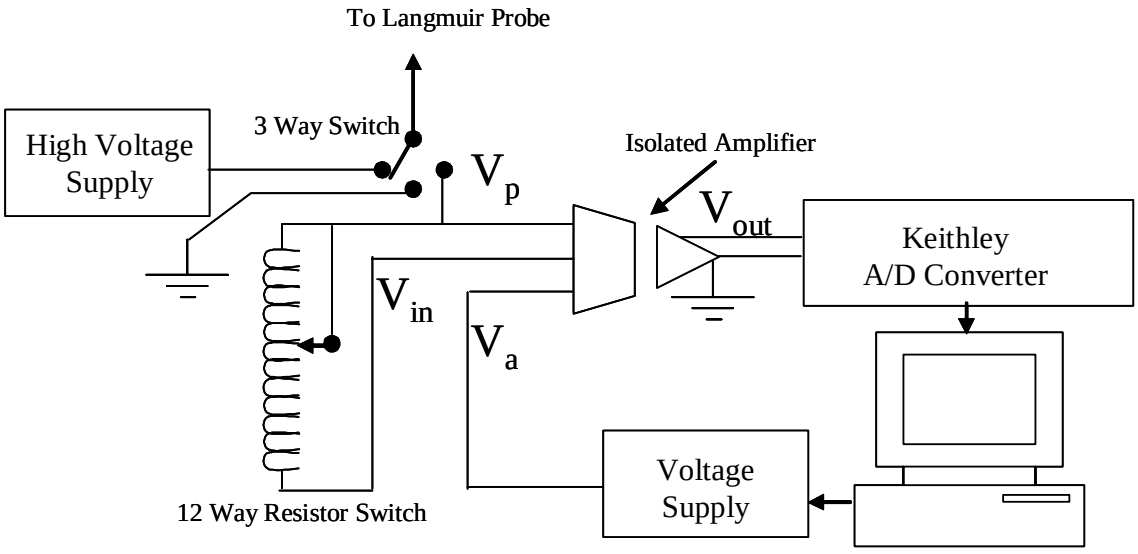

Figure 2.4. The wiring schematic of the Langmuir probe's circuitry.

A plot can be produced of I (current)^2 versus V_p, figure 2.5. The electron density is proportional to the slope, which can be obtained by performing linear least squares fit to the data. In this way, electron currents in microamperes can be measured. The electron densities obtained from these fits are then plotted versus the distance along the flow tube,

see figure 2.6. If only one ion is recombining, analysis of the rate equation for electrons shows that the $[e^-]_z^{-1}$ versus distance, z, plot will yield a linear relationship:

$$\frac{1}{[e^-]_z} - \frac{1}{[e^-]_0} = \alpha_e \frac{z}{v} \tag{2.2}$$

where v is the plasma velocity and α_e is the recombination rate coefficient.

In Figure 2.6, the slope is equal to α_e/ν, α_e is the recombination rate coefficient and ν is the flow velocity of the ions down the tube. Pressures were used that were high enough to inhibit diffusion, thus making recombination the only significant loss process at early times.

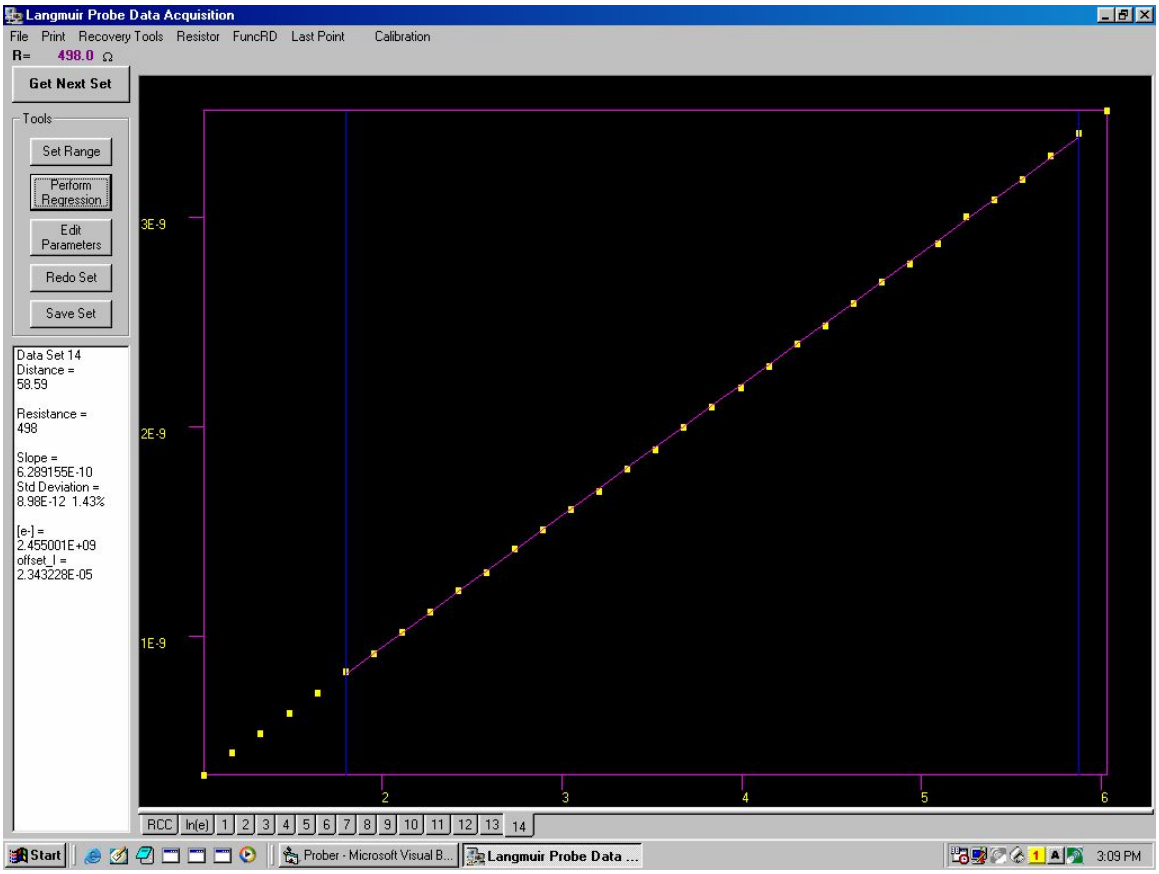

Figure 2.5. A plot of I^2 vs. V_p from the probe program. The slope yields $[e^-]$ according to equation 2.1. The "Set Range" button allows the operator to draw a line across the linear portion of these data. The "Perform Regression" button then can be pressed to calculate the $[e^-]$.

In the inset, figure 2.6, shows the slow decay of electron density upstream of the reactant port, which can be attributed to a combination of ambipolar diffusion of electrons and H_3^+ to the walls of the flow tube, and the slow recombination of H_3^+ ions. The upward curvature of the 1/[e^-] data after the recombination regime occurs because at lower electron densities, ambipolar diffusion begins to compete with the recombination process for [e^-] decay. These studies were repeated at temperatures ranging from 80-600 K. All recombination coefficients are accurate at 300 K to within ± 15%, and to within ± 20% at all other temperatures.

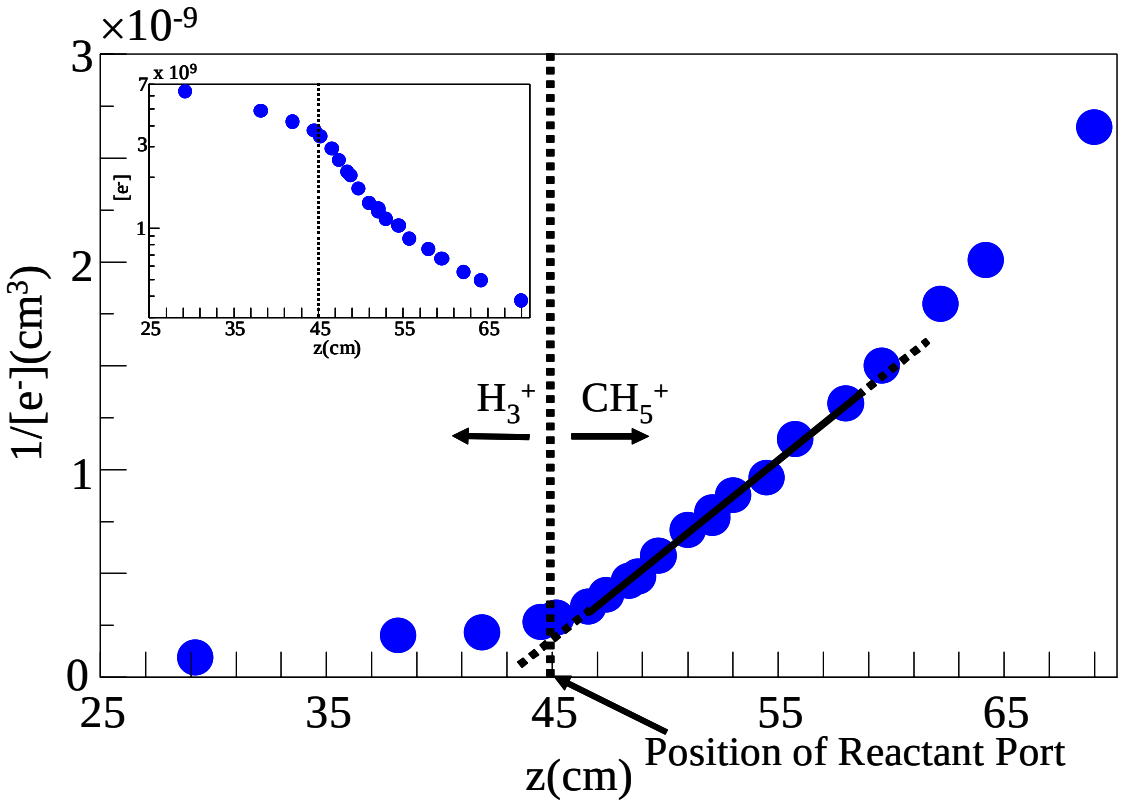

Figure 2.6. A plot of the $[e^-]^{-1}$ vs distance, z, down the flow tube for CH_5^+/e^- DR. The inset shows the electron density decay on a ln-linear plot. In ~1 cm, the proton transfer reaction converts the plasma from a H_3^+/e^- plasma into a rapidly recombining plasma of CH_5^+/e^-. The upward deviation from linearity at 63 cm indicates where, at low electron densities, diffusion begins to compete with recombination for [e^-] decay.

Mass spectra are obtained using a quadrupole mass spectrometer located at the downstream end of the flow tube and are used to identify which ion species are present. Rapidly recombining species are more difficult to detect mass spectrometrically, but several procedures can circumvent this problem. Lowering the electron density (ionization density) slows the neutralizing recombination and allows the ion to be more readily detected. However, if the recombination rate coefficient is very large it is possible to select reaction ports further downstream, i.e., closer to the mass spectrometer, which gives less time for the ions to recombine. A Mathematica model of the kinetics has also been created to confirm the chemistry prior to the addition of specific reactant gas

2.4 MEASURING ION VELOCITIES

Time is one of the most fundamental and complex phenomenon in reality. The timing of a flowing afterglow reaction is no different than a freshman lab experiment measuring the rate constant/coefficient in a beaker. This is because no reactions occur instantaneous, but instead happen over some time frame. Making measurements at specific times during the reaction is crucial for determining the rate at which a reaction proceeds. Unlike a simple beaker, a flowing afterglow's time is also a spatial dimension axial in the flow tube. At a particular position along the flow tube, time of the reaction is dependent solely on the velocity of the flow, and more particularly the velocity of the ions and electrons. Due to viscous drag, the flow of ions down a tube follows a radial profile of axial velocity where the slowest ions are at the wall of the tube. In the absence

of ionic reactions, the ion/electron radial concentration is a Bessel function. Ambipolar diffusion is where the light electrons leave the plasma more rapidly making the plasma positive. This creates an ambipolar field, which accelerates the ions out and slows the electron loss to make the ion and electron losses equal. However, ambipolar diffusion is slow compared to dissociative recombination at ionization densities $>10^7$ cm^{-3}, and flow tube pressures above 1.5 Torr, see figure 2.7. At lower ionization densities, the plasma Debye length gets large so that the electrons interact with the walls and free diffusion becomes dominant i.e., plasma behavior breaks down. The ambipolar diffusion time constant τ_D was measured from to be 0.0469 s for a H_3^+/e^- plasma with flow of helium at 16 standard liter per minute (slm) and a flow tube pressure of 1.5 Torr. Note that the τ_D for diffusion is much larger for H_3^+ than that of most molecular ions studied due to its smaller mass.

Fortunately, the ion velocity can be measured with the Langmuir probe very accurately. Measuring the velocity of the ions is simply a matter of perturbing the flowing plasma. The Opthos (MPG-4M) microwave generator used for plasma generation has an oscillation mode where it can be turned on and off at a certain frequency. A constant positive voltage is applied to the probe and the output voltage from the probe is monitored on an oscilloscope, figure 2.8.

The perturbation from the microwave generator and externally triggers the oscilloscope. An additional microwave cavity upstream of the pulsed cavity maintains a background ionization density. This microwave cavity only supplies a negligible amount of ionization to the flow, and is used as an ignition source because when the power is cycled off, the plasma can fail to reignite. Essentially, one can compare the perturbation to a plug of plasma traveling down the tube. The perturbation is seen on the oscilloscope as the microwave generator is cycled off, indicated by the downward pointing arrow on the trace at the first division of time from the left, figure 2.8.

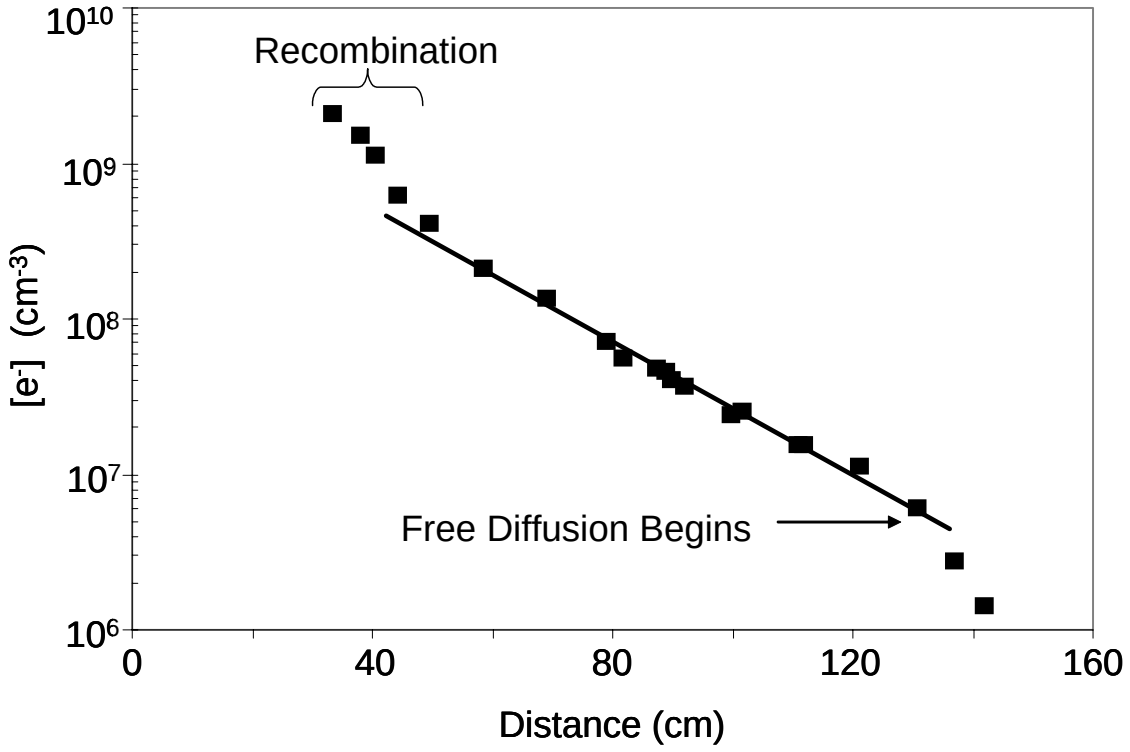

Figure 2.7. The ionization loss due to ambipolar diffusion and slow recombination of a H_3^+/e^- plasma down the entire length of the flow tube. Note that recombination dominates over diffusion at large $[e^-]$ and free diffusion over recombination for small $[e^-]$.

The power off cycle (P_{OFF}) then takes 3.575 ms to register on the probe, which is indicated by the upward pointing arrow on the trace. In figure 2.8., ground is set on the centered x-axis, so when the negative electrons are attracted to the probe the voltage drops negative, below ground. Although the frequency pulse is a square-wave the oscilloscope's trace is not.

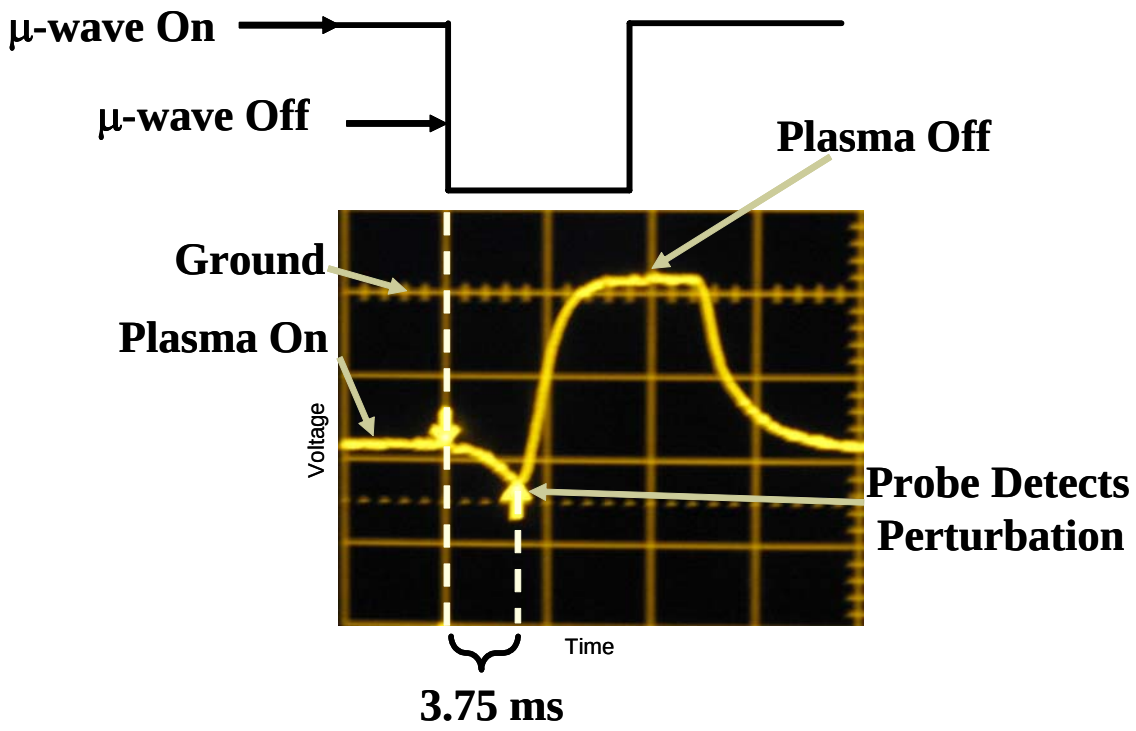

Figure 2.8. This oscilloscope trace shows a large perturbation oscillation of the plasma used to determine the velocity of the ions and electrons down the flow tube.

This is due to ambipolar diffusion of ions and electrons, which distorts the leading and trialing edges of the trace. The time for the initial voltage increase (P_{OFF}) and following decrease (P_{ON}) can both be used as a reference to determine the velocity. The velocities obtained from these two times are usually very similar, see figure 2.9. These two times are measured at various positions along the flow tube axis. A plot of the

distance vs. time gives a linear line and the slope of this line is the equivalent to the average velocity of the ions, figure 2.9.

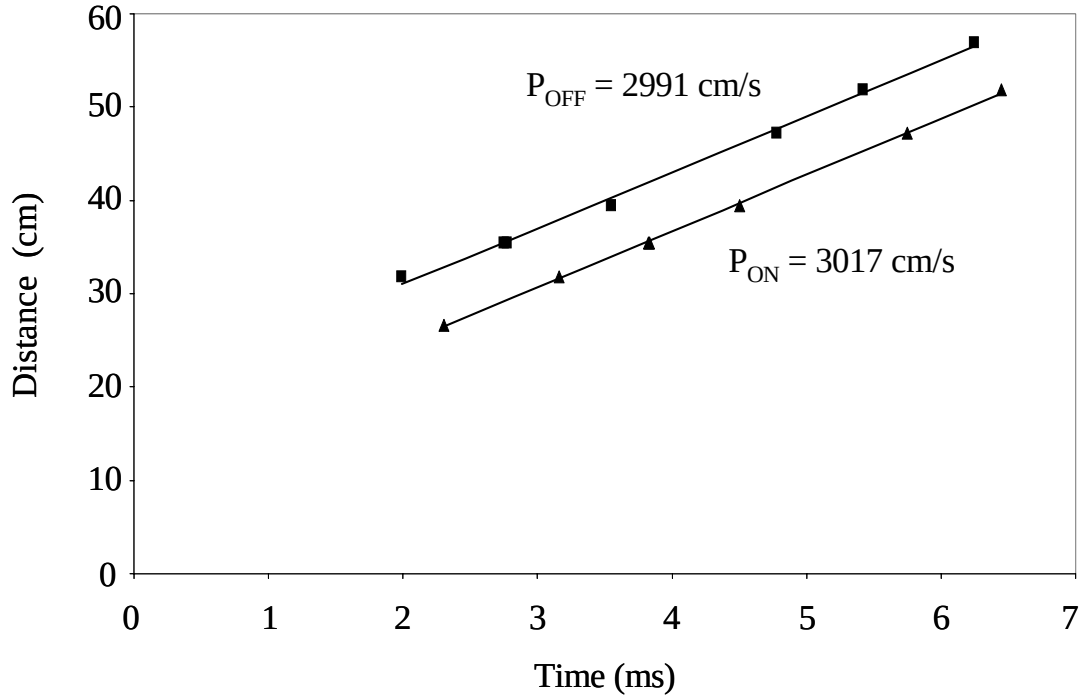

Figure 2.9. An example of a plot of the distance vs. time data obtained at 300 K for a 16 slm He flowing plasma at a flow tube pressure of 3 Torr. The squares represent the first time where the probe first detects the plasma is off and the triangles represent time when probe detects the plasma is cycled back on.

The average velocity of the neutrals and ions depend on three factors; the temperature, pressure, and the flow rate of the buffer gas. In the figure 2.10, the velocity is plotted as a function of temperature and for a series of flow tube pressures with a constant flow rate of 16 slm. From these data, ion velocities can also be extracted at different temperature while keeping the helium number density constant, [He] = 6.5×10^{16} cm^{-3}, and adjusting the flow tube pressure.

The trend line fits for these velocity data at constant pressure are useful for obtaining velocities at various temperatures. In Table 2.1, the fits are mostly 2nd order polynomial trend fits, except for the outer two pressures of 1 and 3 Torr which are linear regression fits.

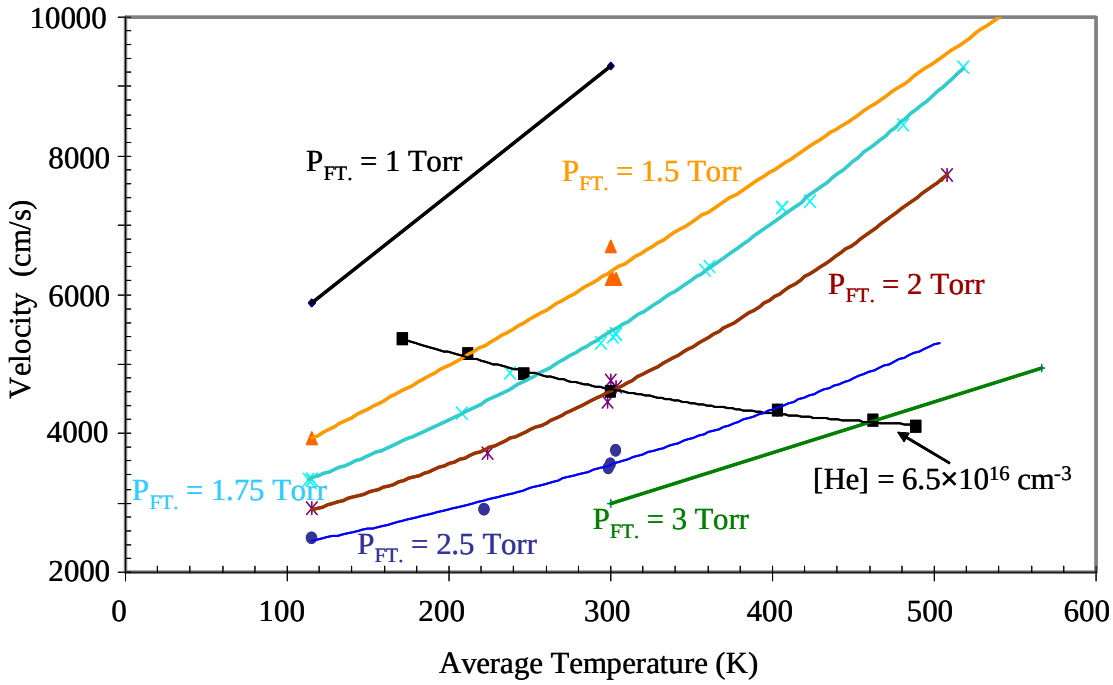

Figure 2.10. Plots of the measured plasma velocities at various temperatures and pressures. The squares correspond to the velocities of the flow while keeping the helium number density constant.

Table 2.1. The trend line fits for the velocity data (y) at constant pressures and constant flow rates of 16 slm as a function of temperature (x).

Flow Tube Pressure	Trend Line Fit
1 Torr	$y = 18.406x + 3768.7$
1.5 Torr	$y = 0.0054x^2 + 10.765x + 2616.6$
1.75 Torr	$y = 0.0157x^2 + 4.4631x + 2741$
2 Torr	$y = 0.0147x^2 + 3.1062x + 2351.2$
2.5 Torr	$y = 0.007x^2 + 3.0361x + 2012.5$
3 Torr	$y = 7.3365x + 787.56$
Various Pressures at Constant Helium Number Density [He] = 6.5×10^{16} cm^{-3}	$y = 0.0091x^2 - 9.8229x + 6769.4$

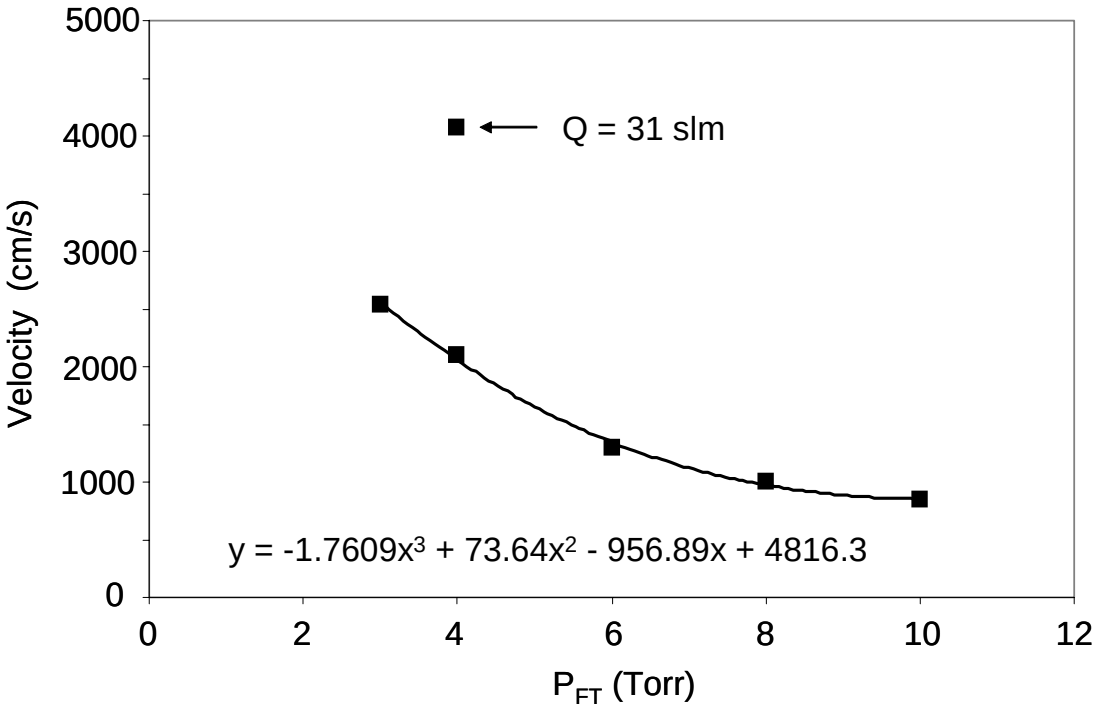

Figure 2.11. A plot of measured plasma velocities at elevated flow tube pressures (P_{FT}) with a constant helium buffer gas flow rate (Q) of 16 slm at 300 K. The 3rd order polynomial fit is given for determining velocities at intermediate pressures. In addition, a velocity measurement at 300 K with Q = 31 slm at a flow tube pressure of 4 Torr is plotted.

2.5 LANGMUIR PROBE PROGRAM

There are 2 computers involved in the Langmuir probe data collection. They will be referred to as the "data acquisition computer", (Zenith 386-SX), and the "Gateway computer", (Gateway E-4200). The data acquisition computer sends the voltage supply the voltage ramp command requested by the Langmuir probe program. The data acquisition computer also receives the return voltages which are converted into digital data by the analog to digital converter, (Keithley A/D). The data acquisition computer then sends the return voltages to the Gateway computer. The Gateway computer runs the main Langmuir probe program to analyze the data on the fly.

To initialize the data acquisition computer, the first command is to initialize the Keithley A/D converter by typing "kinit" and enter. The computer then requests the power to be turned on to the Keithley at this time. After this has been completed, then the Keithley kernel must be loaded by typing "kload" and enter. The final step is to load the sub-routine that communicates with the Gateway computer, which is accomplished by typing "pol" and enter, a acronym for "Probe Of Langmuir". A gated photon counter (SR 400) is used as the voltage supply for the voltage ramp to the probe and must be on for the program to function properly. The (SR 400) is a multi-function instrument can be used for many applications. The (SR 400) receives the commands from the data acquisition computer to apply a specified positive voltage ramp to the probe. The Keithley then converts the return voltage V_{OUT} to digital information.

The first step for collecting data is to power up the probe amplifier, making sure the three-way toggle switch is the center position. In this position, the circuit is grounded so no voltages can pass to the probe or the amplifier. After this, the three-way toggle

switch can be place in the up position and the probe is then ready to be axially moved downstream to a position of interest. By pressing “Get Next Set” the program pops up a text box for a probe position to be entered. Then hitting “enter” on the keyboard or clicking on the “enter” button will begin the data collection. The program will then send the command to start the voltage ramp to the data acquisition computer.

A program was developed in Visual Basic to assist in the data acquisition. The program can be initialized by selecting the “Prober” icon on the Gateway desktop computer. The play button runs the program, and the first step is to choose a located in which the file can be saved; this is typically a new folder previously set-up with the day’s date beginning with the year, then month and date, i.e. for Feb. 20, 2008 it would be “080220”. The next step is to determine the voltage range, the number of data points, and the beginning and ending distance for the electron density plots, figure 2.5.

The defaults for the program are set as 0, 5, 32, 1, 50, and 100 for the beginning voltage (V), ending voltage (V), number of points, number of cycles, beginning distance and ending distance (cm), respectively. These can be changed at the beginning or during the experiment by pressing the “edit parameters” button. Note, the program will stall here if the data acquisition computer has not already been initialized.

2.6 SELECTING THE RESISTOR VALUE FOR THE LANGMUIR PROBE

The program does not automatically pick a resistor value on the input to the amplifier. This must be done by selecting the tab “Resistor” and choosing 1 of 6 available resistors, depending on the ionization density to be studied. The low value

resistors 20, 100, and 500 Ω are used for high ionization densities, (10^{11} to 10^{9} cm^{-3}), and for low ionization densities, (10^{9} to 10^{7} cm^{-3}), 2000, 10000 and 50000 Ω can be used, and all resistors have an accuracy of ± 5%. The resistor value of 500 Ω is used more often because it provides excellent probe characteristics for performing typical recombination experiments where electron number densities are in the range of 1×10^{8} to 1×10^{10} cm^{-3}. Saturating the amplifier by choosing too high of resistor should be avoided. This saturation would be seen in the figure 2.5 when the typically diagonal linear points, as shown, reach the top of the plot and run horizontally across the rest of the plot. Conversely, when the electron number densities are too small for a resistor, the points in figure 2.5 begin to scatter and the digitization becomes visible.

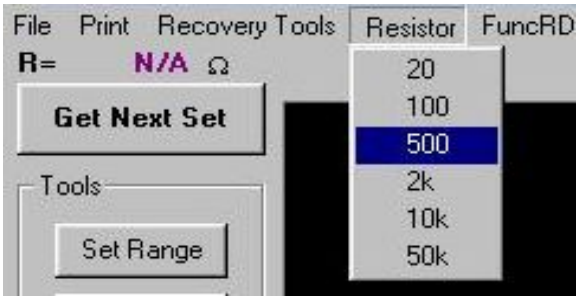

Figure 2.12. The resistor tab allows the user to select one of the six available resistor values on the amplifier. A resistor value of 500 Ω has been selected here. Note that the program only sets this resistance for the [e^{-}] calculation, and that the resistor switch on the amplifier must also be physically moved to a desired resistor value, figure 2.4.

Although initially the linear regression performed on these scatter points tend to give an accurate value for the electron density, when the data becomes too scattered it is becomes necessary to change to a higher resistor value. Even though changing the

resistors values should give the same electron number density, this is not always the case. Small changes in the electron number densities when using different resistor values have been observed, but the errors are typically less than 10%. However, this offset is constant, and can be corrected during the analysis. This offset can probably be fixed if the resistor values were measured again and any drift in the resistance included in the program's calculations.

2.7 CLEANING THE LANGMUIR PROBE

The very first step prior to heating the probe is to check its position. Caution must be taken here because in some plasmas, i.e. O_2^+, heating the probe in these conditions can damage it, even causing it to be burned away. Bringing the probe all of the way upstream into a $He^{+/}He_2^+$ or Ar^+ plasma is recommended for every cleaning. This is very important because heating the probe to ensure that it is clean is performed prior to every measurement. The high voltage power supply is place at a negative 0.13 kV to achieve this heating and cleaning. The three-way toggle switch is pressed down for ~5 seconds before every measurement to apply this -130 V to the probe. The 5 s is typically all that is needed to properly clean the Langmuir Probe. However, consecutive cleanings can be performed for longer times if sticky gases are used and the probe becomes very contaminated.

CHAPTER 3

FLOWING AFTERGLOW STUDIES OF THE TEMPERATURE DEPENDENCIES FOR DISSOCIATIVE RECOMBINATION OF O_2^+, CH_5^+, $C_2H_5^+$, AND $C_6H_7^+$ WITH ELECTRONS[1]

[1]McLain, J. L., Poterya, V., Molek, C. D., Babcock, L. M., Adams, N. G. J. Phys. Chem. A., 2004, 108(32), 6704-6708. Reprinted here with permission of publisher.

3.1 ABSTRACT

A temperature-variable flowing afterglow with an electrostatic Langmuir probe has been used to determine the rate coefficients, α_e, for the recombination of a series of molecular ions with electrons. The α_e for O_2^+, CH_5^+, $C_2H_5^+$, and $C_6H_7^+$ have been determined at temperatures ranging from 80 to 600 K. Data for O_2^+ over the temperature range of 100-500 K establish a single-power law dependence, which is consistent with previous data in this temperature range. The hydrocarbon data show that the α_e are large at room temperature, being 1.1×10^{-6}, 1.2×10^{-6}, and 2.4×10^{-6} cm^3 s^{-1} for CH_5^+, $C_2H_5^+$, and $C_6H_7^+$, respectively, and exhibit significant dependencies on temperature consistent with theoretical models based on the direct and indirect mechanisms. The change between these two dependencies occurs at a temperature of ~300 K. The dissociative recombination of these ions is significant to molecular synthesis in interstellar clouds and the ionosphere of Titan, which is to be probed by the NASA Huygens-Cassini spacecraft that reaches the Saturnian system in July 2004. The relevance of the present data to these media is briefly discussed.

3.2 INTRODUCTION

Dissociative electron–ion recombination is the dominant mechanism for decay of ionization in many plasmas.[1, 2] Electron-ion recombination, recently reviewed by Adams and coworkers[3], shows that majority of recombination rate coefficients (α_e) have been obtained at room temperature and only in cases such as Ne_2^+, Ar_2^+, Kr_2^+, Xe_2^+, NO^+, N_2^+, $H_3O^+(H_2O)_x$, (where x is 1-5), $NH_4^+(NH_4)_x$, (where x is 1-4), $N_2^+ \cdot N_2$, $CO^+ \cdot CO$, $CO^+ \cdot (CO)_2$, $O_2^+ \cdot O_2$, H_3^+, O_2^+, N_2H^+, and HCO^+, has temperature dependent information been obtained.[3-6] Generally though, this information is not sufficiently detailed for temperature dependencies to be deduced. This is unfortunate, since mechanistic information can be obtained from such data. Also temperature dependent data for hydrocarbon ions are critical in modeling the chemistry of the interstellar medium[7] and the Titan ionosphere.[8] To alleviate these problems, temperature dependencies have been determined for hydrocarbon ions of varying complexity (CH_5^+, $C_2H_5^+$, and $C_6H_7^+$ protonated benzene). Early theories of Bates[9] and Bardsley[1, 10] predicted temperature dependencies of $T_e^{-0.5}$ and $T_e^{-1.5}$ for the direct and indirect processes, respectively, where T_e is the electron temperature.

The direct and indirect processes both involve a doubly excited dissociating state of the neutral molecule. The direct mechanism, which can be represented for CH_5^+ by;

$$e^- + CH_5^+ \leftrightarrow CH_5^{**} \rightarrow \text{neutral products} \qquad (3.1)$$

proceeds with the electron being captured directly onto a repulsive, dissociative potential curve of the excited neutralized ion. This is a dielectronic capture, where the recombining electron excites an electron in the ion, and this is resonantly captured with

the incident electron to form the doubly excited neutral repulsive state CH_5^{**}. This state can initially autoionize back to the reactants, but as the products start to separate along the repulsive curve, the energy is converted from potential energy into kinetic energy of separation, soon making autoionization energetically unfavorable and dissociation inevitable.[3]

The indirect process proceeds through an additional intermediate step corresponding to a radiationless electron capture into a Rydberg level CH_5^*, e.g.,

$$e^- + CH_5^+ \leftrightarrow CH_5^* \leftrightarrow CH_5^{**} \rightarrow \text{neutral products} \qquad (3.2)$$

where the binding distance between the electron and the CH_5^+ core is large. This state undergoes a second radiationless transition to the same repulsive state as in the direct process, CH_5^{**}, which then dissociates. Recently, theoretical effort has been concentrated on calculating potential curves for individual systems and determining the probabilities of transitions at curve crossings.[11, 12] Note though that recent theories have included quantum tunneling,[13] so that the absence of a curve crossing does not necessary preclude rapid recombination.[14] Detailed approaches can, at present, only be applied to systems with up to about four atoms and have not been used for the hydrocarbon systems under consideration here. Fortunately, and surprisingly in the present study, the temperature dependencies are consistent with the simpler direct and indirect theoretical approaches as discussed below. The simple mechanistic behavior of these recombinations has enabled generalizations to be made about the recombination coefficients and their temperature

dependence to facilitate the modeling of interstellar molecular clouds and the Titan ionosphere.

3.3 EXPERIMENT

The measurements were made using a variable temperature flowing afterglow apparatus equipped with an axially movable Langmuir probe (VT-FALP). The apparatus has an available temperature range of 80–600 K.

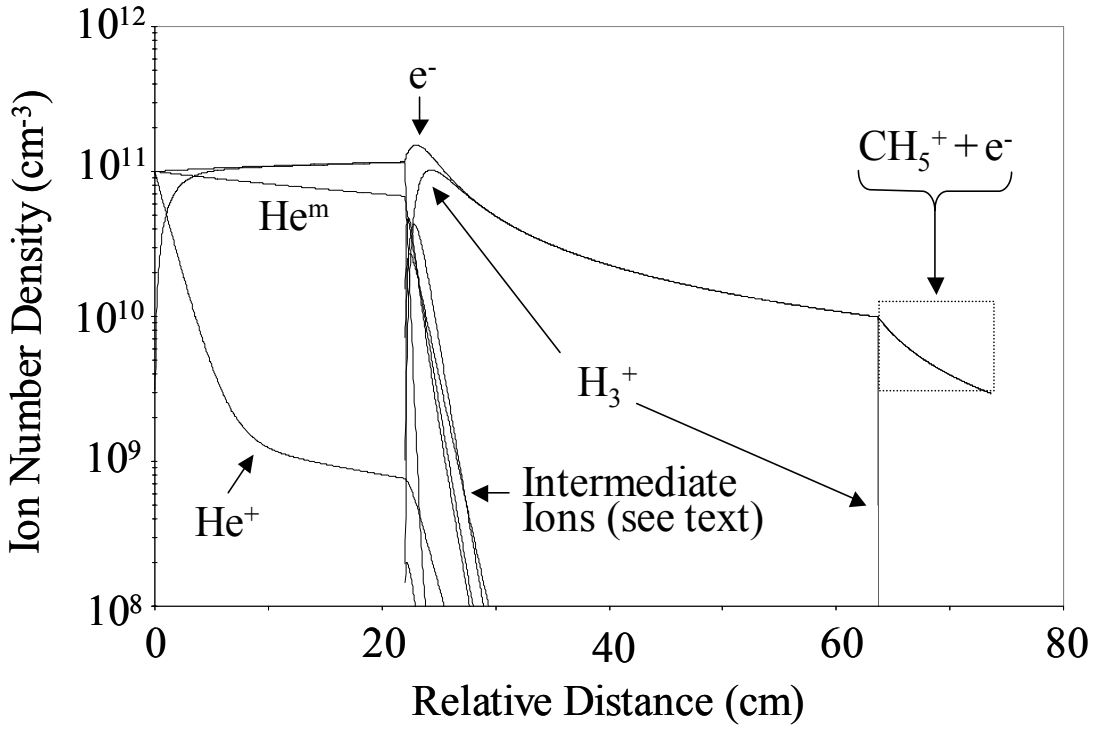

Figure 3.1. A Mathematica model of the ion chemistry occurring as a function of distance along the flow tube for generation of CH_5^+ ions. The inset box is where CH_5^+ recombination occurs, and is where the measurements of electron density (Figure 3.2) are performed to determine α_e. The α_e value for H_3^+ recombination used in the model was 1.10×10^{-7} cm^3 s^{-1}; larger or smaller literature values of this controversial recombination

only slightly affects the ionization density at point where the hydrocarbons are added to the flow.[15]

Table 3.1. Literature rate constants (in cm^3s^{-1}) used in the kinetic model.[16]

Reactant Ion	Reactant Neutral	Product Ion	Reaction Rate Coefficient (300 K)
He^+	He + He	He_2^+	1.00×10^{-31}
He^+	Ar	Ar^+	1.00×10^{-13}
He^+	H_2	(17%) H_2^+	1.00×10^{-13}
		(83%) H^+	
He^m	Ar	Ar^+	7.04×10^{-11}
He_2^+	Ar	Ar^+	2.00×10^{-10}
He_2^+	H_2	He_2H^+	5.30×10^{-10}
Ar^+	H_2	ArH^+	8.90×10^{-10}
H_2^+	Ar	ArH^+	2.10×10^{-9}
H^+	H_2 + He	H_3^+	1.50×10^{-29}
H_2^+	H_2	H_3^+	2.00×10^{-9}
ArH^+	H_2	H_3^+	6.30×10^{-10}
He_2H^+	H_2	H_3^+	3.00×10^{-10}
H_3^+	CH_4	CH_5^+	2.30×10^{-9}
CH_5^+	$CH_4 + CH_4$	$CH_5^+ \cdot CH4$	8.00×10^{-30}
H_3^+	C_2H_6	$C_2H_5^+$	2.40×10^{-9}
$C_2H_5^+$	C_2H_6	Products	4.00×10^{-11}
H_3^+	C_6H_6	$C_6H_7^+$	3.00×10^{-9}
$C_6H_7^+$	C_6H_6	N/A[a]	N/A
H_3^+	e^-	N/A	1.10×10^{-7}

[a] N/A inidicates not available

This type of technique has been described in detail previously[17, 18] and will therefore be only briefly described here. A microwave discharge was used to create ionization in a flowing helium carrier gas (at about 2 Torr) generating helium cations He^+, helium metastables He^m, and electrons. At this pressure, helium cations are converting rapidly to He_2^+ by ternary association.[19] Hydrogen was then injected into the afterglow of the discharge and this reacted with He_2^+ and He^m to give H_3^+ as the dominant ion. The ion

chemistry was verified with a downstream quadrupole mass spectrometer, and supported by detailed models (Figure 3.1) of the ion chemistry involving numerically solving the differential rate equations of this system. The reaction rate coefficients used in the models are given in Table 3.1.[16, 19] Argon was often added upstream to destroy the helium metastables, and through this process several intermediate ions are created. These ions correspond to the concentrations, in Figure 3.1, that become negligible as H_3^+ becomes dominant. The H_3^+ concentration then tracks the electron density until the point at which, in this case, CH_4 is added.

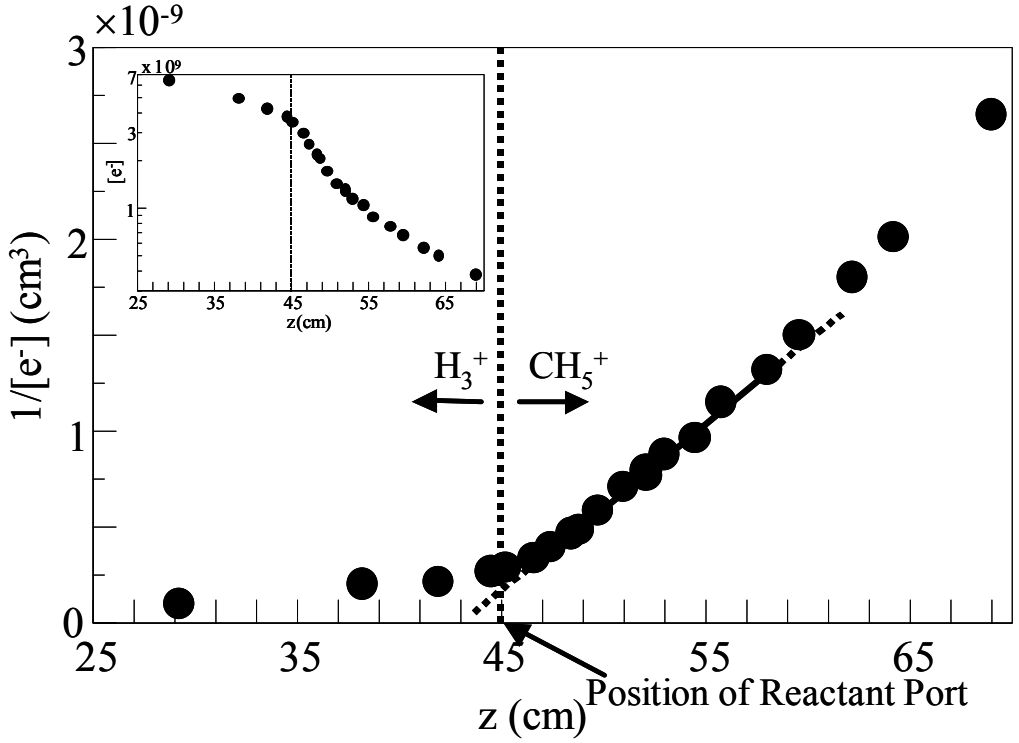

Figure 3.2. A plot of $1/[e^-]$ vs. distance, z, for the electron-ion recombination of CH_5^+ used to determine the recombination rate coefficient (α_e) in conjunction with equation (7). The Reactant Port, where the hydrocarbons enter the flow, is identified by the vertical dotted line and the arrows point to the region where either H_3^+ or CH_5^+ ions dominate. The inset $[e^-]$ vs. distance shows the ln $[e^-]$ variation along the length of the flow tube.

The hydrocarbon gases and vapors (CH_4, C_2H_6, and C_6H_6) were introduced individually into the flow through one of several injector ports positioned along the flow tube. The model (Figure 3.1) confirms that the hydrocarbons were added where H_3^+ was the dominant cation. H_3^+ is known to react rapidly with these neutral hydrocarbons by the proton transfers (dissociative in the case of the C_2H_6 reaction),[20]

$$H_3^+ + CH_4 \rightarrow CH_5^+ + H_2 \quad (3.3)$$

$$H_3^+ + C_2H_6 \rightarrow C_2H_5^+ + 2H_2 \quad (3.4)$$

$$H_3^+ + C_6H_6 \rightarrow C_6H_7^+ + H_2 \quad (3.5)$$

and then the product ions begin to recombine with electrons. Secondary reactions in these systems such as three-body association of the type;

$$CH_5^+ + CH_4 + He \rightarrow CH_5^+ \cdot CH_4 + He \quad (3.6)$$

were also included in the modeling to confirm that only the recombining ion of interest was present. The electron density, [e-], was determined as a function of position along the flow tube, using a Langmuir probe (25 μm diameter, 4mm long) operating in the orbital limited region.[21] Pressures were used that were high enough to inhibit diffusion, thus making recombination the only significant loss process. This allowed a simpler analysis[18] with a dependence of $[e^-]$ on axial position (z) of the form;

$$\frac{1}{[e^-]_{t,z}} - \frac{1}{[e^-]_0} = \alpha_e \frac{z}{v} \quad (3.7)$$

where *v* is the ion velocity and *z* is the axial position along the flow tube. This method of analysis was used for all cases presented in this study; an example of data for the recombination of CH_5^+ is presented in Figure 3.2. In the inset, the slow decay of electron density upstream of the hydrocarbon addition point can be attributed to a combination of ambipolar diffusion of electrons and H_3^+ to the walls of the flow tube, and slow recombination of H_3^+ ions.

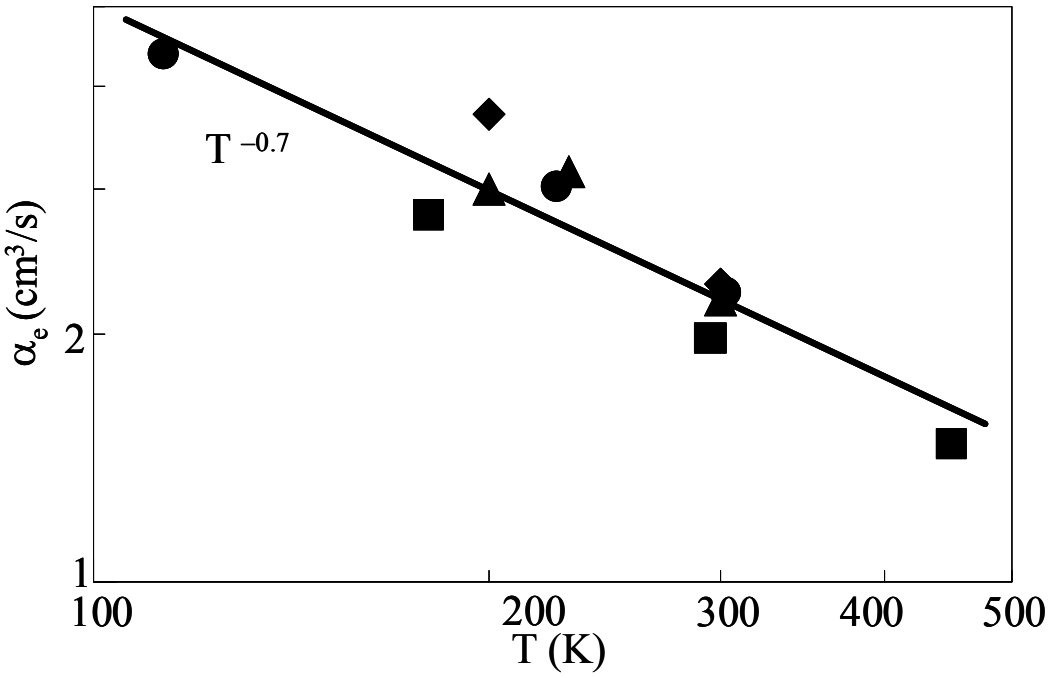

Figure 3.3. A ln-ln plot of α_e vs. temperature for O_2^+ dissociative recombination with electrons. The circles indicate the present data and the squares[5], diamonds[22], and triangles[23] represent previous data in the literature.

Table 3.2. Measured recombination coefficients of O_2^+ ions with electrons. x is the power law index for the temperature dependence, T^{-x}

$\alpha_e(cm^3s^{-1})$ at 300 K	x	Temp. (K)	Method	Ref.
$2.24\pm0.3 \times 10^{-7}$	0.7	100-500	FALP	Present data
$1.95\pm0.2 \times 10^{-7}$	0.7	300-1200	μWA-MS[a]	5
1.95×10^{-7}	0.7	200-600	FALP	18
1.95×10^{-7}	0.66	200-5000	Trap[b]	19

[a] Microwave Afterglow-Mass Spectrometer, [b] Ion Trap

The upward curvature of the $1/[e^-]$ data, after the recombination regime, occurs because at lower electron densities diffusion dominates recombination as the process for $[e^-]$ decay. By performing a linear least squares fit on this plot in the region where recombination is dominant, the recombination rate coefficient (α_e) can be evaluated using equation 7.[3] All recombination coefficients are accurate at 300 K to within ± 15%, and ± 20% at all other temperatures.

3.4 RESULTS AND DISCUSSION

The temperature dependence of the O_2^+ recombination (shown in Figure 3.3) was determined to validate the technique since this recombination has been studied previously in detail.[5, 23-25] Measurements were made at a series of temperatures ranging from 80-500 K to establish the temperature dependence. Table 3.2 lists the present and previous α_e at 300 K and the power of the temperature dependence. Figure 3.3 also shows these data for the recombination of O_2^+, which established an overall temperature dependence. The agreement gives confidence in our technique since the magnitudes of the difference between the various data are within experimental error.

Temperature dependencies for the CH_5^+, $C_2H_5^+$, and $C_6H_7^+$ recombinations are plotted in Figures 3.4-6, respectively. Data for the recombination of hydrocarbon ions was obtained over the same temperature range as for O_2^+ except for $C_6H_7^+$ for which studies were not possible at temperatures below 300 K due to condensation of benzene. The hydrocarbon ions are in their vibrational ground states due to collisional relaxation due to the symmetrical proton transfer.

$$CH_5^{+*} + CH_4 \rightarrow CH_4^* + CH_5^+ \qquad (3.8)$$

The CH_5^+ and $C_2H_5^+$ plots (Figure 3.4-5) show previous α_e data at 300 K that are greater than the 15 % error mentioned earlier. For CH_5^+, α_e data falls neatly within the range of the previous data. To the authors knowledge, detailed modeling of these systems were

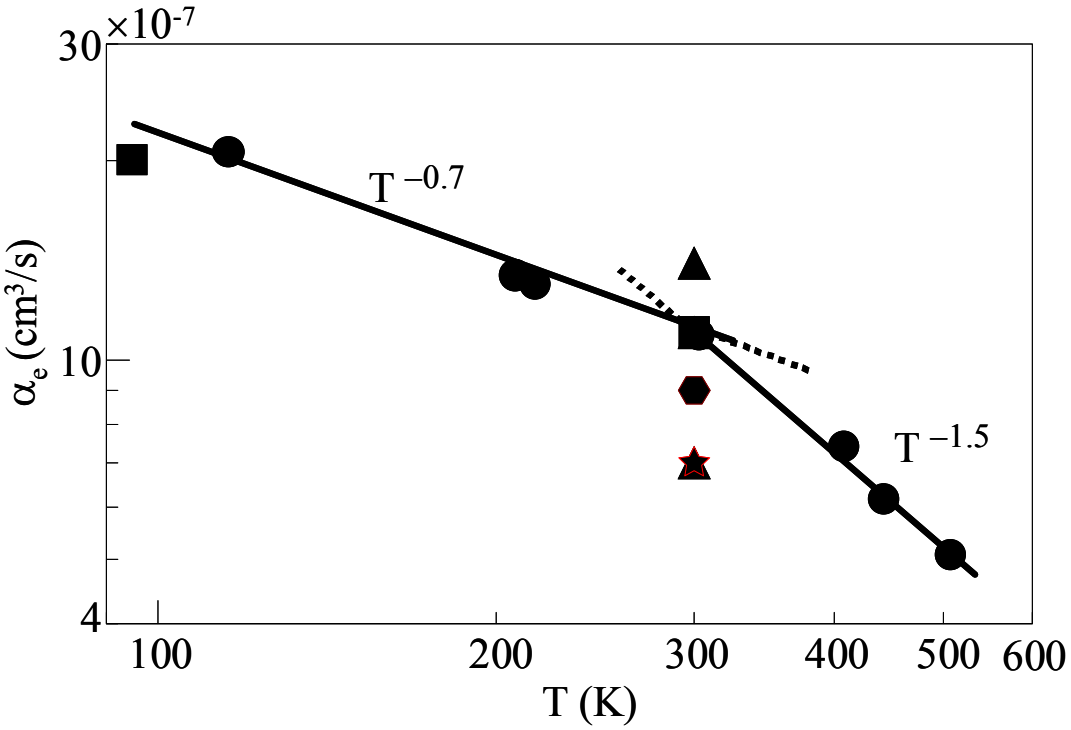

Figure 3.4. A ln-ln plot of α_e vs. temperature for CH_5^+ recombination with the circles indicating the present data and the squares[6], triangles[26], hexagons[27], and stars[28] representing previous data.

not conducted, and the hydrocarbon concentrations used may have been such that precursor ion or cluster ion recombination were occurring to some degree. This was not the case with the present data. All data (see Figures 3.4-6) show similar behavior with higher slopes on ln-ln plot at high temperatures and lower slopes at low temperature.

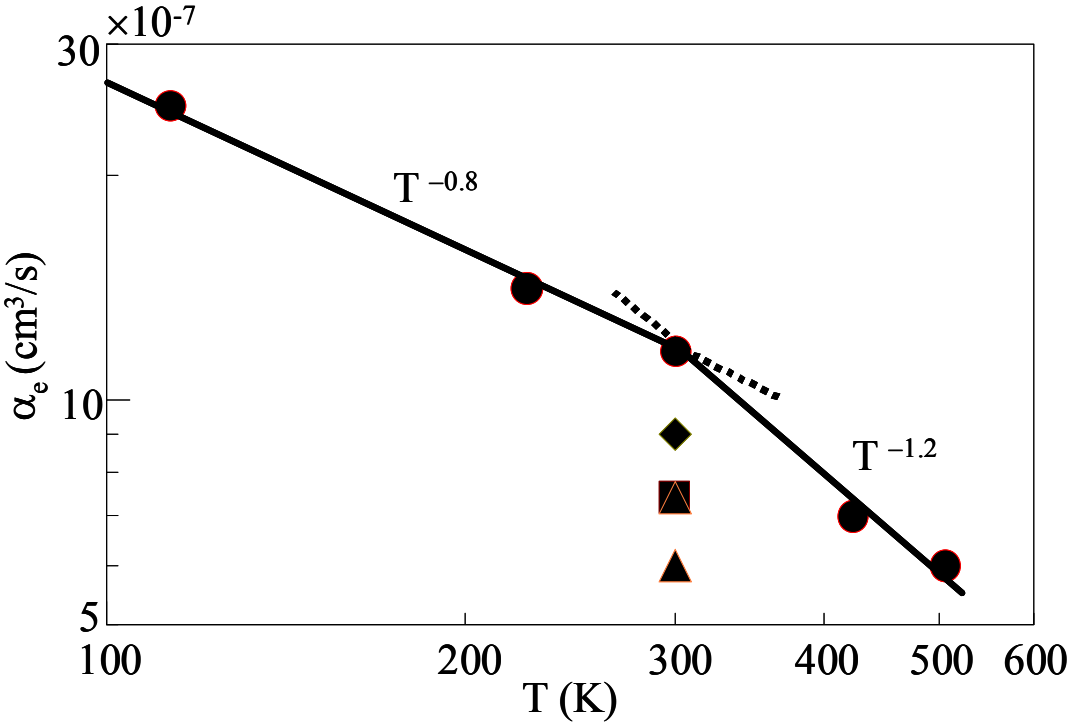

Figure 3.5. A ln-ln plot of α_e vs. temperature for $C_2H_5^+$ recombination with the circles indicating the present experimental data and the square[6], triangles[26], diamonds[27] representing previous 300 K data.

The exponents for these power law dependencies and the α_e at 300 K are listed in Table 3.3. The values for the low temperature region are somewhat above that generally suggested for direct process and that for the high temperature region are approaching that for the indirect process. This is not unexpected since there can be a contribution of the indirect mechanism at low temperatures and the direct mechanism at high temperatures, enhancing and depressing the exponent respectively. Note in Table 3.3 that for CH_5^+ and

$C_2H_5^+$ the change over between the two mechanisms occurs around 300 K, and that for $C_6H_7^+$ is below or at 300 K. Interestingly, no such change occurs for O_2^+ and a dependency around $T^{-0.7}$ has always been obtained over the whole temperature range. In examining the combined data, a pattern emerges with power law dependencies of $T^{-0.7 \text{ to } -0.8}$ at low temperatures and $T^{-1.2 \text{ to } -1.5}$ at high temperatures. There is some consistency of

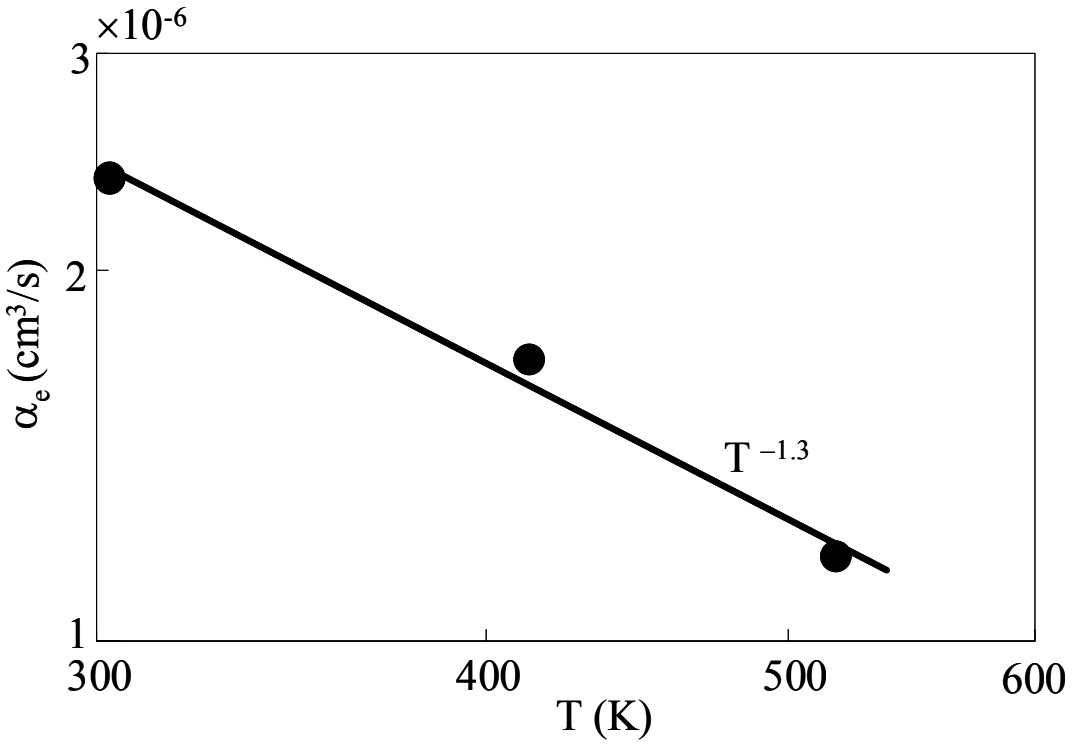

Figure 3.6. A ln-ln plot of α_e vs. temperature for $C_6H_7^+$.

These rate coefficient data with other hydrocarbon data in the literature on the recombination of $C_2H_3^+$ and $C_3H_7^+$ determined using storage rings.[29, 30] Here cross-sections are actually measured and converted into rate coefficients by integrating over a thermal Maxwell Boltzmann speed distribution. For the $C_2H_3^+$ recombination, the

dependence is similar to the present study with $T^{-0.84}$ at low temperatures (50-1000 K) and $T^{-1.38}$ at high temperatures (1000-13000 K), with a break at ~1000 K, somewhat higher than the present study.[30] For the $C_3H_7^+$ recombination,[29] there is a single dependence from 10-1000 K of $T^{-0.68}$.

Table 3.3. Present measured recombination coefficients and temperature dependencies in the low and high temperature regimes for CH_5^+, $C_2H_5^+$, and $C_6H_7^+$ ions. Power Law index (x) in the T^{-x} temperature dependence is also indicated. N/A indicates not available.

		Power Law Index		Change over
Ion	$\alpha_e(cm^3s^{-1})$ at 300 K	Low temp.	High temp.	Temperature (K)
CH_5^+	$1.1\pm0.2 \times 10^{-6}$	0.7	1.5	300
$C_2H_5^+$	$1.2\pm0.2 \times 10^{-6}$	0.8	1.2	300
$C_6H_7^+$	$2.4\pm0.4 \times 10^{-6}$	N/A	1.3	≤300

The $C_3H_7^+$ data is not inconsistent with both the other data on hydrocarbon ions and with the predictions of the direct and indirect mechanisms. The bulk of the present and previous data though gives a dependence slightly steeper than the direct mechanism at low temperatures and slightly less than the indirect mechanism at high temperature. This discussion assumes that the direct and indirect mechanisms are independent, however they are actually coupled with both being accessed in a single recombination. Mixing of these two mechanisms would thus be expected to result in different power law dependencies in the regions where they separately dominate, as is observed. In an early paper[31], Bardsley was not able to determine the relative contributions of the two processes, however, this is automatically done in multichannel quantum defect theory MQDT.[25] To the authors' knowledge, MQDT theory has not been applied to studies involving hydrocarbon ions. In light of the present data, theoretical determinations of the temperature dependencies and of the temperature at which the power law dependence

changes would be valuable. The overall magnitude of α_e for these hydrocarbon ions is relatively similar. There is only a slight increase in the magnitude of α_e between CH_5^+ and $C_2H_5^+$, but as the hydrocarbon complexity increases to $C_6H_7^+$ the recombination rate increases by about a factor of 2.

The ionosphere of Titan has been modeled in the higher altitude region most recently by Fox and Yelle[8] and at lower altitudes by Molina-Cuberos et. Al.[32] In order to model the individual ion densities and the overall ionization/electron density, knowledge of the magnitude of the rate coefficients and their temperature dependencies is required. Fox and Yelle assumed, when there was little experimental data, that the recombination coefficients varied as $(3\text{-}3.5)\times10^{-7}(300/T_e)^{0.5}$ cm^3s^{-1} and Molina-Cuberos et.al. similarly assumed for hydrocarbon ions $(5\text{-}8)\times10^{-7}(300/T_e)^{0.5}cm^3s^{-1}$ (the slightly bigger value assumed is realistic in view of the greater ionic complexity at lower altitudes). It is now necessary for the model calculations to be repeated to take account of the larger values obtained in the present study, which will make a significant difference to the ionization balance at the lower temperatures of the Titan ionosphere. Our generic temperature dependences for hydrocarbon ions would be $(300/T)^{0.7}$ below 300 K and $(300/T)^{1.4}$ above 300 K, with 300 K values of $(1\text{-}2)\times10^{-6}$ cm^3s^{-1}. Thus, at the lowest temperatures in the Titan atmosphere of 100 K the models of Fox and Yelle and Molina-Cuberos would suggest $(5.2–6.1)\times10^{-7}$ cm^3s^{-1} and $(8.7–13.9)\times10^{-7}$ cm^3s^{-1}, respectively, with the present data giving $(23–68)\times10^{-7}$ cm^3s^{-1}.

All of these dependencies are shown in Figure 3.7 where a substantial difference is evident. If the power law dependencies refer to the direct and indirect mechanism then

the changeover might be expected to be related to the temperature at which there is a significant population of vibrationally excited states. Note that for O_2^+ all the data are in the low-temperature regime not inconsistent with the larger vibrational spacing relative to the hydrocarbon ions.

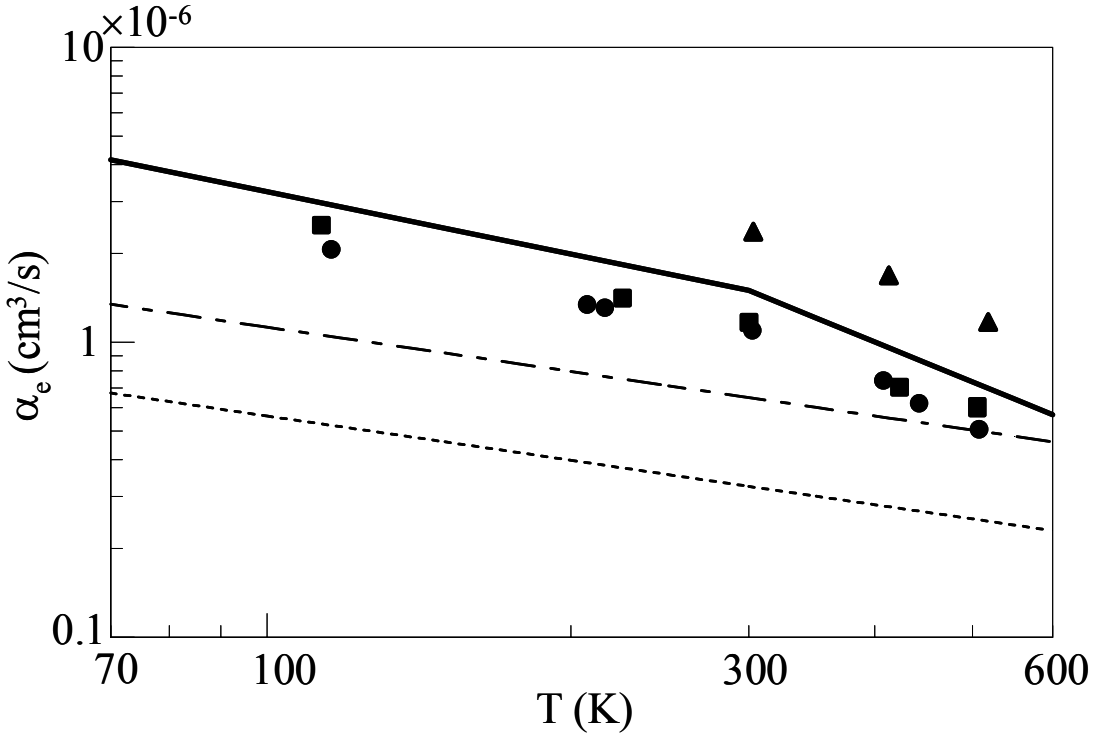

Figure 3.7. A ln-ln plot of α_e vs. temperature for CH_5^+(circles), $C_2H_5^+$(squares), and $C_6H_7^+$(triangles) recombination. The Fox and Yelle model temperature dependence (dotted line), the Molina-Cuberos et.al. model temperature dependence (dot-dash line), and our generic temperature dependence (solid line) are indicated.

However, this does not occur for other small non-hydrocarbon species. For example N_2H^+ shows little temperature dependence over the temperature range 80 to 500 K.[33] However, this may be a special case since there is evidence for quantum tunneling in this recombination,[33, 34] These data indicate important trends for α_e variations with temperature and contain insights into the mechanisms involved.

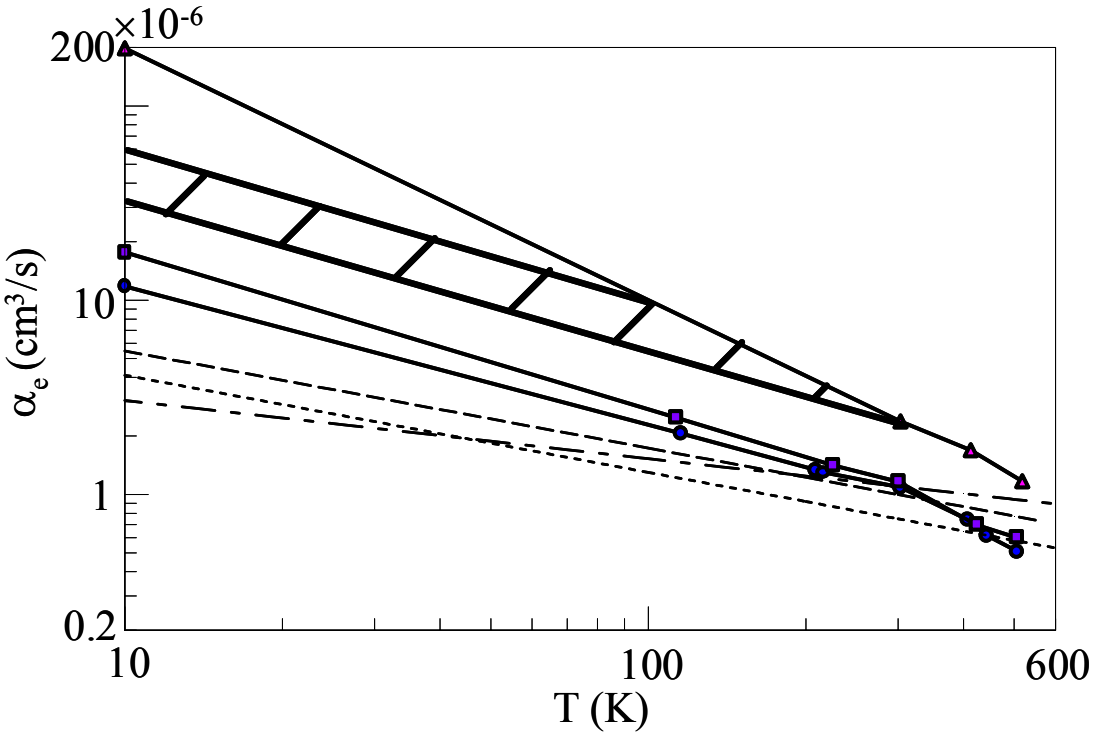

Figure 3.8. A ln-ln plot of α_e vs. temperature for CH_5^+(circles), $C_2H_5^+$(squares), and $C_6H_7^+$(triangles) recombination extrapolated to 10 K, assuming a change over in mechanism between 100-300 K for $C_6H_7^+$. The UMIST[36] temperature dependence for CH_5^+(dot-dash line), $C_2H_5^+$(dotted line), $C_6H_7^+$(dashed line) extrapolated from previous, very limited, data are included.

The recombinations are also significant to interstellar chemistry with the detection of now over 20 hydrocarbon species.[35] The formation of these molecules occur either within the molecular clouds themselves or in the expanding envelopes of old stars.[7] Here, at the lower temperatures of ~10 K, α_e values based on extrapolation of the present data are 1.2×10^{-5} cm^3s^{-1}, 1.8×10^{-5} cm^3s^{-1} for CH_5^+, $C_2H_5^+$, respectively, compared with extrapolation of UMIST data,[36] (usually a single or perhaps 2 data points), which would yield 3.1×10^{-6} cm^3s^{-1}, 4.1×10^{-6} cm^3s^{-1} for CH_5^+, $C_2H_5^+$, respectively. Shown in (Figure 3.8) are the extrapolated temperature dependencies. Figure 3.8 also shows the extrapolated dependence of recombination for $C_6H_7^+$. An assumed change in temperature dependence between 100-300 K was used since it was not possible to observe this for $C_6H_7^+$; this yields a α_e of $(3.0–6.0)\times10^{-5}$ cm^3s^{-1} at 10 K. Assuming no change in the mechanism for $C_6H_7^+$ yields a α_e of 2.0×10^{-4} cm^3s^{-1}, while the UMIST dependence would yield a α_e of 5.5×10^{-6} cm^3s^{-1} at 10 K. The interstellar models need to be recalculated with the new data to make them more realistic.

3.5 CONCLUSIONS

The data presented here imply a generic temperature dependent behavior for electron-ion recombination of hydrocarbon ions, and this is now being extended to other hydrocarbon ions. This is important since such recombinations are relevant to the synthesis of neutral hydrocarbons in the interstellar clouds and the atmospheric chemistry of Titan[8]. In the upper atmosphere, the ions suggested by the Fox and Yelle model are $C_2H_5^+$, CH_5^+ and $HCNH^+$ in order of decreasing abundance and thus the recombination of

the two most abundant ions has been studied here. Determining recombination rate coefficients as a function of temperature will continue with emphasis being placed on more complex organic molecules which exist in interstellar space[35, 37], and extraterrestrial atmospheres[38], such as Titan. The data presented above indicate that these recombination rate coefficients follow a combination of mechanisms. In the absence of detailed theory for these systems the rate coefficients must be measured directly to ensure accurate values for inclusion in the models.

3.6 ACKNOWLEDGEMENTS

Funding under NASA Grant No. NAG5-8951 is gratefully acknowledged.

3.7 REFERENCES

[1] Bardsley, J. N.; Biondi, M. A., Dissociative Recombination. *Adv. At. Mol. Phys.* **1970,** 6, 1-57.

[2] Smith, D.; Adams, N. G., Elementary Interactions between Charged and Neutral Species in Plasmas. *Pure Appl.Chem.* **1984,** 56, 175-188.

[3] Adams, N. G.; Babcock, L. M.; McLain, J. L., Electron-Ion Recombination. In *Encyclopedia of Mass Spectrometry: Theory and Ion Chemistry, Vol.1*, Armentrout, P., Ed. Elsevier: Amsterdam, 2003; Vol. 1, pp 542-555.

[4] Adams, N. G.; Smith, D.; Alge, E., Measurements of Dissociative Recombination Coefficients of H_3^+, HCO^+, N_2H^+ and CH_5^+ at 95 and 300 K using the FALP Apparatus. *J. Chem. Phys.* **1984,** 81, 1778-1784.

[5] Johnsen, R., Microwave Afterglow Measurements of the Dissociative Recombination of Molecular Ions with Electrons. *Int. J. Mass Spectrom. Ion Proc.* **1987,** 81, 67-84.

[6] Adams, N. G.; Smith, D., Laboratory Studies of Dissociative Recombination and Mutual Neutralization and their Relevance to Interstellar Chemistry. In *Rate Coefficients in Astrochemistry*, Millar, T. J.; Williams, D. A., Eds. Kluwer: Dordrecht, 1988; pp 173-92.

[7] Herbst, E., Ion-Molecule Chemistry in Interstellar Clouds: Successes and Problems. *Adv. Gas Phase Ion Chem.* **1998,** 3, 1-47.

[8] Fox, J. L.; Yelle, R. V., Hydrocarbon ions in the ionosphere of Titan. *Geophys. Res. Letts.* **1997,** 24, (17), 2179-2182.

[9] Bates, D. R., Dissociative Recombination. *Phys. Rev.* **1950,** 78, 492-493.

[10] Bardsley, J. N., The Theory of Dissociative Recombination. *J. Phys. B.* **1968,** 1, 365-380.

[11] Talbi, D., *Dissociative Recombination of c-C3H3+*. Kluwer: New York, NY, 2003.

[12] Guberman, S. L., *The Dissociative Recombination of N2+*. Kluwer: New York, NY, 2003.

[13] Bates, D. R., Dissociative Recombination: Crossing and Tunneling Modes. *Adv. Atom. Molec. Opt. Phys.* **1994,** 34, 427-486.

[14] Bell, R. P., *The Tunnel Effect in Chemistry* Chapman and Hall London 1980.

[15] Plasil, R.; Glosik, J.; Poterya, V.; Kudrna, P.; Rusz, J.; Tichy, M.; Pysanenko, A., Advanced Integrated Stationary Afterglow Method for Experimental Study of Recombination of Processes of H_3^+ and D_3^+ Ions with Electrons. *Int. J. Mass Spectrom.* **2002,** 218, 105-130.

[16] Anicich, V., *An Index of the Literature for Bimolecular Gas Phase Cation-Molecule Reaction Kinetics: JPL Publication 03-19*. Jet Propulsion Laboratory: Pasadena, 2003; p 1194.

[17] Smith, D.; Adams, N. G., Studies of Plasma Reaction Processes using a Flowing Afterglow/Langmuir Probe Apparatus. In *Swarms of Ions and Electrons in Gases*, Lindinger, W.; Mark, T. D.; Howorka, F., Eds. Springer-Verlag: Vienna, 1984; pp 284-306.

[18] Adams, N. G.; Smith, D., Flowing Afterglow and SIFT. In *Techniques for the Study of Ion-Molecule Reactions*, Farrar, J. M.; Saunders, J. W. H., Eds. Wiley Interscience: New York, 1988; Vol. 20, pp 165-220.

[19] Ikezoe, Y.; Matsuoka, S.; Takebe, M.; Viggiano, A. A., *Gas Phase Ion-Molecule Reaction Rate Constants through 1986*. Ion Reaction Research Group of the Mass Spectroscopy Society of Japan: Tokyo, 1987.

[20] Milligan, D. B.; Wilson, P. F.; Freeman, C. G.; Meot-Ner, M.; McEwan, M. J., Dissociative Proton Transfer Reactions of H_3^+, N_2H^+ and H_3O^+ with Acyclic, Cyclic and Aromatic Hydrocarbons and Nitrogen Compounds and Astrophysical Implications. *J. Phys. Chem. A* **2002,** 106, 9745-9755.

[21] Swift, J. D.; Schwar, M. J. R., *Electrical Probes for Plasma Diagnostics.* Iliffe: London, 1970.

[22] Alge, E.; Adams, N. G.; Smith, D., Measurements of the Dissociative Recombination Coefficients of O_2^+, NO^+ and NH_4^+ in the Temperature Range 200-600K. *J.Phys.B.* **1983,** 16, 1433-1444.

[23] Walls, F. L.; Dunn, G. H., Measurement of Total Cross Sections for Electron Recombination with NO+ and O2+ using Ion Storage Techniques. *J. Geophys. Res.* **1974,** 79, 1911-1915.

[24] Smith, D.; Goodall, C. V., The Dissociative Recombination Coefficient of O_2^+ Ions with Electrons in the Temperature Range 180-630 K. *Planet.Space Sci.* **1968,** 16, 1177-1188.

[25] Giusti, A., A Multichannel Quantum Defect Approach to Dissociative Recombination. *J. Phys. B.* **1980,** 13, 3867-3894.

[26] Mitchell, J. B. A.; Rebrion-Rowe, C., The Recombination of Electrons with Complex Molecular Ions. *Int. Rev. Phys. Chem.* **1997,** 16, 201-213.

[27] Gougousi, T.; Golde, M. F.; Johnsen, R., Electron-Ion Recombination Rate Coefficient Measurements in a Flowing Afterglow Plasma. *Chem. Phys. Lett.* **1997,** 265, 399-403.

[28] Lehfaoui, L.; Rebrion-Rowe, C.; Laube, S.; Mitchell, B. A.; Rowe, B. R., The Dissociative Recombination of Hydrocarbon Ions .1. Light Alkanes. *J. Chem. Phys.* **1997,** 106, (13), 5406-5412.

[29] Ehlerding, A.; Arnold, S. T.; Viggiano, A. A.; Kalhori, S.; Semaniak, J.; Derkatch, A. M.; Rosen, S.; af Ugglas, M.; Larsson, M., Rates and Products of the

Dissociative Recombination of $C_3H_7^+$ in Low-Energy Electron Collisions. *J Phys. Chem. A* **2003,** 107, 2179-2184.

[30] Kalhori, S.; Viggiano, A. A.; Arnold, S. T.; Rosen, S.; Semaniak, J.; Derkatch, A. M.; af Ugglas, M.; Larsson, M., Dissociative Recombination of $C_2H_3^+$. *Astron. Astrophys.* **2002,** 391, 1159-1165.

[31] Bardsley, J. N., Configuration Interaction in the Continuum States of Molecules. *J. Phys. B.* **1968,** 1, 349-364.

[32] Molina-Cuberos, G. J.; Lopez-Moreno, J. J.; Rodrigo, R., Chemistry of the glactic cosmic ray induced ionosphere of Titan. *Geophys. Res.* **1999,** 104, 21997-22024.

[33] Poterya, V.; McLain, J. L.; Adams, N. G.; Babcock , L. M., *J Phys. Chem.* **2004**, in preparation.

[34] Butler, J. M.; Babcock, L. M.; Adams, N. G., Effects of Deuteration on Vibrational Excitation in the Products of Electron Recombination of HCO^+ and N_2H^+. *Mol. Phys.* **1997,** 91, 81-90.

[35] McCarthy, M. C.; Thaddeus, P., Microwave and Laser Spectroscopy of Carbon Chains and Rings. *Chem. Soc. Revs.* **2001,** 30, 177-185.

[36] Le Teuff, Y. H.; Millar, T. J.; Markwick, A. J., The UMIST Database for Astrochemistry 1999. *A. & A., Suppl, Series* **2000,** 146, 157-168.

[37] Adams, N. G.; Babcock, L. M.; Ray, N. S., Ionic Processes in Low Temperature Interstellar Molecular Plasmas. In *Atomic Processes in Plasmas*, Schultz, D. R.; Meyer, F. W.; Ownby, F., Eds. AIP: Melville, NY, 2002; pp 182-193.

[38] Fox, J. L.; Yelle, R. V., Hydrocarbon Ions in the Ionosphere of Titan. *Geophys. Res. Letts.* **1997,** 24, 2179-2182.

CHAPTER 4

$C_3H_3^+$ ISOMERS: TEMPERATURE DEPENDENCE OF PRODUCTION IN THE H_3^+ REACTION WITH ALLENE AND LOSS BY DISSOCIATIVE RECOMBINATION WITH ELECTRONS[1]

[1]McLain, J. L., Poterya, V., Jackson, D. M., Adams, N .G., Babcock, L. M. J. Phys. Chem. A., 2005, 109(23), 5119-5123. Reprinted here with permission of publisher.

4.1 ABSTRACT

A technique has been developed to simultaneously determine recombination rate coefficients, α_e, and initial concentrations of ion types that coexist in a flowing afterglow plasma. This was tested using the H_3^+ + allene reaction in which two different $C_3H_3^+$ isomers are produced. Use of an electrostatic Langmuir probe enabled the $C_3H_3^+$ isomer branching ratios for propargyl and cyclic $C_3H_3^+$ from this allene reaction and their Re to be determined over the temperature range 172-489 K. The study showed that the cyclic $C_3H_3^+$ to propargyl $C_3H_3^+$ branching ratios from the allene reaction varied from 50/50 at 172 K to 18/82 at 489 K. Over this temperature range, the α_e for both isomers change only slightly. The room temperature Re values for propargyl and cyclic $C_3H_3^+$ are (1.15 ± 0.2) × 10^{-7} and (8.00 ± 0.1) × $10^{-}7$ cm^3 s^{-1}, respectively. The data are discussed relative to current theories and in relation to fuel-rich flame chemistry, interstellar molecular synthesis, and modeling of Titan's atmosphere.

4.2 INTRODUCTION

A Variable Temperature Flowing Afterglow with an electrostatic Langmuir Probe (VT-FALP) has previously been used in our laboratory to obtain recombination rate coefficients (α_e), including those for a series of hydrocarbon ions relevant to the interstellar medium[1] and Titan's atmosphere[2] i.e. CH_5^+, $C_2H_5^+$, and $C_6H_7^+$ (protonated benzene).[3] In these and all of our previous cases, situations have been chosen where one ion type has been dominantly produced in a proton transfer reaction with H_3^+. However, in the H_3^+ dissociative proton transfer reaction with allene ($H_2C_3H_2$), two isomeric ion types dominate the plasma, propargyl and cyclic $C_3H_3^+$. This reaction has previously been studied by Milligan et al[4] in a Selected Ion Flow Tube (SIFT) at room temperature, where the two isomeric forms of $C_3H_3^+$ were distinguished by their different reactivities with CH_3OH yielding a propargyl/cyclic $C_3H_3^+$ product ratio of 70/30. For flowing afterglow plasmas, we have developed techniques to separately determine the proportions of the two ion types coexisting in the plasma and their α_e values. Techniques have been developed previously by Rebrion-Rowe et al.[5] to determine α_e's for minority ions in flowing afterglow plasmas, but this requires use of a movable mass spectrometer and Langmuir probe. Our technique has been applied to the $C_3H_3^+$ isomers produced in the allene reaction over the temperature range 172 to 489 K. Here, the observed temperature independent behavior of the α_e is inconsistent with early theories of the direct[6] and indirect mechanisms,[7, 8] but does correspond to recombination where it is thought that tunneling is involved, i.e. N_2H^+ and perhaps HCO^+.[9, 10] This behavior is contrary to theoretical calculations of potential curves that have shown that there is a favorable

dissociative curve crossing in the cyclic case implying that the direct mechanism would occur efficiently. No such crossing was predicted for the propargyl form. From an applications point of view, C_3H_4 has been detected mass spectrometrically by Cassini in Titan's upper atmosphere,[11] and this could possibly be allene, since there are only two other stable isomers. The present studies thus have relevance to that atmosphere. Also, the interstellar importance of the production and recombination of the two isomeric forms of $C_3H_3^+$ to form the ubiquitous cyclopropenylidene C_3H_2 in dense molecular clouds[12] as well as a linear form (propadienylidene) is discussed.

4.3 EXPERIMENT

A VT-FALP technique was used for all the present measurements, and this has been described in detail in the literature.[13, 14] Thus, only an overview of the most important features of the technique will be given here. The available temperature range is 100–500 K for these experiments. Helium ions were generated with a microwave discharge creating ionization in a flowing helium carrier gas. Hydrogen was then added to the flow downstream of the discharge to produce a plasma with H_3^+ as the dominant ion by a standard reaction sequence.[3] Detailed models of the ion chemistry have been generated to ensure that H_3^+ was the dominant ion present at the point where allene was injected into the flow and a downstream quadrupole mass filter was used to identify all ions present in the flow. At room temperature, H_3^+ reacts rapidly with allene by the dissociative proton transfer,[4]

$$H_3^+ + C_3H_4 \rightarrow c\text{-}C_3H_3^+ + 2H_2 \quad (4.1a)$$

$$\rightarrow p\text{-}C_3H_3^+ + 2H_2 \quad (4.1b)$$

where c-$C_3H_3^+$ and p-$C_3H_3^+$ are the cyclic and propargyl $C_3H_3^+$ ions, respectively.

The cyclic and the propargyl ions then begin to recombine with electrons simultaneously,

$$c\text{-}C_3H_3^+ + e^- \rightarrow \text{neutral products} \quad (4.2)$$

$$p\text{-}C_3H_3^+ + e^- \rightarrow \text{neutral products} \quad (4.3)$$

The ability to measure the electron density at any point along the reaction coordinate using a Langmuir probe illustrates the beauty and simplicity of this technique (see Figure 4.1), and allows both recombination rate coefficients to be determined.

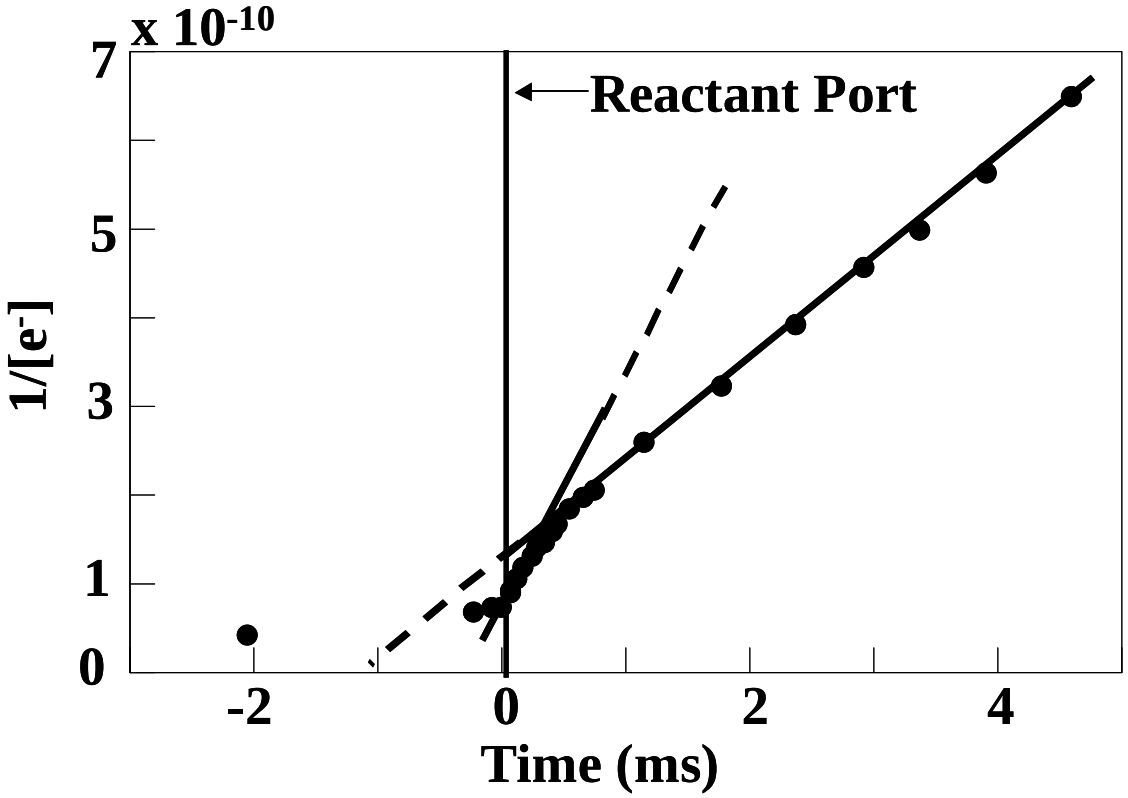

Figure 4.1. A plot of 1/[e^-] vs. time showing the two linear regions caused by the presence of two simultaneously recombining isomers of $C_3H_3^+$ at 300 K. Time zero is where the allene was introduced into the flow and where subsequent recombination of the $C_3H_3^+$ isomers begins.

Techniques have been described previously in detail and used for the recombination of a single ion type.[3, 13, 14] Here, when the loss of a single ion type, x^+, is dominated by recombination, then

$$\frac{d[e^-]}{dt} = -\alpha_e [x^+][e^-] \tag{4.4}$$

where $[e^-]$ is the electron density and $[x^+]$ is the ion density. For a quasi-neutral plasma, $[e^-] = [x^+]$ equation 4.4 can be integrated to yield:

$$\frac{1}{[e^-]_{t,z}} - \frac{1}{[e^-]_0} = \alpha_e \frac{z}{v} \tag{4.5}$$

where v is the ion velocity. Thus a linear plot of $1/[e^-]_z$ versus axial position (z) would be expected, enabling the α_e to be determined. However, in Figure 4.1, the electron density profile is not linear but reveals two approximately linear regions indicating the presence of two recombining ion types and further analysis for these particular recombinations was required. Since the recombination of both ions is occurring simultaneously, equation 4.4 is not valid and numerical integration of the kinetic differential rate equation for the recombinations must be used to obtain an accurate determination of the individual α_e values. For this situation, the kinetic differential rate equation is:

$$\frac{d[e^-]}{dt} = -\alpha_{e,p}[p^+][e^-] - \alpha_{e,c}[c^+][e^-] \tag{4.6}$$

where $[p^+]$ and $[c^+]$ are the densities, and $\alpha_{e,p}$ and $\alpha_{e,c}$ are the recombination rate coefficients for the propargyl and cyclic isomers, respectively. Numerically integrating

this equation to fit the experimental data requires that the initial ion product ratio and the recombination rate coefficients ($\alpha_{e,p}$) and ($\alpha_{e,c}$) are treated as unknowns. This analysis is only possible because of the charge neutrality:

$$[c^+]+[p^+]=[e^-] \tag{4.7}$$

The three unknowns were varied in the numeric integration of equation 4.6 to optimize the fit to the [e^-] versus time experimental data. The best fit of this model to the experimental data is shown in Figure 4.2.

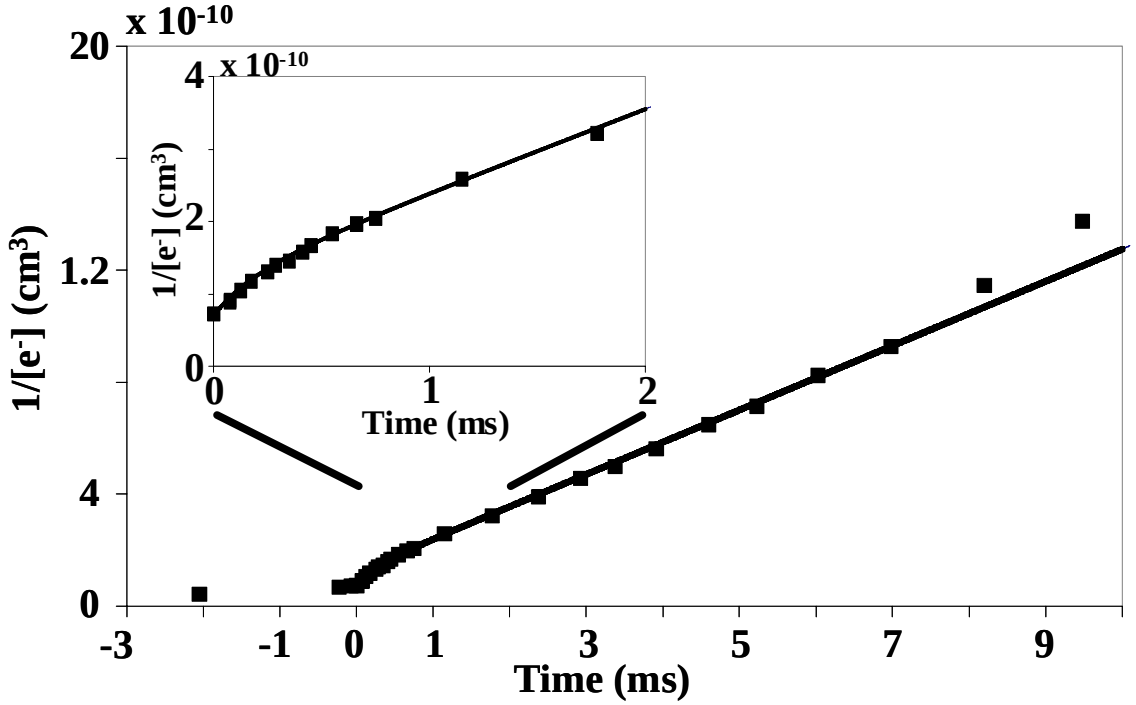

Figure 4.2. A plot of 1/[e^-] vs. time showing the fit of two simultaneously recombining isomers of $C_3H_3^+$, at a temperature of 300 K (α_e are 1.15×10^{-7} and 8.00×10^{-7} cm^3/s for propargyl and cyclic $C_3H_3^+$ respectively), created by numerically integrating the differential rate equation 6. The inset is a plot of the beginning of the fit expanded.

The upward curvature of the data above the fit in Figure 4.2 occurs because, at lower electron densities, diffusion becomes increasingly more important relative to recombination as the process of [e^-] decay. Because of the number of variables involved in the integration of equation 4.6, further fitting was performed to determine the amount of error that is associated with this type of analysis. The sensitivity analysis showed that if the product ion distribution was varied by more than 3%, the experimental electron density profile could not be accurately fitted.

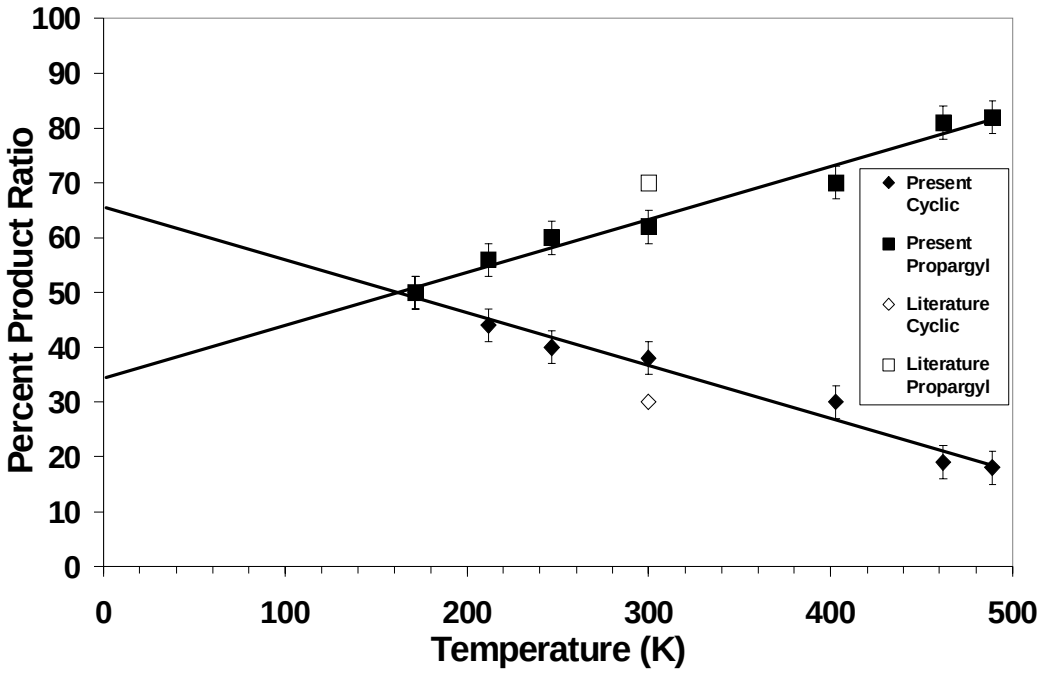

Figure 4.3. The temperature dependence of the product ion distribution (%) for the propargyl and the cyclic $C_3H_3^+$ produced in the H_3^+ dissociative proton transfer with allene (C_3H_4). The linear fits are extrapolated to interstellar molecular cloud temperatures. Open symbols indicate previous data[4].

In addition, changing the values of $\alpha_{e,p}$ and $\alpha_{e,c}$ by more than 8% also caused a poor fit. Measurements were made at temperatures varying from 172-489 K to determine the temperature dependencies of the α_e's (Figure 4.4). All recombination rate coefficients are accurate to within ± 15% at 300 K, and ± 20% at all other temperatures. The product ion distributions are accurate to within ± 5 in the percentage.

4.4 RESULTS AND DISCUSSION

4.4.1 $H_3^+ + C_3H_4$

The reaction of H_3^+ with allene has been studied previously at 300 K,[4] and this showed that two isomers of $C_3H_3^+$ are formed in a distribution of 70% propargyl to 30% cyclic $C_3H_3^+$. At room temperature, our ratio of the small α_e product to the large α_e product is 62% to 38% (see Figure 4.3) identifying the ions and their temperature dependent production and showing that the less abundant cyclic form has the larger α_e. The product ion distribution at the lowest temperature of 172 K is 50/50. Thus, these distributions show a trend tending towards a ratio of the propargyl over the cyclic form of 82/18 at the highest temperature of 489 K. Pathways to the production of both isomers are exothermic, with the cyclic isomer formation having 100 kJ/mol more excess energy than the propargyl ion formation. This is because the cyclic ion is more stable than the propargyl ion, so at low temperatures, production of the cyclic isomer is likely to dominate. Increasing the temperature of the system allows less time for the cyclic isomer

to be produced, leaving the product as more of the less stable propargyl ion form. The propargyl form begins to dominate the plasma at T >172 K.

4.4.2 c/p-$C_3H_3^+ + e^-$

The α_e's for the c/p-$C_3H_3^+$ isomers show little to no temperature dependence, although there is a slight increase at the higher temperatures (Figure 4.4). This is different from previous hydrocarbon data,[3] where the temperature dependence can be written as a simple power law dependence:

$$\alpha_e(T) = \alpha_e(300K)\left(\frac{T}{300K}\right)^X \tag{4.8}$$

Simple theoretical models have indicated *X* to be around -1.5 for the indirect mechanism,[7, 8] and -0.5 for the direct mechanism.[6] Temperature independent behavior is not unique since it has been observed in the N_2H^+ and HCO^+ recombinations.[9, 10] In these cases, there are no favorable crossing dissociative curves and a tunneling mechanism could be invoked. Alternatively, several Rydberg states could be accessed sequentially for which case, to the authors' knowledge, the *X* dependence in equation 8 has not been determined theoretically. The cyclic isomer recombines at a rate that is a factor of 6 faster than the propargyl isomer, α_e's averaging 8.5×10^{-7} and 1.5×10^{-7} cm^3/s for the cyclic and the propargyl $C_3H_3^+$, respectively. This difference is not unexpected since there is evidence that a favorable dissociative curve crossing exist for the cyclic[15] and not for the propargyl[16] form. However, why both these ions have little to no temperature dependence is still an open question. This implies that the curve crossings that exist for

the cyclic isomer and their form must be positioned in such a way that changing the temperature has an insignificant effect on the α_e.

Table 4.1. Hydrocarbon ion-molecule reactions that produce $C_3H_3^+$ as the dominant ion.[17] The lines join the reacting combinations. The species in bold indicate their presence in the Fox and Yelle model of the ionosphere of Titan.[2]

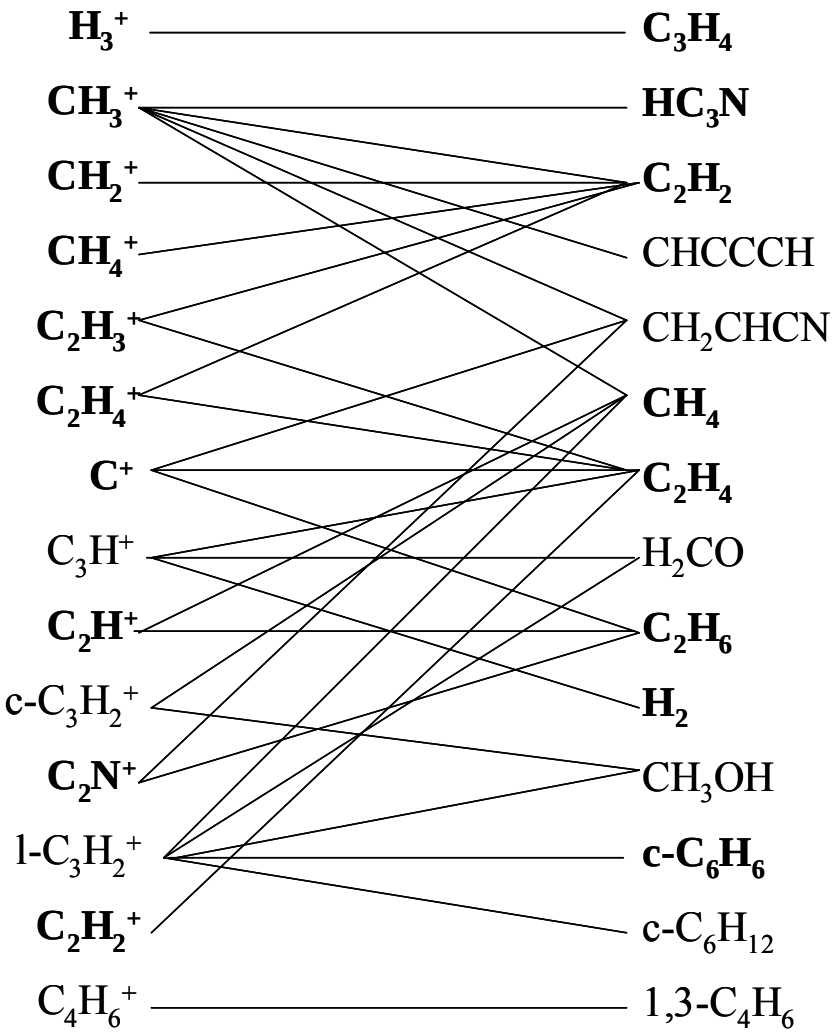

Although not observed yet, $C_3H_3^+$ must contribute to the ion chemistry in the Titan's atmosphere. $C_3H_3^+$ has been observed as the dominant ion produced in many ion-molecule hydrocarbon reactions (see Table 4.1) including hydrocarbon ions and neutrals thought to be present in the Titan atmosphere, and is produced in numerous other ion-

molecule reactions.[17] As in the allene reaction, $C_3H_3^+$ might be expected to be produced in different isomeric forms. c-$C_3H_3^+$ ion is very stable and does not react with many abundant neutrals within that atmosphere, i.e. not with H_2, N, N_2, NH_3, CH_4, C_2H_2, C_2H_4, C_3H_4, or c-C_6H_6, and would thus be available for recombination. Note though that p-$C_3H_3^+$ reacts at about the gas phase kinetic rate with NH_3, C_2H_2, C_2H_4, and c-C_6H_6.[17] These $C_3H_3^+$ isomers need to be included in the atmospheric models.

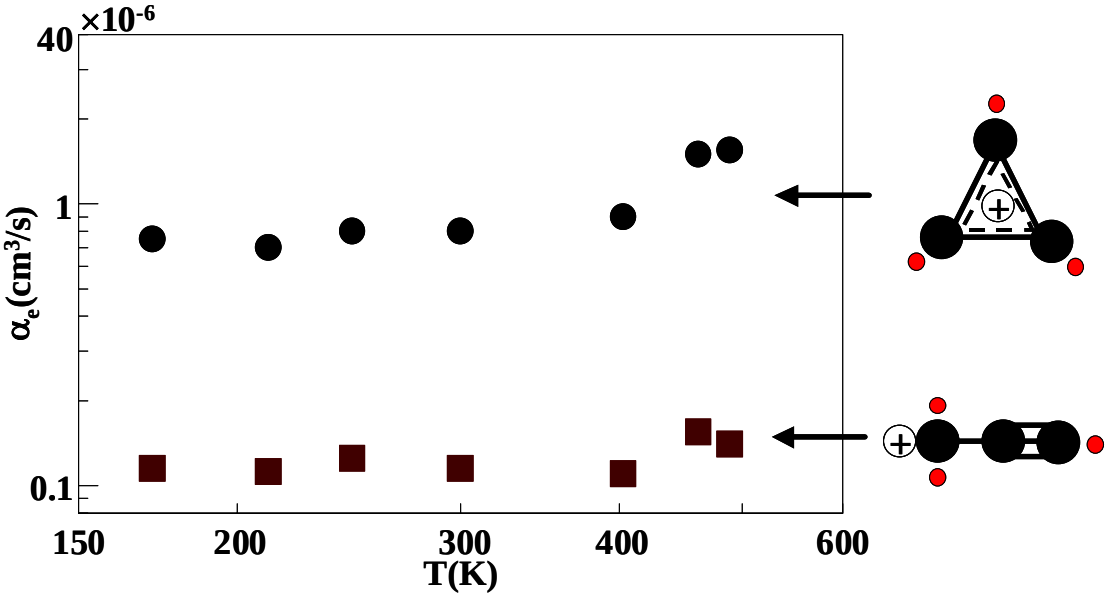

Figure 4.4. A plot of the α_e versus temperature for the propargyl and the cyclic $C_3H_3^+$ isomers.

The data also have relevance to the observed abundance ratio of the cyclic-C_3H_2 to linear H_2CCC (propadienylidene) in the cold cloud TMC-1, where the ratio is about 30/1.[12] The possible formation mechanism for these species has been attributed to the association reaction $C_3H^+ + H_2$ followed by dissociative recombination of the $C_3H_3^+$ isomers.[18] However, it is possible that the H_3^+ + allene reaction and a myriad of other

reactions (see Table 4.1) could also contribute. This observed abundance ratio might not only be due to the difference in the recombination rate coefficients i.e. a factor of 6 faster for the cyclic isomer, but also due to the product ion distribution trend for reactions such as the allene reaction (see Figure 4.3), which if extrapolated to low temperatures (around 10 K for a cold molecular clouds), would give the cyclic/propargyl ratios of 65/35 in the direction of the observations.

4.5 CONCLUSIONS

The recombination rate coefficients, α_e's, for cyclic and propargyl $C_3H_3^+$ and the $C_3H_3^+$ product ion distributions for the reaction of H_3^+ with C_3H_4 (allene) have been obtained over the temperature range 172 to 489 K. The α_e of the cyclic isomer exceeds the α_e of the propargyl isomer by a factor of 6, α_e's averaging 8.5×10^{-7} and 1.5×10^{-7} cm^3/s for the cyclic and the propargyl $C_3H_3^+$, respectively. This difference is consistent with recent theoretical work on the ion and dissociative neutral potential curves crossings.[15, 16] However, that the α_e for the two $C_3H_3^+$ isomers have little to no temperature dependence over this temperature range, is inconsistent with simple theory and is difficult to explain without more detailed theoretical calculations. Interestingly, the product ion distributions for the precursor $H_3^+ + C_3H_4$ could be obtained by numerical analysis of the recombination differential rate equation, and these distributions change with temperature from a 50/50 propargyl/cyclic ratio at the lowest temperature of 172 K to a ratio of 82/18 at the highest temperature of 489 K. $C_3H_3^+$ can be produced by many hydrocarbon ion-molecule reactions and is likely to have an important role in the ion chemistry of Titan's atmosphere. Also, the H_3^+ + allene reaction could contribute to the

30 to 1 observation of the cyclopropenylidene C_3H_2 to propadienylidene C_3H_2 ratio if this trend is extrapolated to cold molecular cloud temperatures around 10 K. This is the first time that recombination rates and product ion distributions have been simultaneously obtained.

4.6 ACKNOWLEDGEMENTS

Funding under NASA Grant No. NAG5-8951 is gratefully acknowledged.

4.7 REFERENCES

[1] Thaddeus, P.; McCarthy, M. C., Carbon Chains and Rings in the Laboratory and in Space. *Spectrochimica Acta* **2001,** A57, 757-774.

[2] Fox, J. L.; Yelle, R. V., Hydrocarbon Ions in the Ionosphere of Titan. *Geophys. Res. Letts.* **1997,** 24, 2179-2182.

[3] McLain, J. L.; Poterya, V.; Molek, C. D.; Babcock, L. M.; Adams, N. G., Flowing Afterglow Studies of the Temperature Dependencies for Dissociative Recombination of O_2^+, CH_5^+, $C_2H_5^+$ and $C_6H_7^+$ with Electrons. *J. Phys. Chem. A* **2004,** 108, 6704-6708.

[4] Milligan, D. B.; Wilson, P. F.; Freeman, C. G.; Meot-Ner, M.; McEwan, M. J., Dissociative Proton Transfer Reactions of H_3^+, N_2H^+ and H_3O^+ with Acyclic, Cyclic and Aromatic Hydrocarbons and Nitrogen Compounds and Astrophysical Implications. *J. Phys. Chem. A* **2002,** 106, 9745-9755.

[5] Mitchell, B. A.; L., L.; Laube, S.; Mosteafoui, T.; Rebrion-Rowe, C., *The Recombination of Hydrocarbon Ions with Electrons*. World Scientific: Singapore, 1999.

[6] Bates, D. R., Dissociative Recombination. *Phys. Rev.* **1950,** 78, 492-493.

[7] Bardsley, J. N., The Theory of Dissociative Recombination. *J. Phys. B.* **1968,** 1, 365-380.

[8] Bardsley, J. N.; Biondi, M. A., Dissociative Recombination. *Adv. At. Mol. Phys.* **1970,** 6, 1-57.

[9] Butler, J. M.; Babcock, L. M.; Adams, N. G., Effects of Deuteration on Vibrational Excitation in the Products of Electron Recombination of HCO^+ and N_2H^+. *Mol. Phys.* **1997,** 91, 81-90.

[10] Poterya, V.; McLain, J. L.; Adams, N. G.; Babcock , L. M., Mechanisms of Electron-Ion Recombination of $N_2H^+/(N_2D^+)$ and $HCO^+/(DCO^+)$ Ions: Temperature Dependence and Isotopic Effect. *J. Phys. Chem. A* **2005,** 109, 7181-7186.

[11] Wessen, A. http://saturn.jpl.nasa.gov. http://saturn.jpl.nasa.gov

[12] Irvine, W. M., Organic Molecules in the Gas Phase of Dense Interstellar Clouds. *Adv. Space Res.* **1995,** 15, 35-43.

[13] Smith, D.; Adams, N. G., Studies of Plasma Reaction Processes using a Flowing Afterglow/Langmuir Probe Apparatus. In *Swarms of Ions and Electrons in Gases*, Lindinger, W.; Mark, T. D.; Howorka, F., Eds. Springer-Verlag: Vienna, 1984; pp 284-306.

[14] Adams, N. G.; Smith, D., Flowing Afterglow and SIFT. In *Techniques for the Study of Ion-Molecule Reactions*, Farrar, J. M.; Saunders, J. W. H., Eds. Wiley Interscience: New York, 1988; Vol. 20, pp 165-220.

[15] Talbi, D., *Priv. Comm.* **2004**.

[16] Talbi, D., Dissociative Recombination of c-$C_3H_3^+$. In *Dissociative Recombination of Molecular Ions with Electrons*, Guberman, S. L., Ed. Kluwer: New York, 2003; pp 203-208.

[17] Anicich, V., *An Index of the Literature for Bimolecular Gas Phase Cation-Molecule Reaction Kinetics: JPL Publication 03-19*. Jet Propulsion Laboratory: Pasadena, 2003; p 1194.

[18] Adams, N. G.; Smith, D., On the Synthesis of c-C_3H_2 in Interstellar Clouds. *Ap. J.* **1987,** 317, L25-L27.

CHAPTER 5

PRESSURE DEPENDENT STUDY OF THE ELECTRON-ION RECOMBINATION OF PROTONATED CYANIDES $(RCN)H^+$ AND THEIR PROTON-BOUND DIMER IONS $(RCN)_2H^+$ WHERE R IS H, CH_3, AND CH_3CH_2[1]

[1]McLain, J. L., Molek, C. D., Osborn, D., Adams, N .G., To be submitted to Int. J. Mass. Spect., 2008.

5.1 INTRODUCTION

In Titan's atmosphere and the interstellar medium (ISM), cyanides are extremely important due to their large abundances. The amount of interest on this topic is evident by the abundance of literature on RCN and $(RCN)H^+$ (R = H, CH_3, CH_3CH_2).[1-9] $HCNH^+$ was predicted[1-4] to be the dominate ion in Titan's atmosphere and this was confirmed by the Cassini Ion and Neutral Mass Spectrometer (INMS).[5] Its number density has approached 1000 cm^{-3}, a value almost 10 times that of any other ions in the altitude range ~1000-1300 km. $HCNH^+$ also has been detected in the ISM along with vibrationally excited HCN.[6, 7] CH_3CNH^+ is a important ion in models of Titan's ionosphere contributing significantly to the total positive ionization density.[10] Observations have tentatively found CH_3CN in TMC-1 and Sgr B2,[8] and pure rotational transitions also were measured for CH_3CNH^+ in the range of 325 -500 GHz in 2006.[9] $CH_3CH_2CNH^+$ has also been included in models of Titan's atmosphere but few kinetic studies has been performed on this ion and its reactivity.[11] Because of this, the present study was performed to determine the dissociative recombination rate coefficients (α_e) of these ions for use in chemical modeling applications. During these studies it became evident that the proton-bound dimers were rapidly produced. For this a VT-FALP (Variable Temperature, Flowing Afterglow Langmuir Probe) apparatus has been used. The dissociative recombinations of $RCNH^+$ ions with electrons is straightforward since the reactions with the H_3^+ precursor gives only proton transfer.[12-14] On addition of RCN, these ions begin to recombine with electrons immediately and the reciprocal electron density profile with the flow tube position were very linear indicating that only one ion species is recombining in the plasma. Although this linearity is observed at all

concentrations of RCN, the rate of electron density decay increases significantly in all cases with increasing concentration of [RCN]. It became apparent that this increase in the rate of the electron decay is a result of the three-body association of $RCNH^+$ with RCN to form proton-bound dimer ions. These types of dimer ions have been shown to have exceptionally large recombination rate coefficients.[15-17] As has also been predicted by theory,[15] this association is rapid due to the large dipole moments of these cyanides. Since the electron density profile is now not of a single ionic species recombining but a mixture of two ionic species recombining simultaneously, numerical solution of the kinetic rate equations became necessary to obtain an accurate fit to all of the data.[18]

5.2 EXPERIMENT

The VT-FALP technique was used for these electron-ion recombination measurements. This technique has been described in detail in the literature and will only be discussed briefly here.[19, 20] A He^+/He_2^+ plasma (with helium metastables, He^m) flow was produced by a microwave discharge in helium flowing with a throughput of 16 slm in a flow tube (1 m long and 7 cm in diameter) at a pressure of 1.5 Torr. Argon was added upstream in the flow at a concentration of ~5 x 10^{13} cm^{-3} to destroy all He^m and He_2^+ producing a predominantly Ar^+/e^- plasma Hydrogen was then added further downstream to form a H_3^+/electron plasma by a standard reaction sequence.[21] These ions were sampled through an orifice to a downstream quadrupole mass filter/ion counting detection system which was used to identify all ions present in the plasma. Kinetic models were produced to confirm the ion chemistry occuring prior to the addition of RCN and examples of these have already been presented literature.[21] The HCN gas was

synthesized from the reaction H_2SO_4 + NaCN using a standard procedure.[22] The 99.9 % acetonitrile (CH_3CN) was obtained from Aldrich® and 99 % propanenitrile (CH_3CH_2CN) from Alfa Aesar®. Their neat vapors were often used to create the ions of interest after a series of freeze/pump/thaw procedures to remove any dissolved impurity gases. Dilutions with helium were used to obtain lower concentrations accurately. The recombining ion types were created by the reactions:

$$H_3^+ + RCN \rightarrow [RCNH^+]^* + H_2 \qquad (5.1)$$

$$[RCNH^+]^* + RCN \rightarrow RCNH^+ + RCN^* \qquad (5.2)$$

At this point, only protonated-RCN ions were observed in the plasma. Reaction (5.1) has been shown at room temperature to be simply a proton transfer reaction for all of the cyanides and all have rate coefficients approaching ~1×10^{-8} cm^3 s^{-1}.[13, 14, 23] Resonant proton transfer, reaction 5.2, rapidly quenches any vibrationally excited species created by the exothermicity of the primary proton transfer reaction before recombination occurs. At the higher RCN concentrations, the association, reaction 5.3, can be stabilized by a helium third body to create the proton-bound dimer which then can also recombining with electrons.

A movable Langmuir probe (25 μm in diameter and 4.3 mm long) operating in the orbital limited regime, was used to determine the electron density $[e^-]$ at various positions along the flow tube. $[e^-]$ and $[e^-]^{-1}$ are plotted as a function of time, figure 5.2, and the α_e's are determined by numerical solution of the rate equations. When ambipolar diffusion losses are not included, the simple form of the rate equation is $1/[e^-]_t - 1/[e^-]_0 = \alpha_e t$. Although, ambipolar diffusion is small in our experiment, this effect was included into the models. At the highest concentrations, approaching 1×10^{14} cm^{-3}, the Langmuir

probe had to be cleaned considerably longer than normal. Usually, after every voltage sweep a negative 130 V is applied for ~5 seconds to heat the probe so as to obtain exceptionally linear probe characteristics.

5.3 RESULTS AND DISCUSSION

The form of the electron density profiles depended significantly on RCN concentration which was varied from 1×10^{9} to approaching 1×10^{14} cm^{-3}. This is because of the association of $RCNH^{+}$ with RCN to produce the $(RCN)_2H^{+}$, reaction 5.3. To model the recombination, it was necessary to fit the data by numerically solving the kinetic equations for the production and recombination of the ions present in the afterglow to obtain the individual rates coefficients (k) for association and the α_e's. To be valid, the models have to fit all of the data obtained at different RCN concentrations, with constant α_e for $RCNH^{+}$ and $(RCN)_2H^{+}$ ions, Figs. 5.2-4.

One of the main models used is given in reaction 5.3, and plotted in figure 5.1 as a function of [RCN]. This shows that at a [RCN] = ~1×10^{11} cm^{-3} the α_e for the protonated monomer species can be obtained directly from the slope of the $1/[e^-]$ vs time data.

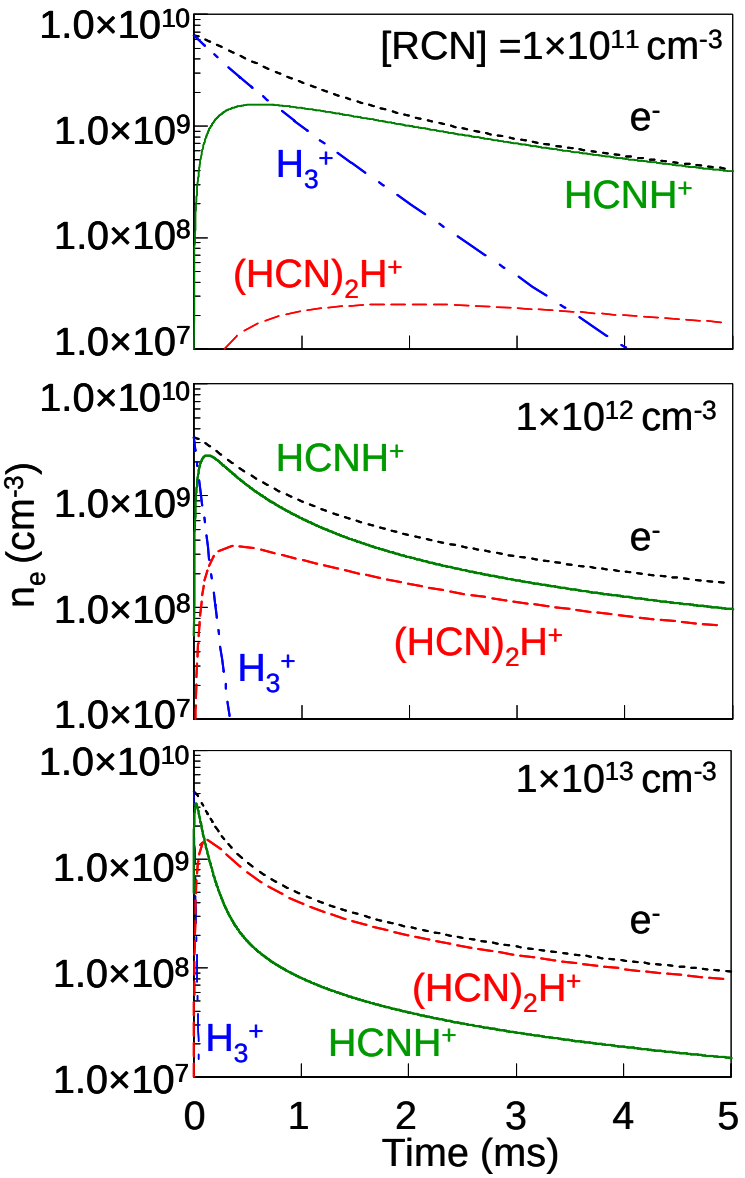

Figure 5.1. Electron and major ion concentrations in the model are plotted as a function of time in the flow tube. The black dotted lines represent $[e^-]$, and the blue dashed-dotted lines are the $[H_3^+]$, which reacts rapidly with HCN for the 1×10^{12} and 1×10^{13} cm^{-3} plots, disappearing in < 1 ms. The green solid lines are the $(HCN)H^+$ and the red dashed lines are the $(HCN)_2H^+$. For this illustration, the kinetic model for the reaction of H_3^+ with HCN was arbitrarily chosen, but this behavior is consistent with the CH_3CN and CH_3CH_2CN studies.

This is because [RCN] is too small for any substantial amount of the dimer to form.

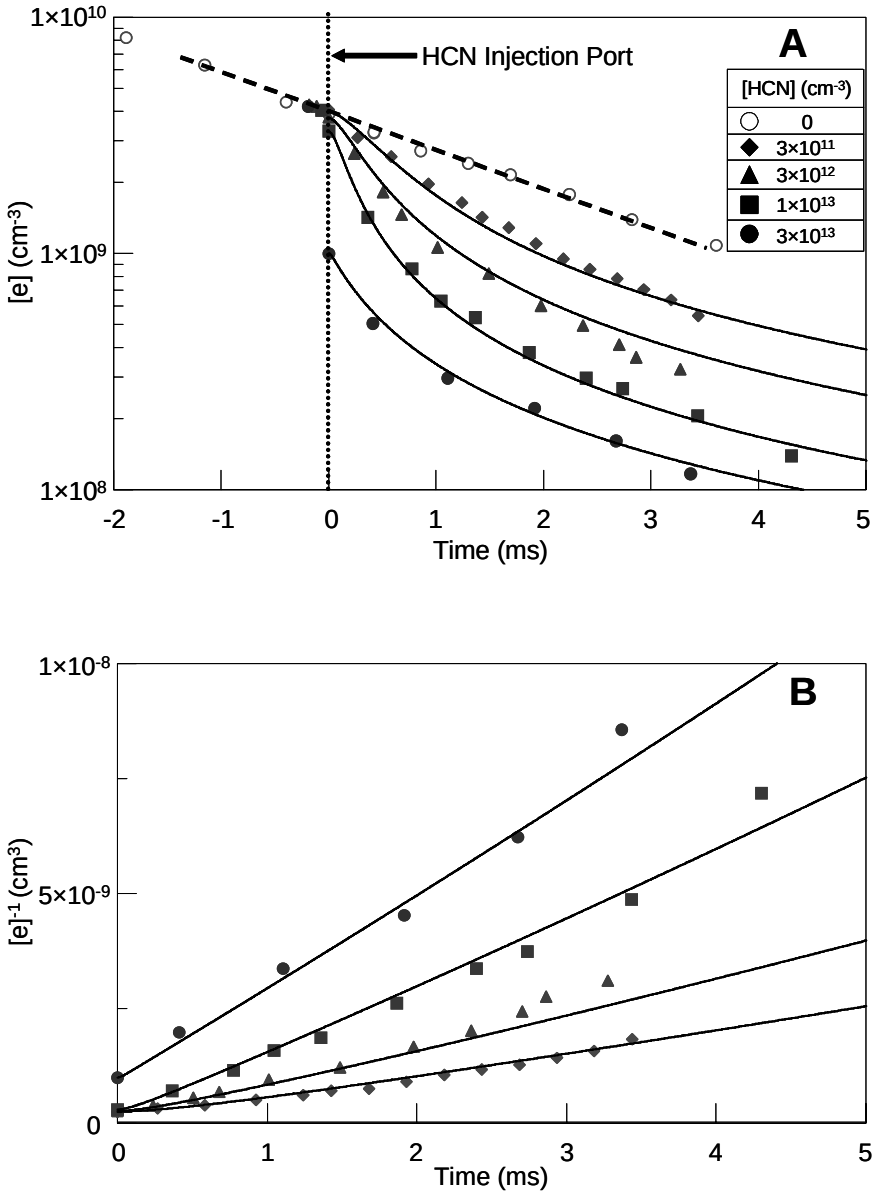

Figure 5.2. Plot A illustrates electron density decays, and the kinetic model fit to the experimental data at a series of [HCN] concentrations. The open circles are with no HCN added to the flow and therefore the electron density decay is only due to the recombination and diffusion of H_3^+, $\alpha_e = 1.1\times10^{-7}$ cm^3 s^{-1}. Time zero represents the position in the flow tube at which HCN was added. Plot B shows a typical plot of 1/[e] versus time for determining the α_e directly from the slope. The solid lines represent the fit of the model to the experimental data to show the validity of the model even though two ionic species are recombining simultaneously.

Conversely, at the highest concentrations used >1×10^{13} cm^{-3}, the proton-bound dimer forms immediately <0.5 ms by the association, reaction (5.3), and is very much the dominant ion in the plasma after ~1 ms so that from these data the slope is equivalent to the α_e of just the proton-bound dimer.

$$\begin{array}{ccc} & & k_3 \\ RCNH^+ + HCN + He & \rightleftharpoons & (RCN)_2H^+ + He \\ \downarrow e^- & & k_{-3} \quad \downarrow e^- \end{array} \qquad (5.3)$$

The three-body association rate coefficient k_3 for association reaction 5.3 to produce these dimers are large. $k_3 = 2.0\pm1\times10^{-26}$ cm^6 s^{-1} is determined from the model fits, see Table 5.1. When considering the effective binary rate coefficient with a [He] = 5.0×10^{16} cm^{-3}, the present value $k_{eff} = k_3[He]$ for CH_3CN is only slightly smaller ($k_{eff} = 1.0\times10^{-9}$ cm^3 s^{-1}) than with the value previously obtained for CH_3CN ($k_{eff} = 2.1\times10^{-9}$ cm^3 s^{-1}) in a flowing afterglow by studying the ion-molecule reactions in the conventional way.[17] To further improve the model and to obtain a more accurate fit, a two-body reverse reaction rate coefficient of $k_{-3} = 1.0\pm2\times10^{-13}$ cm^3 s^{-1} for HCN and CH_3CN and $4.0\pm3\times10^{-14}$ cm^3 s^{-1} for CH_3CH_3CN were also included. This reverse reaction is typical for an intermediate complex $[(RCN)_2H^+]^*$ dissociating back into reactants before it can be stabilized by collisions with helium, reaction 5.4. Therefore, a new reaction 4 model, including the excited intermediate complex was created. This more complex model only provided the same quality of fit as with the reaction 5.3 model with the addition of an extra recombination rate coefficient for the excited intermediate.

$$\begin{array}{ccccc} & & k_4 & & k_{4s} \\ RCNH^+ + HCN + He & \rightleftharpoons & [(RCN)_2H^+]^* + He & \rightarrow & (RCN)_2H^+ + He \\ \downarrow e^- & & k_{-4} \quad \downarrow e^- & & \downarrow e^- \end{array} \qquad (5.4)$$

However, it is not unreasonable to consider a α_e for the intermediate if the lifetime of the excited complex is relatively long. But the possibility of an excited intermediate is worth noting because the models in reaction 5.3 and 5.4 require a reverse reaction.

Remarkably, the quality of the fitting to the model is impressive after assigning the four rate coefficients, Table 5.1., because then the only parameter varied in the experiments and in the kinetic model was the concentration of [RCN]. In these studies, the [RCN] was varied by approximately four orders of magnitude, increasing the production and subsequent recombination of the dimer ions, figures 5.2-4. Plot A in figure 5.2., shows the recombination and diffusion of H_3^+ in open circles, which is noticeably slower compared to the recombination of the $HCNH^+$ and $(HCN)_2H^+$. While the rate of diffusion for H_3^+ is larger than for the higher mass molecular ions, its α_e is much smaller. Plot A in figure 5.2., has been presented to show the electron density decay at all [HCN]. Notice that the electron number density is decreased by an order of magnitude due to these rapidly recombining ions.

Table 5.1. Rate coefficients (k) and recombination rate coefficients (α_e) which provide the best fit to the electron density decays at all concentrations of RCN. The α_M and α_D represent the protonated monomer and the proton bound dimer, respectively. Uncertainty for the k's and the α's are ±30% and ±15%, respectively. The $k_{1(Theor.)}$ are the theoretical rate coefficients that were calculated using combined variational transition state theory and classical trajectory theory.[24]

	HCN	CH_3CN	CH_3CH_2CN
$k_{1(Lit.)}$ ($cm^3\ s^{-1}$)	9.5×10^{-9}	9.8×10^{-9}	9.9×10^{-9}
$k_{1(Theor.)}$ ($cm^3\ s^{-1}$)	8.5×10^{-8}	1.1×10^{-8}	1.2×10^{-8}
k_3 ($cm^6\ s^{-1}$)	2.0×10^{-26}	2.0×10^{-26}	2.0×10^{-26}
k_{-3} ($cm^3\ s^{-1}$)	1.5×10^{-13}	2.0×10^{-13}	4.0×10^{-14}
$\alpha_{M\ (Exp.)}$ ($cm^3\ s^{-1}$)	3.6×10^{-7}	3.4×10^{-7}	4.6×10^{-7}
$\alpha_{M\ (Lit.)}$ ($cm^3\ s^{-1}$)	FA[29] $3.5\pm0.9\times10^{-7}$ SR[30] 2.8×10^{-7}	FA[28] $3.3\pm1\times10^{-7}$ SR[31] $8.1\pm0.8\times10^{-7}$	FA[28] $4.7\pm2\times10^{-7}$
$\alpha_{D\ (Exp.)}$ ($cm^3\ s^{-1}$)	2.4×10^{-6}	FA[17] 2.8×10^{-6}	2.3×10^{-6}
$\alpha_{D\ (Lit.)}$ ($cm^3\ s^{-1}$)	NA	FA $2.8\pm1\times10^{-6}$	NA

The three-body association and the reverse rate coefficients were varied to determine how much uncertainty would be associated with these values as obtained with the kinetic model, and a standard deviation from the data was calculated for every case. These rate coefficients have an uncertainty of $\lesssim$ ±30% for all reactions. The three-body association rates for all of the reactions are very close to one another, and this is not surprising since the dipole moments (*d*) for these three cyanides are also very similar, *d* = 2.98, 3.92, 4.02

Debye for HCN, CH_3CN, and CH_3CH_2CN, respectively.[25] If the forward and reverse reactions are fast compared to electron-ion recombination of $(RCN)_2H^+$ and $RCNH^+$, then an equilibrium can be established, and this has been shown previously to give the appearance of one $\alpha_{eff.}$.[26] Alternatively, when the forward reaction is fast compared to the reverse, then a dynamic equilibrium can be established due to the rapid recombination rates. In figures 5.2B, 5.3 and 5.4, the experimental data along with the fit shows that the $1/[e^-]$ vs. time plots are consistently linear with only very slight deviations due to ambipolar diffusion.

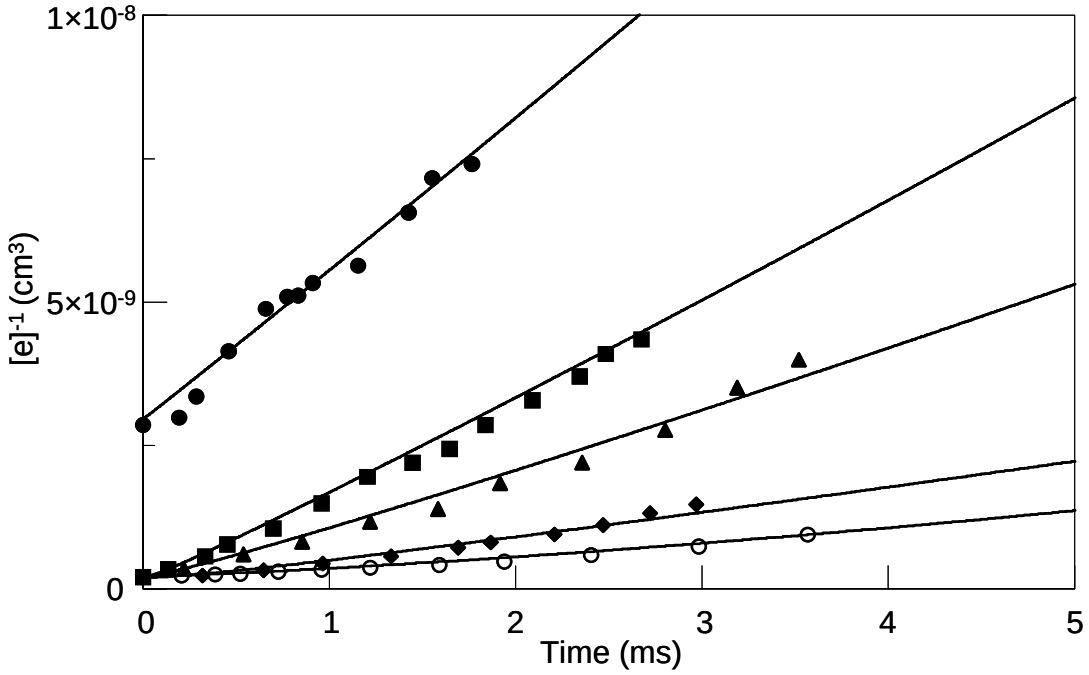

Figure 5.3. Plot of the experimental data and fit for $[CH_3CN]$ = (open-circles) 1×10^{10} cm^{-3}, (diamonds) 1×10^{11} cm^{-3}, (triangles) 1×10^{12} cm^{-3}, (squares) 1×10^{13} cm^{-3}, and (solid-circles) 8×10^{13} cm^{-3}. If only one ionic species is dominant, the α_e is equivalent to the slope. The lines represent the fits for 4 orders of magnitude change in $[CH_3CN]$.

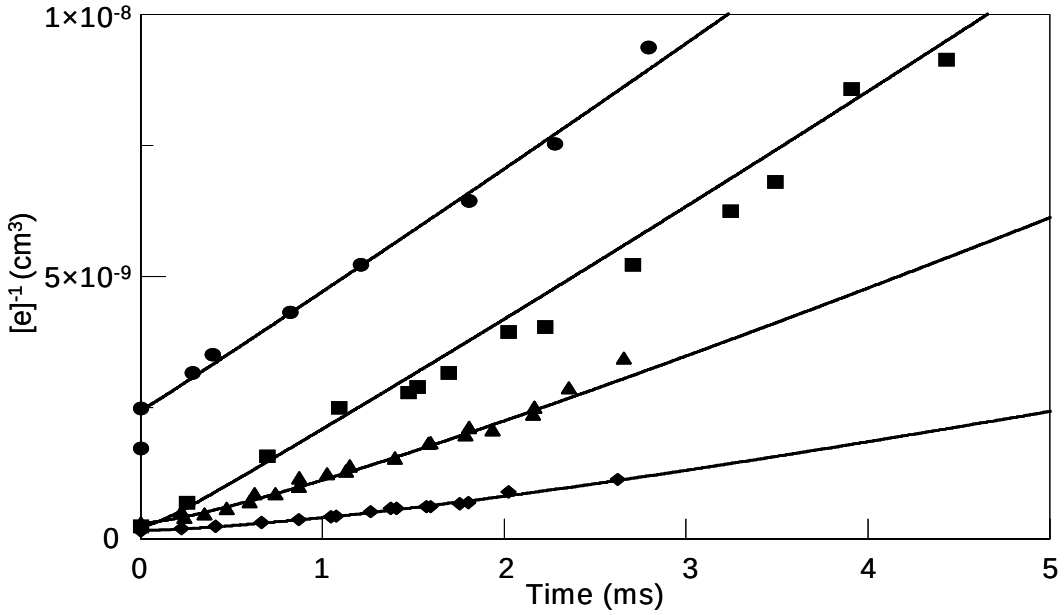

Figure 5.4. Plot of the present data and fit (solid-lines) for [CH_3CH_2CN] = (diamonds) 1×10^{11} cm^{-3}, (triangles) 1×10^{12} cm^{-3}, (squares) 1×10^{13} cm^{-3}, (circles) 3×10^{13} cm^{-3}. The lines represent the fits for 3 orders of magnitude change in [CH_3CH_2CN].

At low [RCN] concentrations, the recombination is controlled by only the recombination of the monomer and diffusion, figure 5.4. As the concentration of RCN increases, the dimer production increases, which begins to contribute more to the total ionization, until eventually the dimer is present at a relatively short time after injection ~1 ms. At the highest concentration of RCN, there is a rapid decrease in the electron number density at < 1 ms. The type of reactant port used was a single nozzle situated slightly above the center of the flow tube and positioned to flow upstream at ~45° off axis. The appearance of a drop in [e^-] near a port has been shown before in the literature[27] to be caused by the position of the injection port, which if positioned too close in proximity to the Langmuir probe can create a drop in electron density. Although this also shows a rapid decrease in the electron number density near the port, after the Langmuir probe is moved past the port position, if the port is small, the electron density profile appears as if this drop never

occurred, which is not the case in our experiment. Such a rapid decrease can be created if the flow tube is being coated with an insulating layer of the reactant vapor, lowering the return area for the probe. Fortunately, as the distance from the injection port increases, a smaller amount of vapor is available to coat the flow tube, and as the electron density decreases the effect on the return voltage also decreases. The Langmuir probe did have to be cleaned considerably more at these higher concentrations to obtain consistent electron number density measurements. The α_e after this initial drop is consistent with previous measurements for the α_e for $(CH_3CN)_2H^+$ at 300 K and to the author's knowledge is the only proton-bound dimer in the series to have been measured previously.[17] The magnitudes of the α_e's for $RCNH^+$ compared to the α_e's of $(RCN)_2H^+$ for the three cyanides shows that the proton-bound dimers can have substantially larger α_e's. This can be explained by the reaction proceeding via electron capture, which neutralizes the proton, and releases the attached molecules that efficiently carry away the excess energy of recombination. The double-electron transition normally required for dissociative recombination therefore occurs in a single-electron transition, which are much more probable than double-electron transitions.[16] In comparing the measured α_e's with the literature there is good agreement with previous flowing afterglow measurements where available.[28, 29] The FA and SR denote previous flowing afterglow and storage ring measurements. The α_e's $HCNH^+$ for the SR is only slightly lower than the current measurement and certainly within the combined errors, while the α_e's for the CD_3CND^+ appears much higher than both of the FA measurements.[30] Note that, the comparison is not exact because CD_3CN was used instead of CH_3CN and the proton transfer reaction was with deuterium instead of hydrogen.[31]

The α_e's for $HCNH^+$ and CH_3CNH^+ are very similar and compared to the α_e of the $CH_3CH_2CNH^+$ are only slightly lower, <30%. But when comparing the α_e's for the proton-bound dimers of the three systems there are important differences. The α_e for the $(HCN)_2H^+$ is ~25% lower than the α_e for the $(CH_3CN)_2H^+$. Interestingly, this trend does not continue for the α_e for the $(CH_3CH_2CN)_2H^+$, which instead decreases. The decrease in the α_e for $(CH_3CH_2CN)_2H^+$ may be caused by the larger ethyl chains sterically hindering the electron capture. This implies that the recombination of these proton-bound dimers is very site specific and there is not much variation in α_e with increasing dimer size, this has previously been shown to be the case for proton-bound H_2O clusters,. In these clusters the $(H2O)_nH^+$, where n = 2, 3, 4, 5 the α_e's only varied from (2.5, 3.0, 3.0, 3.6)$\times 10^{-6}$ cm^3 s^{-1}, respectively.[15, 32]

5.4 CONCLUSIONS

A comprehensive study using the VT-FALP technique for the H_3^+ + RCN reaction reveals that the recombination of $RCNH^+$ ion is not just simple recombination reaction but that proton-bound dimers begin to contribute more to the electron density decay when the [RCN] is increased above ~10^{11} cm^{-3}. The two α_e for the $RCNH^+$ and $(RCN)_2H^+$ have been determined and compared to previous data when available, Table 5.1. The protonated-cyanides have relatively modest $\alpha_e < 5\times 10^{-7}$ cm^3 s^{-1} while their proton-bound dimer ions have substantially larger $\alpha_e > 10^{-6}$ cm^3 s^{-1} at 300 K. Both individual α_e's can be obtained directly from the slope of the $1/[e^-]$ vs time plots without the use of the fitting model if the appropriate concentrations are chosen ([RCN] ~10^{11} cm^{-3} and $\gtrsim 10^{13}$ cm^{-3}, for

the $RCNH^+$ and $(RCN)_2H^+$, respectively). These specific concentrations can easily be determined by solving the kinetic reaction models as long as the rate coefficients are available for the proton transfer and association reactions. The HCN, CH_3CN and CH_3CH_2CN proton transfer reaction from H_3^+ are extremely rapid ~1 x 10^{-8} cm^3 s^{-1} compared to a typical gas kinetic rate coefficient 2 x 10^{-9} cm^3 s^{-1} due to their large dipole moments and the small mass of H_3^+. Although a simple three-body mechanism, reaction 5.3 model, was used to model all of the present data, a reverse reaction was added to obtain the presented fits. This indicates that the clusters are excited and can either recombine or dissociate back into the protonated monomer. Therefore, the more complete mechanism, Reaction 5.4 model, was also explored where an excited intermediate species was introduced into the model. However, this required an additional electron loss process by assigning the excited intermediate a recombination rate coefficient and did not improve the quality of the fit. The degree of excitation in these cluster ions is not known, but with these features being present in both models, the recombination of the excited intermediate most likely contributes to the electron decay at intermediate flows of RCN. But, when concentration of RCN is increased sufficiently, the association rate is fast enough that measurements of the α_e's for the proton-bound dimers can be obtained.

5.5 ACKNOWLEDGEMENTS

Funding under NSF Grant No. 0212398 and NASA Grant No. NAG5-8951 is gratefully acknowledged.

5.6 REFERENCES

[1] Fox, J. L.; Yelle, R. V., Hydrocarbon Ions in the Ionosphere of Titan. *Geophys. Res. Letts.* **1997,** 24, 2179-2182.

[2] Keller, C. N.; Anicich, V.; Cravens, T. E., Model of Titan's Ionosphere with Detailed Hydrocarbon Ion Chemistry. *Planet. Space Sci.* **1998,** 46, 1157-1174.

[3] Wilson, E. H.; Atreya, S. K., Current State of Modeling the Photochemistry of Titan's Mutually Dependent Atmosphere and Ionosphere. *J. Geophys. Res.* **2004,** 109, E06002.

[4] Anicich, V.; Wilson, P.; McEwan, M. J., A SIFT Study of Some Reactions in Titan's Atmosphere: Reactions of N^+, N_2^+, and HCN^+ with CH_4, C_2H_2 and C_2H_4. *J. Am. Soc. Mass Spectrom.* **2004,** 15, 1148-55.

[5] Cravens, T. E.; Robertson, I. P.; Waite, J. H.; Yelle, R. V.; Kasprzak, W. T.; Keller, C. N.; Ledvina, S. A.; Nieman, H. B.; Luhmann, J. G.; McNutt, R. L.; Ip, W.-H.; de la Haye, V.; Mueller-Wodarg, I.; Wahlund, J.-E.; Anicich, V. G.; Vuitton, V., Composition of Titan's Ionosphere. *Geophys. Res. Letts.* **2006,** 33, L07105.

[6] Ziurys, L. M.; Turner, B. E., $HCNH^+$: A new interstellar molecular ion. *Astron. J.* **1986,** 302, L31-36.

[7] Ziurys, L. M.; Turner, B. E., Detection of interstellar vibrationally excited HCN. *Astron. J.* **1986,** 300, (L19-23).

[8] Turner, B. E.; Friberg, P.; Irvine, W. M.; Saito, M.; Yamamoto, S., Interstellar Cyanomethane. *Astrophys. J.* **1990,** 355, (2), 546-61.

[9] Amano, T.; Hashimoto, H.; Hirao, K., Submillimeter-wave spectroscopy pf $HCNH^+$ and CH_3CNH^+. *J Mol Structure* **2006,** 795, 190-193.

[10] Molina-Cuberos, G. J.; Lopez-Moreno, J. J.; Rodrigo, R.; Lara, L. M., Chemistry of the Galactic Cosmic Ray Induced Ionosphere of Titan. *J.Geophys. Res.* **1999,** 104, 21997-22024.

[11] Bouchoux, G.; Minh, T. N.; Longevialle, P., Unimolecular Chemistry of Protonated Ethyl Cyanide and Ethyl Isocyanide: An Experimental and Molecular Orbital Study. *J. Am. Chem. Soc.* **1992,** 114, 10000-10005.

[12] Mackay, G. I.; Betowski, D.; Payzant, H. I., Rate constants at 297 K for proton-transfer reactions with HCN and CH_3CN. Comparisons with classical theories and exothermicity. *J Phys. Chem. A* **1976,** 80, 2919-2922.

[13] Clary, D. C.; Smith, D.; Adams, N. G., Temperature Dependences of Rate Coefficients for Reactions of Ions with Dipolar Molecules. *Chem.Phys.Letts.* **1985,** 119, 320-326.

[14] Anicich, V., Evaluated Bimolecular Ion-Molecule Gas Phase Kinetics of Positive Ions for use in Modeling Planetary Atmospheres, Cometary Comae, and Interstellar Clouds. *J. Phys. Chem. Ref. Data* **1993,** 22, (6), 1469-1569.

[15] Bates, D. R., Super Dissociative Recombination. *J. Phys. B* **1991,** 24, 703-709.

[16] Mitchell, J. B. A.; Rebrion-Rowe, C., The Recombination of Electrons with Complex Molecular Ions. *Int. Rev. Phys. Chem.* **1997,** 16, 201-213.

[17] Plasil, R.; Glosik, J.; Zakouril, P., Formation and Recombination of Protonated Acetonitrile Clusters. *J. Phys. B* **1999,** 32, 3575-83.

[18] McLain, J. L.; Poterya, V.; Jackson, D. M.; Adams, N. G.; Babcock , L. M., $C_3H_3^+$ Isomers: Temperature Dependencies of their Production in the H_3^+ Reaction with Allene and their Loss by Dissociative Recombination with Electrons. *J. Phys. Chem. A* **2005,** 109, 5119-5123.

[19] Smith, D.; Adams, N. G., Studies of Plasma Reaction Processes using a Flowing Afterglow/Langmuir Probe Apparatus. In *Swarms of Ions and Electrons in Gases*, Lindinger, W.; Mark, T. D.; Howorka, F., Eds. Springer-Verlag: Vienna, 1984; pp 284-306.

[20] Adams, N. G.; Smith, D., Flowing Afterglow and SIFT. In *Techniques for the Study of Ion-Molecule Reactions*, Farrar, J. M.; Saunders, J. W. H., Eds. Wiley Interscience: New York, 1988; Vol. 20, pp 165-220.

[21] McLain, J. L.; Poterya, V.; Molek, C. D.; Babcock, L. M.; Adams, N. G., Flowing Afterglow Studies of the Temperature Dependencies for Dissociative Recombination of O_2^+, CH_5^+, $C_2H_5^+$ and $C_6H_7^+$ with Electrons. *J. Phys. Chem. A* **2004,** 108, 6704-6708.

[22] Ziegler, K., Hydrogen cyanide (anhydrous). *Org. Syn.* **1927,** 7, 50-52.

[23] Mackay, G. I.; Betowski, D.; Payzant, H. I., Rate constants at 297 K for proton-transfer reactions with HCN and CH3CN. Comparisons with classical theories and exothermicity. *J. Phys. Chem. A* **1976,** 80, 2919-2922.

[24] Su, T.; Chesnavich, W. J., Parametrization of the Ion-Polar Molecule Collision Rate Constant by Trajectory Calculations. *J. Chem. Phys.* **1982,** 76, (10), 5183-5185.

[25] Nelson, R. D., Selected Values of Electric Dipole Moments for Molecules in the Gas Phase. *NSRDS-NBS 10* **1971**.

[26] Novotny, O.; Plasil, R.; Pysanenko, A.; Korolov, I.; Glosik, J., The recombination of D_3^+ and D_5^+ ions with electrons in deuterium containing plasma. *J. Phys. B* **2006,** 39, 2561-2569.

[27] Smith, D.; Adams, N. G.; Dean, A. G.; Church, M. J., The Application of Langmuir Probes to the Study of Flowing Afterglow Plasmas. . *J. Phys. D.* **1975,** 8, 141-152.

[28] Geoghegan, M.; Adams, N. G.; Smith, D., Determination of the Electron-Ion Dissociative Recombination Coefficients for Several Molecular Ions at 300K. *J. Phys. B* **1991,** 24 2589-2599

[29] Adams, N. G.; Smith, D., Measurements of the Dissociative Recombination Coefficients for Several Polyatomic Ion Species at 300K. *Chem. Phys. Letts.* **1988,** 144, 11-14.

[30] Semaniak, J.; Minaev, B. F.; Derkatch, A. M.; Hellberg, F.; Neau, A.; Rosen, S.; Thomas, R.; Larsson, M.; Danared, H.; Paal, A.; af Ugglas, M., Dissociative Recombination of $HCNH^+$: Absolute Cross-Sections and Branching Ratios. *Ap. J. Suppl.* **2001,** 135, 275-83.

[31] Geppert, W.; al, e., Formation of biomolecule precursors in space. *XXV International Conference on Photonic, Electronic and Atomic Collisions. J Phys. Conf. Ser.* **2007,** 88.

[32] Bates, D. R., Dissociative Recombination of Polyatomic Ions. *J. Phys. B* **1991,** 24, 3267-3284.

CHAPTER 6

FLOWING AFTERGLOW STUDIES OF TEMPERATURE DEPENDENCIES FOR ELECTRON-ION DISSOCIATIVE RECOMBINATION OF $HCNH^+$, CH_3CNH^+ AND $CH_3CH_2CNH^+$ AND THEIR PROTON-BOUND DIMERS[1]

[1]McLain, J. L., Adams, N .G., To be submitted to J. Phys. Chem. A., 2008.

6.1 INTRODUCTION

Titan, the largest satellite of Saturn, is very unique because it is the only moon in our solar system that has a significant atmosphere. Titan's atmosphere, mostly composed of N_2, also contains ~2% hydrocarbons, which is mainly methane and ethane. These molecules are ionized by the solar radiation, solar wind particles, and cosmic rays, which initiate chemical reactions.[1-3] The reactions produce a complex mixture of organic molecules and eventually tholins, which gives Titan its reddish haze. Early models predicted[4-7] $HCNH^+$ to be the dominate ion in Titan's ionosphere. Later the Cassini Ion and Neutral Mass Spectrometer (INMS) confirmed that the concentration of $HCNH^+$ is much larger than other ions in the altitude range ~1000-1300 km.[8] CH_3CNH^+ also contributes significantly to the total positive ionization density in models of Titan's ionosphere.[1] In addition $CH_3CH_2CNH^+$ has been included in models of Titan, but experimental data on this ion are limited.[9] HCN, $HCNH^+$ and CH_3CN have also been detected throughout the ISM.[10-12] Because of these needs, the temperature dependence for electron-ion dissociative recombination (DR) of these ions and their proton-bound dimer have been studied. In particular, a VT-FALP (Variable Temperature-Flowing Afterglow Langmuir Probe) apparatus has been used to determine recombination rate coefficients (α_e) as a function of temperature. The proton transfer from a H_3^+ precursor to the cyanide series produces only the protonated cyanide analogue.[13-15] On addition of the neutral cyanides, the protonated ions begin to recombine with electrons. Unlike many protonated hydrocarbon ions studied previously,[16] these protonated cyanides can dimerize rapidly forming the proton-bound cluster ions. This rapid association is due to the large dipole moments of the cyanides.[17] When the concentration of the neutral cyanides approach 10^{14}

cm^{-3}, the proton bound dimer ions become the dominant recombining ion in the plasma. In a previous study, we have determined α_e for $HCNH^+$, CH_3CNH^+, $CH_3CH_2NH^+$, $(HCN)_2H^+$, $(CH_3CN)_2H^+$, and $(CH_3CH_2CN)_2H^+$ at 300 K as well as the association rate coefficients.[16, 18] For the astrophysical applications the data are required at temperatures below 300 K to be directly applicable. These cluster ions have been shown to have exceptionally large recombination rate coefficients.[17, 19, 20] Because of this, in the present study the α_e's have been measured at various temperatures to determine their temperature dependencies for these applications.

6.2 EXPERIMENT

A flowing afterglow apparatus was used to determine α_e as a function of temperature. This technique utilizes a movable Langmuir probe to determine the electron density profile as a function of reaction time. Since this technique has been described in detail in the literature, only a brief overview will be given here.[21, 22] A microwave discharge ionizes a He carrier gas to create a quasi-neutral He^+/e^- plasma, where the ion and electron number densities are always equal. Downstream of the μ-wave discharge, He^+ associates with He to produce He_2^+. The μ-wave discharge also creates helium metastables, He^m. Argon is then added downstream to destroy He_2^+ and He^m. The ions of interest are created by the proton transfer reaction from H_3^+. H_2 is added to the Ar^+/e^- plasma, and converts the plasma rapidly into a H_3^+/e^- plasma. All of the ion-molecule reactions leading to the H_3^+/e^- plasma have been modeled and presented previously in the literature.[16] After the H_3^+/e^- plasma is established, the neutral cyanides are added producing protonated cyanides. In flowing afterglow experiments, ambipolar diffusion

losses are usually negligible compared with electron-ion recombination, and when the plasma contains only one recombining ion, the rate equation can be simplified to:

$$1/[e^-]_t - 1/[e^-]_0 = \alpha_e t \qquad (6.1)$$

The temperature range of the flow tube can be varied between 80 to 700 K. This is achieved with resistive heaters and cooling tubes both attached to a copper jacket clamped to the flow tube Cryogenic fluid is pumped through the cooling tubes to obtained temperatures below 300 K. The temperature measurements were made with 6 Type K thermocouples equally spaced down the flow tube's Cu jacket. Initially, the hydrogen cyanide gas was obtained from Matheson® but all of the measurements with HCN presented here this reactant gas was synthesized from the reaction H_2SO_4 + NaCN using a standard procedure.[23] Methyl cyanide (CH_3CN) with a purity of 99.9 % was obtained from Aldrich®, and 99 % ethyl cyanide (CH_3CH_2CN) was obtained form Alfa Aesar®. The neat vapors were used after a series of freeze/pump/thaw cycles to remove any dissolved impurity gases. Dilutions with helium were used to obtain concentrations low enough to inhibiting association reactions. In equation 6.1-5., an example is given of the chemistry for HCN under these conditions; and the methyl and ethyl cyanide reactions are analogous:

$$H_3^+ + HCN \rightarrow [HCNH^+]^* + H_2 \qquad (6.2)$$

$$[HCNH^+]^* + HCN \rightarrow HCNH^+ + HCN^* \qquad (6.3)$$

$$HCNH^+ + e^- \rightarrow \text{neutral products} \qquad (6.4)$$

$$HCNH^+ + HCN + He \rightleftharpoons (RCN)_2H^+ + He \qquad (6.5)$$

$$\downarrow e^- \rightarrow \text{neutral products}$$

When the concentrations of the cyanides used were small enough to inhibit association, equation. 6.5, only the protonated-cyanides ions were observed in the plasma by a downstream mass spectrometer. Equation. 6.3 has been shown at room temperature to be simply a proton transfer reaction for all of the cyanides, and these have rate coefficients of approximately 1×10^{-8} cm^3 s^{-1}.[13-15] Resonant proton transfer, equation. 6.2, rapidly quenches any vibrationally excited ions created by the exothermicity of the proton transfer reaction from H_3^+. Equation 6.4 depicts the DR for ground state $HCNH^+$ given only "neutral products". The neutral products for these DR can also be determined with the current experimental setup, and such future experiments are planned. This technique has been detailed previously in the literature for N_2H^+ and CH_5^+.[24]

While the protonated cyanide ions control the decay of electrons at low cyanide concentration, at larger cyanide concentrations the proton bound dimer can be formed by the three-body association reaction with He, an example is given for the HCN dimer ion $(HCN)_2H^+$ in equation 6.5.

These proton-bound dimer ions also recombine rapidly with electrons and with α_e's much larger than the analogous protonated cyanide monomer. This behavior can be seen in figure 6.1 when the rate increases as the concentration of neutral HCN is increased. The three-body association reactions for these cyanides are all very rapid. This is not surprising since the dipole moments (d) are very large, d = 2.98, 3.92, 4.02 Debye for HCN, CH_3CN, and CH_3CH_2CN, respectively.[25] All of these systems have recently been studied at room temperature and association rate coefficients and recombination rate coefficients for the protonated cyanides and the proton bound dimer cyanides determined, Chapter 5.

6.3 RESULTS AND DISCUSSION

6.3.1 PRESSURE DEPENDENCIES

The recombination rate coefficients (α_e) has been obtained for $HCNH^+$, CH_3CNH^+, $CH_3CH_2CNH^+$, $(HCN)_2H^+$, $(CH_3CN)_2H^+$, and $(CH_3CH_2CN)_2H^+$ for temperature ranging from ~200 K to ~600 K. The lowest temperatures achieved are directly related to the freezing point of the cyanide. In these experiments, the ions are completely thermalized at the temperature of the He carrier gas.

Initially, a pressure dependent study was performed to determine the concentrations required to obtain the α_e of the protonated cyanides and their proton bound dimer ions separately, see Chapter 5. Fortunately, the vapor pressures for these cyanides were large enough that high concentration of the cyanides, approaching 1×10^{14} cm^{-3}, could be achieved. A plot of the α_e measured versus the concentration of [HCN] can be seen in figure 6.1. DR for H_3^+ controls the decay of electron at low concentrations $<10^9$ cm^{-3}, where the α_e for H_3^+ was measured to be 1.1×10^{-7} $cm^3\,s^{-1}$ at 300 K, consistent with previous measurements. The effective rate coefficient (α_{eff}) then increases at $\sim10^9$ cm^{-3} to a constant value of 3.5×10^{-7} $cm^3\,s^{-1}$ centered at 3×10^{10} cm^{-3}, which is the α_e for the $HCNH^+$ ions. Another increase in α_{eff} is observed above $\sim1\times10^{11}$ cm^{-3} until another constant region was observed $>2\times10^{12}$ cm^{-3}, where the average α_e for the dimer $(HCN)_2H^+$ ions of 2.4×10^{-6} $cm^3\,s^{-1}$ is obtained. These data for figure 6.1 were obtained to show the regions where the concentration of the HCN produced a plasma dominated by either $HCNH^+$ or $(HCN)_2H^+$ and the intermediate values of the α_{eff}. The concentration dependent plots for the CH_3CN and CH_3CH_2CN are similar to that of figure 6.1 for HCN.

These constant sections also correspond to the same concentration where the kinetic models indicate that just one recombining ion dominates. These plots indicate very clearly that unless such plots are made and the correct concentrations of the cyanides used erroneous values of the α_e can very easily be obtained

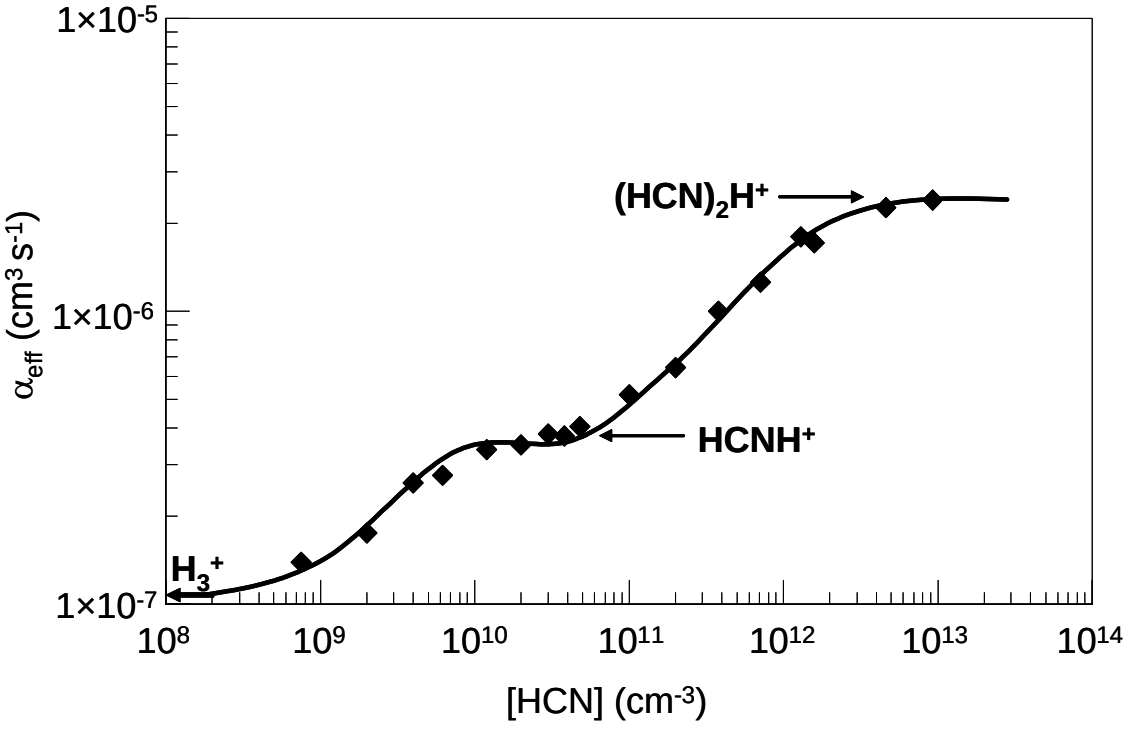

Figure 6.1. A plot of α_{eff} vs [HCN]. The regions where H_3^+, $HCNH^+$ and $(HCN)_2H^+$ control the loss of electrons can be seen from these data. The solid line through these data has been included to emphasize the constant α_{eff} regions corresponding to the α_e for $HCNH^+$ and $(HCN)_2H^+$.

Without such information it would be very dangerous to try to determine α_e for the specific species since any value between that of H_3^+ and the proton bound dimer can be obtained.

6.3.2 TEMPERATURE DEPENDENCIES

The temperature dependencies for DR of $HCNH^+$, CH_3CNH^+, $CH_3CH_2CNH^+$, $(HCN)_2H^+$, $(CH_3CN)_2H^+$, and $(CH_3CH_2CN)_2H^+$ all exhibit power law dependencies. All α_e were obtained for cyanide concentrations in the appropriate plateau regions. Power law dependencies are predicted by simple recombination theories for DR. These theories for DR introduced by Bates[26] in 1950 and Bardsley[27, 28] in 1968 were called the direct and indirect mechanisms. Both mechanisms involve a doubly excited electronic state of the neutralized ion. In the direct mechanism, the recombining electron excites another electron in the ion. Both are resonantly captured and form a doubly excited neutralized ion. Although this excited state can initially autoionize back to the reactants, as the products start to separate along a repulsive curve if available, the energy is converted from potential energy into kinetic energy of separation, and when the predicted energy drops below the lowest rovibronic state of the ion, dissociation becomes inevitable.[29] The power law temperature dependence for this process is $T_e^{-0.5}$, where the subscript e implies the electron temperature.

In the indirect mechanism, an additional step is required because a "direct" route to the repulsive, dissociative potential curve does not cross the ground state potential surface of the ion. The additional step corresponds to a radiationless electron capture into a vibrational level of a Rydberg state, where the binding distance between the electron and the ion core is large. Then, this state undergoes a second radiationless transition to the same repulsive state as in the direct process, which can then dissociate. The power law temperature dependence for this process is $T^{-1.5}$.

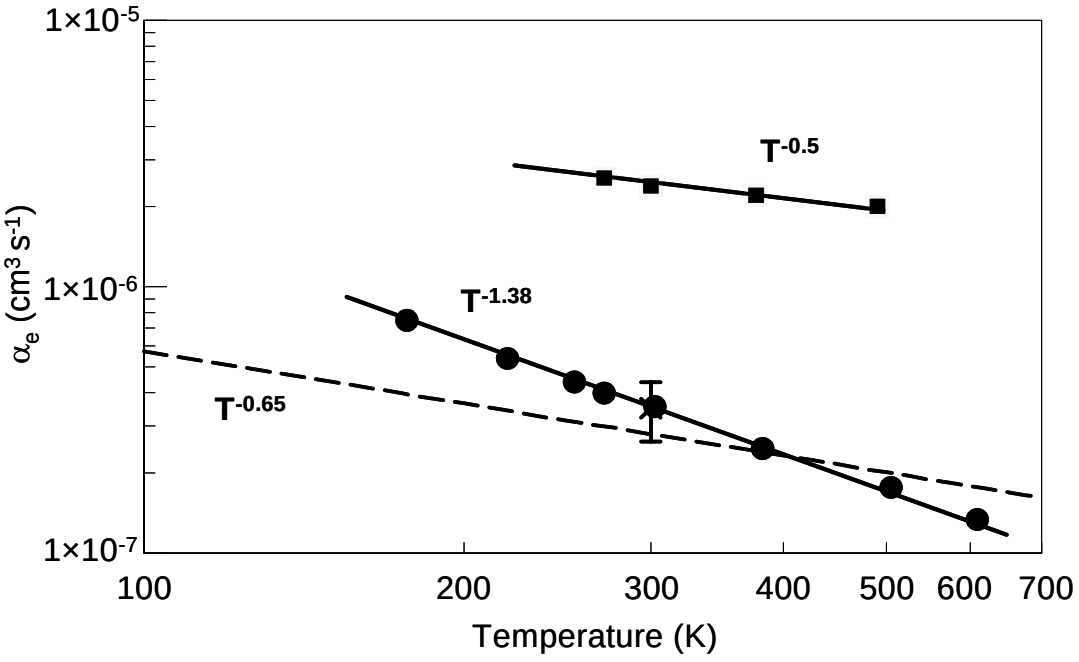

Figure 6.2. A ln-ln plot of α_e vs. temperature of the present data for $HCNH^+$ (circles) with a power law dependence fit of $T^{-1.38}$ and $(HCN)_2H^+$ (squares) with a fit of $T^{-0.5}$. The star with the error bars attached at 300 K is a previous flowing afterglow measurement for $HCNH^+$.[30] The dashed line represents previous storage ring data for $HCNH^+$ with $\alpha_e(T)= 2.8\times10^{-7}\ cm^3\ s^{-1}\ (300/T)^{0.65}$.[31]

6.3.3 TEMPERATURE DEPENDENCIES FOR THE PROTONATED CYANIDES

The α_e vs temperature data for $HCNH^+$, CH_3CNH^+, $CH_3CH_2CNH^+$ are plotted in figures 6.2-4, represented by circles. A comparison of the temperature dependencies for the three protonated ions reveals a trend of the power law dependencies decreasing as the mass of the ions increase. The power law temperature dependence for the cyanides are $\alpha_e(T) = 3.5\times10^{-7}\ cm^3\ s^{-1}\ (300/T)^{1.38}$ for $HCNH^+$, $\alpha_e(T)= 3.4\times10^{-7}\ cm^3\ s^{-1}\ (300/T)^{1.03}$ for CH_3CNH^+, and $\alpha_e(T)= 4.6\times10^{-7}\ cm^3\ s^{-1}\ (300/T)^{0.81}$ for $CH_3CH_2CNH^+$. The α_e's for $HCNH^+$ and CH_3CNH^+ at 300 K are very close, indicative of similar mechanisms. But when an addition of an ethyl group is added to the CN, an increase in the α_e at 300 K is observed. This increase in α_e at 300 K and the $T^{-0.81}$ temperature dependence could indicate that the direct mechanism for this recombination is occurring more efficiently, than with the other two ions.

For the $HCNH^+$, theoretical calculations have predicted that there is not a neutral dissociative curve crossing through the ground state potential surface of the ion.[32] This implies that there is not a direct route to neutral products and that the direct mechanism cannot occur efficiently. Therefore, when the electron is captured by the ion there must be an additional intermediate step involved to facilitate DR, as with the indirect mechanism. The temperature dependence of $T^{-1.38}$ is in very good agreement with the temperature dependence indicated by theory of the indirect process of $T^{-1.5}$. However, there are significant discrepancies in the temperature dependencies between the present data and the storage ring data. Note that at 300 K there is agreement within error between these values and an earlier FA measurement.[33] The storage ring data indicate a

temperature dependence closer to the value obtained for the direct mechanism. One of the disadvantages reported in storage ring measurements is that the ion excitation states have not always been well determined.[34] If the $HCNH^+$ is in an rovibrationally excited state, then this could give a smaller temperature dependence since theoretical calculations show that a dissociative curve crossing does not exist through the ground state potential surface of the ion.[32] This excitation could also explain the smaller α_e, since vibrationally excited ions have been shown to have smaller recombination rate coefficients.

If we replace the proton in HCN with a methyl or ethyl group then the number of dissociative neutral channels is increased, increasing the probability of a favorable dissociative curve crossing and of a larger contribution to the direct mechanism.

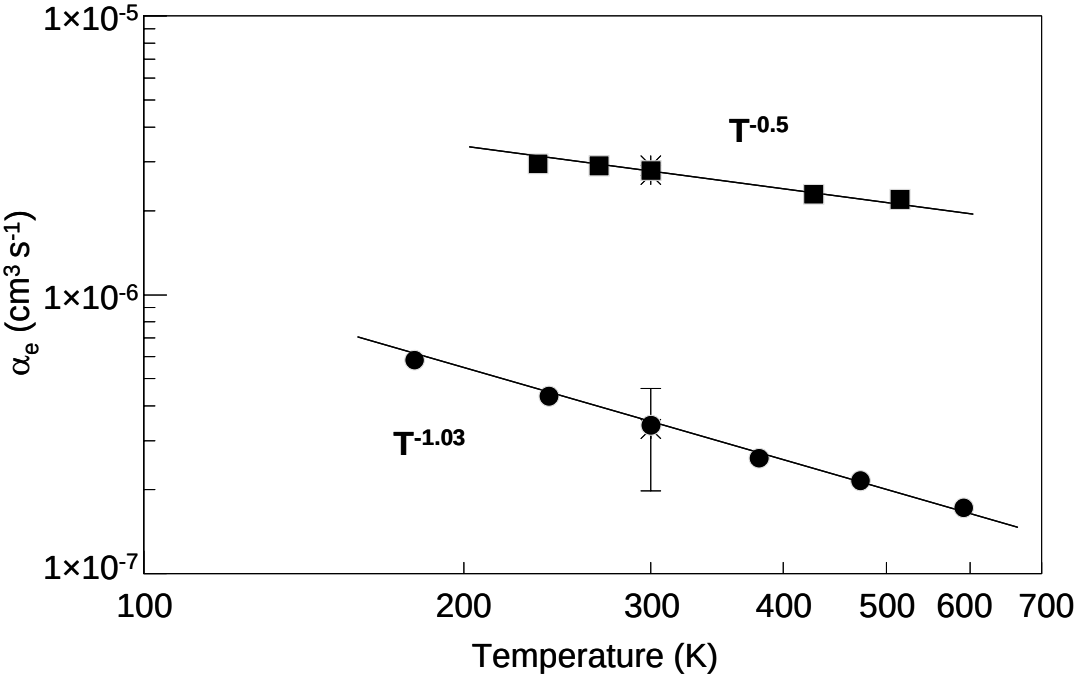

Figure 6.3. A ln-ln plot of α_e vs. temperature of the present data for CH_3CNH^+ (circles) with a power law dependence fit of $T^{-1.03}$ and $(CH_3CN)_2H^+$ (squares) with a fit of $T^{-0.5}$. The stars with the error bars attached represent previous FA measurements for the monomer[35] CH_3CNH^+ and the proton bound dimer[20] $(CH_3CN)_2H^+$.

The trend is consistent for the direct mechanism to be contributing more to the recombination. The fact that the temperature dependence for these larger molecular ions did not give a temperatures dependence of $T^{-0.5}$ is not surprising since the indirect mechanism could still be contributing to the unknown neutral product channel. Unfortunately, to the author's knowledge the same theoretical calculations for $HCNH^+$ have not been made for the CH_3CNH^+ and $CH_3CH_2CNH^+$ ions.

6.3.4 TEMPERATURE DEPENDENCIES FOR THE PROTON-BOUND DIMERS

The α_e for these proton-bound dimers are significantly larger than those of the protonated cyanide monomers. As predicted by Bates,[17] who coined the phrase "super recombination", for cluster ions of this type. The temperature dependencies for $(HCN)_2H^+$, $(CH_3CN)_2H^+$, and $(CH_3CH_2CN)_2H^+$ are all very similar at $T^{-0.5}$. Since the number dissociative channels in these proton bound dimers is much larger than that of their protonated analogue there is a greater possibility of a favorable curve crossing and the direct mechanism would occur more efficiently. The values of the α_e for these dimers are also very similar. This has been predicted for such systems where the H^+ is sandwiched between two molecules.[17, 36] In these cases, the recombining electron attaches to the molecule at the H^+ site. This very site specific recombination implies a similar mechanism is occurring. However, there are small differences as the functional group on the CN is varied. The α_e increases slightly from $\alpha_e(T) = 2.4\times10^{-6}$ cm^3 s^{-1} $(300/T)^{0.5}$ for $(HCN)_2H^+$ to $\alpha_e(T)= 2.8\times10^{-6}$ cm^3 s^{-1} $(300/T)^{0.5}$ for $(CH_3CN)_2H^+$, but when an ethyl functional group is attached to the CN the value decreases slightly to $\alpha_e(T)=$

2.3×10^{-6} cm^3 s^{-1} $(300/T)^{0.5}$ for $(CH_3CH_2CN)_2H^+$. The decrease in the α_e for $(CH_3CH_2CN)_2H^+$ may be caused by the larger ethyl chain sterically hindering the electron capture by the H^+. We plan to make similar studies for proton bound aromatic ring hydrocarbons ($C_6H_6^+$, $C_5H_5N^+$, etc.) where the proton could be truly sandwiched between the two rings. This would also show whether the π electrons in the rings will influence the recombination.

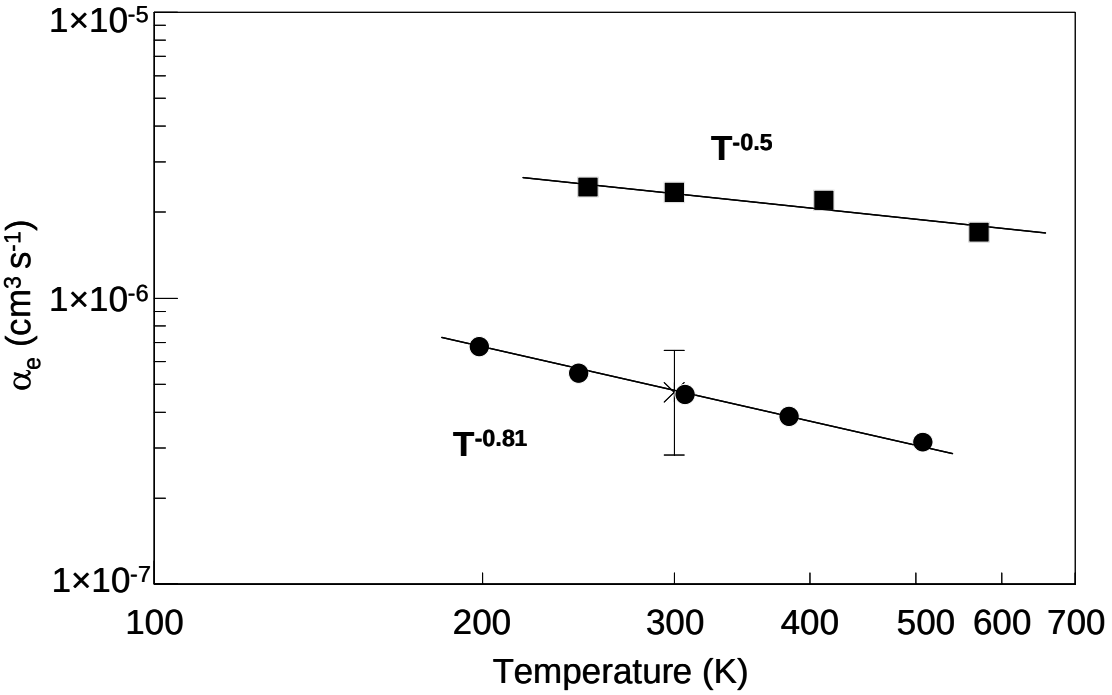

Figure 6.4. A ln-ln plot of α_e vs. temperature of the present data for $CH_3CH_2CNH^+$ (circles) with a power law dependence fit of $T^{-0.81}$ and $(CH_3CH_2CN)_2H^+$ (squares) with a fit of $T^{-0.5}$. The star with the error bars attached at 300 K represent previous FA measurements for $CH_3CH_2CNH^+$.[35]

6.3 CONCLUSIONS

The α_e for DR for $HCNH^+$, CH_3CNH^+, $CH_3CH_2CNH^+$, $(HCN)_2H^+$, $(CH_3CN)_2H^+$, and $(CH_3CH_2CN)_2H^+$ have been obtained as a function of temperature. The protonated cyanide series was chosen because of their importance to the Titan ionosphere[1, 4-8] and their predicted abundances in the interstellar medium[10-12]. The proton transfer reaction from H_3^+ to these cyanides rapidly produces the protonated molecular ion, which then rapidly recombine with electrons. However, if the concentration of the neutral cyanide is sufficiently large, association can produce proton-bound dimer ions. Since the α_e's for these dimer ions is much larger than their protonated analogue, the effective rate coefficient α_{eff} increases with increasing reactant concentration. These α_{eff}'s become constant in the regions where the either the protonated cyanide ions or the proton bound dimer ion becomes the dominant recombining ion in the plasma. Thus great care has to be taken in choosing the cyanide concentrations at which measurements are made. These data also demonstrate that when measuring the α_e's in a flowing afterglow for other molecular ions, especially where large dipole moments exist, clustering reactions should always be considered.

6.5 ACKNOWLEDGEMENTS

Funding under NSF Grant No. 0212368 is gratefully acknowledged.

6.6 REFERENCES

[1] Molina-Cuberos, G. J.; Lopez-Moreno, J. J.; Rodrigo, R.; Lara, L. M., Chemistry of the Galactic Cosmic Ray Induced Ionosphere of Titan. *J.Geophys. Res.* **1999,** 104, 21997-22024.

[2] Nagy, A. F.; Cravens, T. E., Titan's Ionosphere: A Review. *Planet. Space Sci.* **1998,** 46, 1149-1155.

[3] Garland, M.; Lilensten, J.; Toublanc, D.; Maurice, S., The Ionosphere of Titan: Ideal Diurnal and Nocturnal Cases. *Icarus* **1999,** 140, 92-105.

[4] Fox, J. L.; Yelle, R. V., Hydrocarbon Ions in the Ionosphere of Titan. *Geophys. Res. Letts.* **1997,** 24, 2179-2182.

[5] Keller, C. N.; Anicich, V.; Cravens, T. E., Model of Titan's Ionosphere with Detailed Hydrocarbon Ion Chemistry. *Planet. Space Sci.* **1998,** 46, 1157-1174.

[6] Wilson, E. H.; Atreya, S. K., Current State of Modeling the Photochemistry of Titan's Mutually Dependent Atmosphere and Ionosphere. *J. Geophys. Res.* **2004,** 109, E06002.

[7] Anicich, V.; Wilson, P.; McEwan, M. J., A SIFT Study of Some Reactions in Titan's Atmosphere: Reactions of N^+, N_2^+, and HCN^+ with CH_4, C_2H_2 and C_2H_4. *J. Am. Soc. Mass Spectrom.* **2004,** 15, 1148-55.

[8] Cravens, T. E.; Robertson, I. P.; Waite, J. H.; Yelle, R. V.; Kasprzak, W. T.; Keller, C. N.; Ledvina, S. A.; Nieman, H. B.; Luhmann, J. G.; McNutt, R. L.; Ip, W.-H.; de la Haye, V.; Mueller-Wodarg, I.; Wahlund, J.-E.; Anicich, V. G.; Vuitton, V., Composition of Titan's Ionosphere. *Geophys. Res. Letts.* **2006,** 33, L07105.

[9] Bouchoux, G.; Minh, T. N.; Longevialle, P., Unimolecular Chemistry of Protonated Ethyl Cyanide and Ethyl Isocyanide: An Experimental and Molecular Orbital Study. *J. Am. Chem. Soc.* **1992,** 114, 10000-10005.

[10] Turner, B. E.; Friberg, P.; Irvine, W. M.; Saito, M.; Yamamoto, S., Interstellar Cyanomethane. *Astrophys. J.* **1990,** 355, (2), 546-61.

[11] Ziurys, L. M.; Turner, B. E., HCNH+: a new interstellar molecular ion. *Astrophys. J.* **1986,** 302, L31-6.

[12] Ziurys, L. M.; Turner, B. E., Detection of interstellar vibrationally excited HCN. *Astrophys. J.* **1986,** 300, L19-23.

[13] Clary, D. C.; Smith, D.; Adams, N. G., Temperature Dependences of Rate Coefficients for Reactions of Ions with Dipolar Molecules. *Chem.Phys.Letts.* **1985,** 119, 320-326.

[14] Anicich, V., Evaluated Bimolecular Ion-Molecule Gas Phase Kinetics of Positive Ions for use in Modeling Planetary Atmospheres, Cometary Comae, and Interstellar Clouds. *J. Phys. Chem. Ref. Data* **1993,** 22, (6), 1469-1569.

[15] Mackay, G. I.; Betowski, D.; Payzant, H. I., Rate constants at 297 K for proton-transfer reactions with HCN and CH3CN. Comparisons with classical theories and exothermicity. *J. Phys. Chem. A* **1976,** 80, 2919-2922.

[16] McLain, J. L.; Poterya, V.; Molek, C. D.; Babcock, L. M.; Adams, N. G., Flowing Afterglow Studies of the Temperature Dependencies for Dissociative Recombination of O_2^+, CH_5^+, $C_2H_5^+$ and $C_6H_7^+$ with Electrons. *J. Phys. Chem. A* **2004,** 108, 6704-6708.

[17] Bates, D. R., Super Dissociative Recombination. *J. Phys. B* **1991,** 24, 703-709.

[18] McLain, J. L.; Poterya, V.; Jackson, D. M.; Adams, N. G.; Babcock , L. M., $C_3H_3^+$ Isomers: Temperature Dependencies of their Production in the H_3^+ Reaction with Allene and their Loss by Dissociative Recombination with Electrons. *J. Phys. Chem. A* **2005,** 109, 5119-5123.

[19] Mitchell, J. B. A.; Rebrion-Rowe, C., The Recombination of Electrons with Complex Molecular Ions. *Int. Rev. Phys. Chem.* **1997,** 16, 201-213.

[20] Plasil, R.; Glosik, J.; Zakouril, P., Formation and Recombination of Protonated Acetonitrile Clusters. *J. Phys. B* **1999,** 32, 3575-83.

[21] Smith, D.; Adams, N. G., Studies of Plasma Reaction Processes using a Flowing Afterglow/Langmuir Probe Apparatus. In *Swarms of Ions and Electrons in Gases*, Lindinger, W.; Mark, T. D.; Howorka, F., Eds. Springer-Verlag: Vienna, 1984; pp 284-306.

[22] Adams, N. G.; Smith, D., Flowing Afterglow and SIFT. In *Techniques for the Study of Ion-Molecule Reactions*, Farrar, J. M.; Saunders, J. W. H., Eds. Wiley Interscience: New York, 1988; Vol. 20, pp 165-220.

[23] Ziegler, K., Hydrogen cyanide (anhydrous). *Org. Syn.* **1927,** 7, 50-52.

[24] Molek, C. D.; Poterya, V.; Adams, N. G.; McLain, J. L., New Technique for Quantitative Measurements of Products for Dissociative Recombination. *Int. J Mass Spec.* **2007**, in preparation.

[25] Nelson, R. D.; al., e., Selected Values of Electric Dipole Moments for Molecules in the Gas Phase. *NSRDS-NBS 10* **1971**.

[26] Bates, D. R., Dissociative Recombination. *Phys. Rev.* **1950,** 78, 492-493.

[27] Bardsley, J. N., The Theory of Dissociative Recombination. *J. Phys. B.* **1968,** 1, 365-380.

[28] Bardsley, J. N.; Biondi, M. A., Dissociative Recombination. *Adv. At. Mol. Phys.* **1970,** 6, 1-57.

[29] Adams, N. G.; Babcock, L. M.; McLain, J. L., Electron-Ion Recombination. In *Encyclopedia of Mass Spectrometry: Theory and Ion Chemistry, Vol.1*, Armentrout, P., Ed. Elsevier: Amsterdam, 2003; Vol. 1, pp 542-555.

[30] Adams, N. G.; Smith, D., Measurements of the Dissociative Recombination Coefficients for Several Polyatomic Ion Species at 300K. *Chem. Phys. Letts.* **1988,** 144, 11-14.

[31] Semaniak, J.; Minaev, B. F.; Derkatch, A. M.; Hellberg, F.; Neau, A.; Rosen, S.; Thomas, R.; Larsson, M.; Danared, H.; Paal, A.; af Ugglas, M., Dissociative Recombination of $HCNH^+$: Absolute Cross-Sections and Branching Ratios. *Ap. J. Suppl.* **2001,** 135, 275-83.

[32] Talbi, D.; Ellinger, Y., Potential Energy Surfaces for the Electronic Dissociative Recombination of $HCNH^+$: Astrophysical Implications on the HCN/HNC Abundance Ratio. *Chem. Phys. Lett.* **1998,** 288, 155-164.

[33] Smith, D.; Adams, N. G., Studies of Plasma Reaction Processes Using a Flowing-Afterglow/Langmuir Probe Apparatus. In *Swarms of Ions and Electrons in Gases*, Lindinger, W.; Mark, T. D.; Howorka, F., Eds. Springer-Verlag/Wien: New York 1984; pp 195-217.

[34] Larsson, M., Dissociative Recombination in Ion Storage Rings. *Int. J. Mass Spectrom Ion Proc.* **1995,** 149-50, 403-14.

[35] Geoghegan, M.; Adams, N. G.; Smith, D., Determination of the Electron-Ion Dissociative Recombination Coefficients for Several Molecular Ions at 300K. *J. Phys. B* **1991,** 24 2589-2599

[36] Bates, D. R., Dissociative Recombination of Polyatomic Ions. *J. Phys. B* **1991,** 24, 3267-3284.

CHAPTER 7

CONCLUSIONS AND FUTURE DIRECTIONS

The understanding of DR has come a long way since it was first mentioned by Kaplan in 1931 to explain the emissions from the nightglow and the aurora borealis.[1] In the beginning, many scientist had the notion that DR would be a slow process until Bates and Massey tentatively proposed that DR may, after all, be rapid.[2] Since then, the process of DR has been promoted as the most important loss process of plasmas containing molecular ions. Bates surmised that if an earlier idea by Massey is incorrect and that the coupling of the nuclear and electronic motions is not involved, then the way the process may occur is much simpler.[3] Bates reasoned that if the potential energy curve is crossed near its minimum by a repulsive potential energy curve belonging to a resonant electronic state, a double-electron radiationless transition may occur whereby the ion plus the captured electron enters this resonant state. The atoms then begin to separate because of their mutual repulsion, the inverse process of autoionization is prevented and DR is stabilized. Many theories have been suggested since then which do not require this curve crossing and still exhibit DR as a rapid process.[3-9]

DR plays an vital role in the synthesis of complex molecules in interstellar clouds and planetary atmospheres by creating both radical and strongly bound neutral molecules.[10] Therefore, DR couples the ion and neutral chemistries in extraordinary ways. In Titan's ionosphere, the most abundant ions suggested by the Fox and Yelle model were $C_2H_5^+$, CH_5^+ and $HCNH^+$ in order of decreasing abundance. However, the arrival of the Cassini-Huygens spacecraft confirmed that the concentration of $HCNH^+$ is

much larger than the other ions in the altitude range ~1000-1300 km.[11] The α_e for DR of $HCNH^+$, CH_3CNH^+, $CH_3CH_2CNH^+$ have been obtained as a function of temperature. The protonated cyanide series was chosen because of its importance to the Titan ionosphere[11-16] and their predicted abundances in the interstellar medium.[17-19] The α_e for O_2^+, CH_5^+, $C_2H_5^+$, c/l-$C_3H_3^+$ and $C_6H_7^+$ have also been determined at temperatures ranging from 80 to 600 K. All of these ions studied exhibit significant dependencies on temperature consistent with the simple theoretical models, except for $C_3H_3^+$. The α_e for the cyclic and linear-$C_3H_3^+$ isomers have little to no temperature dependence over this temperature range, and this is difficult to explain without more detailed theoretical calculations. Interestingly, the product ion distributions for the precursor $H_3^+ + C_3H_4$ could be obtained by numerical analysis of the recombination differential rate equation, and these distributions change with temperature. This is the first time that recombination rates and product ion distributions have been simultaneously obtained from recombination data.

A comprehensive study using the VT-FALP technique for the H_3^+ + RCN reaction reveals that the recombination of $RCNH^+$ is not just a simple recombination reaction but that the dimers; $(HCN)_2H^+$, $(CH_3CN)_2H^+$, and $(CH_3CH_2CN)_2H^+$ begin to increasingly contribute to the electron density decay when the [RCN] is increased above ~10^{11} cm^{-3}. The protonated-cyanides have relatively modest $\alpha_e \lesssim 5\times10^{-7}$ cm^{-3} s^{-1} while their proton-bound dimer ions have substantially larger $\alpha_e > 10^{-6}$ cm^{-3} s^{-1} at 300 K. Great detail has to be taken in choosing the cyanide concentration at which measurements are made and if this is not done erroneous values of α_e are likely to be obtained. These data also demonstrate that when measuring the α_e's in a flowing afterglow for other molecular

ions, especially where large dipole moments exist, clustering reactions should always be considered.

Determining recombination rate coefficients as a function of temperature will continue with emphasis being placed on more complex organic molecules which exist in interstellar space[20, 21], and extraterrestrial atmospheres, such as Titan.[12] α_e's for molecular ions which are of much interest that can be measured as a function temperature using this technique include: $C_4H_3^+$, $C_4H_4^+$, HC_3NH^+, HC_5NH^+ c-$C_6H_6^+$, c-$C_5H_5N^+$, c-$C_5H_5NH^+$, c-$C_4H_4N_2^+$, c-$C_4H_4N_2H^+$, etc. These aromatic ring compounds are becoming of increasing importance with the detection of c-$C_6H_6^+$ in the interstellar clouds and $C_5H_5N^+$ and c-$C_6H_7^+$ also in Titan's atmosphere. Such heterocyclics have similarities to thymine, a component of base pairs of DNA, and may be considered as prebiotic molecules. In addition, the π electrons in these rings may influence their DR, and this needs to be investigated. This is can also be expanded to include oxygen containing molecular ions such as: $HCOH_2^+$, $CH_3OCH_4^+$, $(CH_3)_2OH^+$, $CH_3CH_2OCH_2CH_4^+$, $CH_3OH_2^+$, $CH_3CH_2OH_2^+$, and many analogous isomers. All of these measurements pose great challenges for future researchers in this area. For most of these molecular ions, the effects of dimerization will have to be explored to ensure accurate α_e's. And for several of these systems, the neutral reactants are unstable and must be carefully synthesized in the laboratory.

Another important aspect of these types of measurements both obtained previously and in the future will be to investigate the neutral products of recombination. This is especially important now since discrepancies have come to light between flowing afterglow and storage ring measurements (H_2O^+, H_3O^+, CH_5^+) and these are unresolved.

We have developed a novel technique to determine these neutral products with mass spectrometric measurements, and this has already proven itself to be a very useful technique in the field.[22] These neutral products of recombination have become an increasingly important feature for researchers to improve their models of the environments where dissociative recombination is crucial.

7.1 REFERENCES

[1] Kaplan, J., In Light of the Night Sky. *Phys Rev.* **1931,** 38, (5), 1048.

[2] Bates, D. R.; Massey, H. S. W., *Proc. R. Soc. Lond. A* **1947,** 192, 1.

[3] Bates, D. R., Dissociative Recombination: Crossing and Tunneling Modes. *Adv. Atom. Molec. Opt. Phys.* **1994,** 34, 427-486.

[4] Bardsley, J. N., The Theory of Dissociative Recombination. *J. Phys. B.* **1968,** 1, 365-380.

[5] Guberman, S. L., Dissociative Recombination without a Curve Crossing. *Phys. Rev. A* **1994,** 49, R4277.

[6] Mitchell, J. B. A.; Guberman, S. L., *Dissociative Recombination: Theory, Experiment and Applications I.* World Scientific: Singapore, 1989.

[7] Zajfman, D.; Mitchell, J. B. A.; Schwalm, D.; Rowe, B. R., *Dissociative Recombination: Theory, Experiment and Applications III*. World Scientific: Singapore, 1996.

[8] Larson, A.; Orel, A. E., Ion-pair formation and product branching ratios in dissociative recombination of HD^+. *Phys Rev. A* **2001,** 64, (6), 062701-1.

[9] Hickman, A. P., Dissociative recombination of electrons with H_2^+. *J Phys. B* **1987,** 20, (9), 2091.

[10] Fox, J. L.; Yelle, R. V., Hydrocarbon ions in the ionosphere of Titan. *Geophys. Res. Letts.* **1997,** 24, (17), 2179-2182.

[11] Cravens, T. E.; Robertson, I. P.; Waite, J. H.; Yelle, R. V.; Kasprzak, W. T.; Keller, C. N.; Ledvina, S. A.; Nieman, H. B.; Luhmann, J. G.; McNutt, R. L.; Ip, W.-H.; de la Haye, V.; Mueller-Wodarg, I.; Wahlund, J.-E.; Anicich, V. G.; Vuitton, V., Composition of Titan's Ionosphere. *Geophys. Res. Letts.* **2006,** 33, L07105.

[12] Fox, J. L.; Yelle, R. V., Hydrocarbon Ions in the Ionosphere of Titan. *Geophys. Res. Letts.* **1997,** 24, 2179-2182.

[13] Keller, C. N.; Anicich, V.; Cravens, T. E., Model of Titan's Ionosphere with Detailed Hydrocarbon Ion Chemistry. *Planet. Space Sci.* **1998,** 46, 1157-1174.

[14] Wilson, E. H.; Atreya, S. K., Current State of Modeling the Photochemistry of Titan's Mutually Dependent Atmosphere and Ionosphere. *J. Geophys. Res.* **2004,** 109, E06002.

[15] Anicich, V.; Wilson, P.; McEwan, M. J., A SIFT Study of Some Reactions in Titan's Atmosphere: Reactions of N^+, N_2^+, and HCN^+ with CH_4, C_2H_2 and C_2H_4. *J. Am. Soc. Mass Spectrom.* **2004,** 15, 1148-55.

[16] Molina-Cuberos, G. J.; Lopez-Moreno, J. J.; Rodrigo, R.; Lara, L. M., Chemistry of the Galactic Cosmic Ray Induced Ionosphere of Titan. *J.Geophys. Res.* **1999,** 104, 21997-22024.

[17] Turner, B. E.; Friberg, P.; Irvine, W. M.; Saito, M.; Yamamoto, S., Interstellar Cyanomethane. *Astrophys. J.* **1990,** 355, (2), 546-61.

[18] Ziurys, L. M.; Turner, B. E., HCNH+: a new interstellar molecular ion. *Astrophys. J.* **1986,** 302, L31-6.

[19] Ziurys, L. M.; Turner, B. E., Detection of interstellar vibrationally excited HCN. *Astrophys. J.* **1986,** 300, L19-23.

[20] Adams, N. G.; Babcock, L. M.; Ray, N. S., Ionic Processes in Low Temperature Interstellar Molecular Plasmas. In *Atomic Processes in Plasmas*, Schultz, D. R.; Meyer, F. W.; Ownby, F., Eds. AIP: Melville, NY, 2002; pp 182-193.

[21] McCarthy, M. C.; Thaddeus, P., Microwave and Laser Spectroscopy of Carbon Chains and Rings. *Chem. Soc. Revs.* **2001,** 30, 177-185.

[22] Adams, N. G.; Molek, C. D.; McLain, J., New Flowing Afterglow Technique for Determining Products of Dissociative Recombination: CH_5^+ and N_2H^+. *J. Phys. Conf. Ser.* **2007**, in press.